

**Water Availability to Vegetation Across a Semiarid Shrubland and Grassland  
Ecotone, Sevilleta Wildlife Refuge, New Mexico**

by

Eric W. Bhark

Submitted in partial fulfillment  
of the requirements for the degree of  
Master of Science of Hydrology

New Mexico Institute of Mining and Technology  
Department of Earth and Environmental Science  
Socorro, New Mexico

August, 2002

---

## ABSTRACT

The 20<sup>th</sup> century shrub invasion of semiarid grasslands in New Mexico is one example of the transition of a semiarid herbaceous to woody plant ecosystem. A key factor controlling plant productivity and reproduction in semiarid environments is water availability in the soil. We characterize the hydrologic changes resulting from the shrub invasion, specifically the hydrologic advantage that shrubs hold over grasses, to pinpoint the primary factor(s) that contribute to the invasion. Observations are based on measurements of near surface soil moisture and soil-water potential across the transition. We focus on the differences between the grass and shrub environments. Our previous research has shown that in both environments, maximum spatial soil moisture variations exist at the plant-to-interspace scale, on the order of meters. Therefore, we now focus on individual plant canopy and interspace patches. We hypothesize that the critical hydrologic difference(s) contributing to the shrub invasion exist at this scale.

During the 2001 summer monsoon season we used the TDR (time domain reflectometry) method to measure soil water content. In both environments, TDR probe arrays are installed laterally covering the surface of eight plant canopies in total and their adjacent interspaces, using 128 probes. One array in each environment contains TDR probes inserted both at the surface and at depths. In addition, soil matric potential is measured adjacent to selected TDR probes. Soil-water potential is measured using a total of 64 heat dissipation sensors. The measurement arrays are designed to observe spatial, in both vertical and lateral orientations, and temporal movement of soil-water at the

canopy-interspace scale during natural precipitation events and subsequent soil drydown. Measurements are made and recorded hourly.

We focus on initial dry soil conditions, wetting events, and subsequent dry down sequences following natural rainfall events. Results suggest that it is the time period during precipitation, when water is redistributed over the ground surface, which is most critical to plant water availability. During precipitation events, shrub canopies accumulate a greater percentage of precipitation applied to a ground surface area than grass canopies, most critically during low precipitation events on the order of millimeters. The advantage of shrubs is twofold. One, their woody structure permits significant rainfall interception and stemflow directly to the plant root zone. Two, the large shrubland bare soil patches, coupled with low bare soil infiltration rates, provide runoff during precipitation that infiltrates into more permeable canopy soils. On the contrary, the plant structure of canopies in grassland, coupled with the depressed microtopography of bare soil patches, results in formation of ponds at bare soil depressions during precipitation, increasing infiltration into bare soil where it is not readily available to grasses.

<b>TABLE OF CONTENTS</b>	<b>Page</b>
Abstract	ii
Table of Contents	iv
List of Tables	vi
List of Figures	vii
Approval	ix
1. Introduction	1
1.1. Shrub Invasion of Semiarid Grassland	1
1.2. The Influence of Water Availability on Shrub Invasion	1
1.3. Surface-water Redistribution during Rainfall	2
1.4. Surface-water Redistribution during Soil Drying	6
1.5. Objectives	7
2. Study Area	10
3. Methods	13
3.1. Field Data	13
3.2. Laboratory Data	24
4. Results	29
4.1. Soil Texture and Hydraulic Properties	29
4.1.1. Soil Particle Size Analysis	29
4.1.2. Field Results	34
4.1.3. Laboratory Results	41
4.2. Water Availability	47
4.2.1. Volumetric Soil-Water Content beneath Canopies and Interspaces	47
4.2.2. Comparison of Soil-Water Content beneath Shrub and Grass Canopies	53
4.3. The Influence of Precipitation on Soil-Water Potential	53

## TABLE OF CONTENTS

	<b>Page</b>
4.3.1. Vertical Soil-Water Potential Gradients	59
4.3.2. Lateral Soil-Water Potential Gradients	63
5. Discussion	67
5.1. Shrubland	67
5.2. Grassland	69
6. Conclusions	70
References	74
Appendix I: Bhark, E.W. and Small, E.E., 2002	A-1

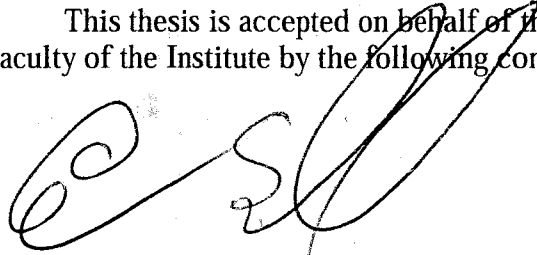
<b>List of Tables</b>	<b>Page</b>
Table 1: Soil column sample particle size analysis	30
Table 2: van Genuchten hydraulic parameters from grain size, soil columns, field data - A soil horizon	33
Table 3: van van Genuchten hydraulic parameters from grain size, soil columns, field data - B soil horizon	34
Table 4: van Genuchten model parameters for five standard soil classes	39
Table 5: Effective saturated hydraulic conductivity [ $\text{cm min}^{-1}$ ] of soil column samples and surface infiltration rates of field soils	41

<b>List of Figures</b>	<b>Page</b>
Figure 1: Root density depth profile in shrubland and grassland	5
Figure 2: Infiltration variograms in shrubland and grassland, reproduced from Bhark and Small, 2000	9
Figure 3: Location of field sites, Sevilleta Wildlife Refuge, central New Mexico	11
Figure 4: Overhead photos (meter scale) of shrubland and grassland	12
Figure 5: Scatterplot comparison of actual volumetric soil-water content versus TDR measurements	15
Figure 6: General schematic of five plant canopy locations in shrubland and grassland at which measurement arrays are established	18
Figure 7: Schematic of laterally oriented heat dissipation sensor arrays in shrubland and grassland	21
Figure 8: Schematic of vertically oriented TDR probe and heat dissipation sensor array in shrubland	22
Figure 9: Schematic of vertically oriented TDR probe and heat dissipation sensor array in grassland	23
Figure 10: Photograph of soil hydraulic property measurements in the laboratory during soil drydown	26
Figure 11: Water retention curves derived from grain size analyses from 0 – 10 cm	31
Figure 12: Water retention curves derived from grain size analyses from 10 – 35 cm	32
Figure 13: Water retention and $K(\theta)$ curves derived from field measurements at 5 cm	36
Figure 14: Water retention and $K(\theta)$ curves derived from field measurements at 15 cm	37
Figure 15: Water retention and $K(\theta)$ curves derived from soil column measurements of 0 – 10 cm depth soil sample	44
Figure 16: Water retention and $K(\theta)$ curves derived from soil column measurements of 10 – 35 cm depth soil sample	45

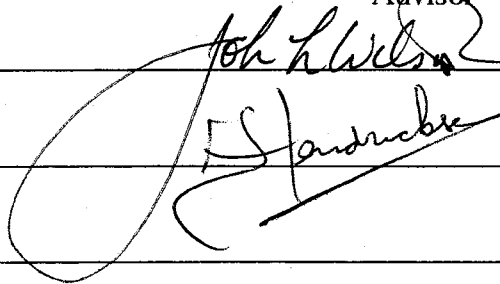
<b>List of Figures</b>	<b>Page</b>
Figure 17: Volumetric soil-water content time series at 5, 15 and 25 cm in the shrubland	49
Figure 18: Volumetric soil-water content time series at 5, 15 and 25 cm in the grassland	52
Figure 19: Soil-water diffusivity plots for shrub and grass canopy soils	57
Figure 20: Section 5 summary figure: Direction of vertical and lateral soil-water potential gradients for two time periods	58
Figure 21: Time series of vertical soil-water flux direction in shrubland and grassland	61
Figure 22: Time series of lateral soil-water flux direction in shrubland and grassland	66
Figure 23: 2001 precipitation intensity at 5 Points Station	69
Figure A-1: Field site locations at 5 Points Station, Sevilleta Refuge, NM	A-26
Figure A-2: Sketch of TDR probe insertion method into soil	A-27
Figure A-3: Photo of typical soil wetting front following precipitation	A-28
Figure A-4: Infiltration along transects at shrubland and grassland field sites	A-29
Figure A-5: Canopy: Interspace infiltration ratio plotted against precipitation size	A-30
Figure A-6: Infiltration variograms from transect measurements in shrubland and grassland	A-31



This thesis is accepted on behalf of the  
Faculty of the Institute by the following committee:



Adviser



8/15/02

Date

I release this document to the New Mexico Institute of Mining and Technology.



Student's Signature

8/15/02

Date

## **1. Introduction**

### **1.1. Shrub Invasion of Semiarid Grassland**

In the early 19<sup>th</sup> century, large areas of grassland were present in the southwestern U.S. Over the past 200 years, the density of shrubs such as mesquite (*Prosopis glandulosa*) and creosotebush (*Larrea tridentata*) has increased dramatically, converting these ecosystems from herbaceous to woody-dominated (Buffington and Herbel, 1965; Archer et al., 1994; Grover and Musick, 1990; Bahre and Shelton, 1993). Similar invasions of grasslands by shrubs have been observed worldwide, e.g., West Africa and Australia (Graetz, 1994). The following factors have been proposed to explain shrub invasion in the southwest: livestock grazing, altered fire regime, drought or climatic change, and increased atmospheric CO<sub>2</sub> concentration (Archer, 1994; Van Auken, 2000; Drewa and Havstad, 2001). However, it is not possible to establish a clear cause-effect relationship between these factors and observed vegetation changes. There is only limited data to constrain the history of shrub invasion (e.g., Buffington and Herbel, 1965) and interactions between these different factors could lead to complex ecosystem changes (Archer, 1994).

### **1.2. The Influence of Water Availability on Shrub Invasion**

In arid to semiarid ecosystems, precipitation is sufficiently low that water is the most critical factor controlling plant productivity and reproduction (Noy-Meir, 1973; Rodriquez-Iturbe, 2000). In Sonoran and Chihuahuan desert ecosystems, the influence of soil fertility, for example available nitrogen, is considered to be of secondary importance, as the effects of enhanced soil fertility are typically only observed once the limitations from available soil-water are eliminated (Ettershank et al., 1978; Cunningham et al.,

1979; Sharifi et al., 1988). Precipitation in these ecosystems occurs infrequently in discrete events, therefore limiting primary periods of water availability to periods of precipitation.

To simplify matters, we categorize the means by which precipitation is made available to plants in the shrubland and grassland ecosystems into two temporal components. First, we consider the period during precipitation, which includes how precipitation is distributed and redistributed on the ground surface, and subsequently infiltrates into the soil, over the surface area of consideration. Within this time period of precipitation, we define physical properties and processes that control the redistribution of surface water as precipitation. These properties and processes therefore also control spatial patterns of infiltration. These are (1) plant structure, e.g., woody, herbaceous, (2) surface ponding and runoff of precipitation, controlled by both surface soil hydraulic properties and spatial patterns of plant canopy and bare soil patch location, and (3) microtopography. We next define the second temporal component of water availability to plants as the period immediately following the earlier stage of precipitation and infiltration, where soil-water is spatially redistributed as soils dry. We define the physical properties and processes that control the soil-water redistribution as (1) difference in soil texture and corresponding soil hydraulic properties beneath plant canopies and bare soil patches, and (2) root-water uptake.

### **1.3. Surface-water Redistribution during Rainfall**

Considering the first component of water availability to plants, or how water is made available to plants through the spatial redistribution of surface water during precipitation, we review what is presently known about the surface hydrologic system in

semiarid shrubland and grassland ecosystems, focusing on the three physical properties that we suggest control surface hydrology in these systems.

Perhaps the most well documented of these processes is the influence of plant structure on the redistribution of surface water and infiltration. In semiarid shrublands, canopy interception accounts for a significant percentage ( $> 10\%$ ) of annual precipitation (Tromble, 1988; Dunkerly and Booth, 1999). In creosotebush, although the majority of interception falls through the canopy, surface soil nutrient enrichment (relative to bare soil) beneath shrubs indicates that stemflow is crucial to the process of shrub encroachment (Whitford, 1997). Similarly, it was shown that redirection of interception via stemflow channels water to subsurface storage along root systems that act as preferential flow paths, thereby redirecting water to locations where it is not available to surrounding vegetation with shallower root systems (Martinez-Meza and Whitford, 1996; Devitt and Smith, 2002). The effects of stemflow become more pronounced as the size of shrub canopies, root systems, and stem angles (with respect to the horizontal) increase.

In semiarid grasslands, there is no study to date that examines the influence of grass canopies, particularly those of black grama and blue grama, on the redistribution of surface soil-water during precipitation. Although grass interception research has been conducted, the results often neglect to quantify the percentage of interception that is channelized by grass stalks and contributes to infiltration, e.g., Thurow et al. (1987). More importantly, the grass species studied (e.g., big bluestem, buffalograss, curlymesquite) are sufficiently different from the grass species observed in this study (black grama) that a comparison of results is of no value.

Changes in geomorphology observed across the grass-to-shrub transition are also characteristic of desertification, and have been shown to strongly influence the availability of water to plants. These processes include the remainder of the aforementioned physical properties that we believe contribute to the redistribution of surface soil-water during precipitation: plant structure, the occurrence of ponding and surface runoff of precipitation, and microtopography. Shrubs are typically spaced further apart than grasses, a feature probably attributable to the large and deep shrub root systems, extending on average to depths ( $> 5$  m) at least three times greater than those of grass roots (Gibbens and Lenz, 2001). From 50 x 50 x 80 cm (L x W x Depth) soil pits excavated beneath one plant canopy and adjacent interspace at our shrubland and grassland field sites, we observed a similar relationship between root density and depth (Figure 1). Because individual shrub and grass canopies cover approximately equal surface areas, the larger spatial separation between shrubs than grasses entails that bare soil patches, also referred to as interspaces, are significantly larger in shrubland than grassland. During precipitation, intensified rainsplash reduces infiltration capacity in the large shrubland interspaces (Abrahams et al., 1995; Lyford and Qashu, 1969). Consequently, more overland flow is observed in shrublands (Abrahams et al., 1995; Schlesinger et al., 2000), increasing soil erosion and exposing finer textured, and therefore less permeable, soils at the surface (e.g., Kieft et al., 1998). Conversely, the local environment beneath a shrub canopy, protected from soil erosion (rainsplash, overland flow) by the plant, contains more permeable soils that permit faster infiltration than at bare soil patches (Wainwright et al., 1999; Dunkerley, 2000). As the size and connectivity of bare soil patches increases, it is expected that the volume of surface

runoff per unit soil surface area increases, significantly affecting the redistribution of surface water and spatial patterns of infiltration during precipitation. However, to the author's knowledge, no study to date examines bare soil connectivity in semiarid grassland or shrubland.

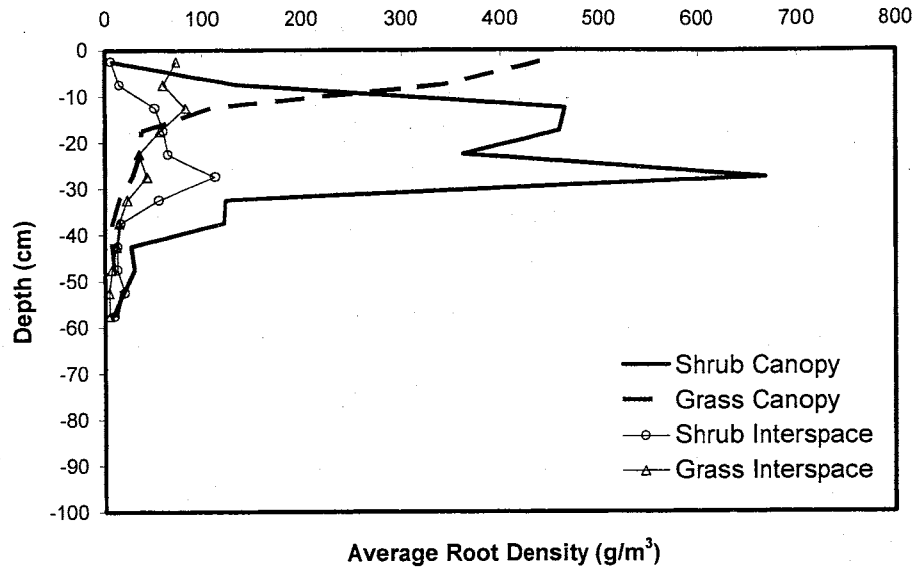


Figure 1: Root density depth profile in shrubland and grassland derived from measurement of soil beneath one shrub canopy, one grass canopy, and corresponding interspaces (Section 1.3). Maximum root density is located in the surface 15 cm beneath grass canopies. Beneath shrub canopies the maximum root density is located from ~10 to 30 cm.

Although differences in soil moisture have been observed between these ecosystems (Schlesinger et al., 1990; Kieft et al., 1998), the sampling schemes used in these studies were not linked to wetting-drying cycles, so it is difficult to assess changes in soil moisture availability to grasses and shrubs. However, Bark and Small (Appendix 1) found that both shrub (creosotebush) and grass (black grama) canopies are infiltration sinks following precipitation in their respective environments, and that the difference between canopy and interspace infiltration is typically greater in the shrubland. This result is in part explained by the 'zone of influence' beneath shrubs, a term defined as the surface area beneath and adjacent to shrubs where the infiltration rate is at least 10%

greater than that at bare soil patches (Dunkerly, 2000a; 2000b). Within this zone, the infiltration rate decreases nonlinearly from the shrub stem out into bare soil. The hydrologic distinction between canopy and bare soil in the shrubland therefore becomes fuzzy, contrary to previous studies that assume a sharp boundary between soil types (e.g., Bhark and Small, Appendix 1). However, distinct differences between canopy and interspace soil properties (Kieft et al., 1998; Dunkerly, 2000a) clearly indicate that the redistribution of surface soil water during precipitation is central to the study of water availability to plants.

#### **1.4. Soil-water Redistribution during Soil Drying**

We now consider the second component of water availability to plants, the redistribution of near subsurface soil-water following the earlier stage of precipitation and infiltration. Again, we suggest that this component is controlled by difference in soil texture and corresponding soil hydraulic properties beneath plant canopies and bare soil patches and root-water uptake. In a semiarid pinon-juniper woodland, Breshears (1997) showed that soil moisture derived from precipitation varied at spatial and temporal scales that corresponded with plant structure and the effects that plant structure had on the local environment (similar to those effects discussed above in semiarid shrublands). In particular, soil-water potential was lower (more negative) beneath plants following precipitation, which would suggest a net flux of soil-water from the wetter interspace soils towards the dryer canopy soils. However, differences in soil hydraulic properties were not measured. In addition, it was not certain if the deficit in soil moisture beneath plant canopies was a result of canopy interception and water loss relative to interspaces, or of root-water uptake.

Although no such studies are completed in either semiarid grassland or shrubland, there is sparse data from which inferences can be made. Gile et al. (1998) showed that creosotebush root morphology and distribution are strongly influenced by evolving subsurface soil textures (typically calcification), such changes controlling hydraulic conductivity and soil-water movement in the subsurface. Although this was not shown for semiarid grass root systems, it is known that the shallow root systems of black grama ( $\leq 1.6$  m), relative to shrubs ( $\geq 5.0$  m), have large radial spreads, thought to be an adaptation to access soil-water from small precipitation events (Gibbenz and Lenz, 2001). Therefore, root densities of semiarid shrubs and grasses, particularly of creosotebush and black grama, are high in the upper soil horizons, indicating direct competition for soil-water at the ecotone. Difference in soil texture beneath plant canopies and bare soil may therefore be significant in establishing the direction of soil-water flux following precipitation. Thus, there is indirect evidence that the redistribution of soil-water, resulting from soil texture differences beneath different plants and beneath bare soil, is a central component to plant water availability.

### **1.5. Objectives**

In this study, our goal is to understand how the transition from grass-to-shrub dominated semiarid ecosystems affects the spatial and temporal distribution of soil-water that is available to plants. It is clear that multiple processes strongly influence patterns of surface and near subsurface soil-water, which dictate the availability of water to plants. We conjecture that five physical properties and processes exclusively control the availability of water to plants during and after periods of precipitation. These are (1) plant structure, (2) ponding and surface runoff of precipitation, (3) microtopography, (4)



surface and near subsurface soil hydraulic parameters at plant canopies and bare soil, and (5) root water uptake. We are confident that each of these properties plays a crucial role in the redistribution of precipitation as soil-water, and we attempt to discern which properties are most significant. However, we do not directly measure the influence of each property on the redistribution of soil-water, with the exception of (4), soil texture and hydraulic parameters at plant canopies and bare soil. Instead, we measure the net effects that such properties have on soil-water redistribution during soil wetting and drying events, from which we are able to infer the relative significance of each property.

In order to fully understand how the ecosystem shift influences the availability of water to plants would require formation of a near-surface hydrologic balance in each system. This however is impractical for a single study as each component, e.g., transpiration, evaporation, and infiltration, requires individual examination. We therefore make broad scale measurements in the shrubland and grassland ecosystems in an attempt to pinpoint the components of such a hydrologic balance that are most critical to the issue of water availability to plants. We observe the spatial and temporal movement of near-surface soil-water in both environments over a series of natural precipitation events. In addition, near-surface soil hydraulic properties are measured, such properties having a strong influence on the flux of water into and through a soil medium.

The scale that we measure over is the canopy-interspace scale, on the order of meters. Bhark and Small (Appendix 1) showed that the maximum scale of soil-moisture and infiltration variability in these ecosystems exists at the plant-interspace (meter) scale, where the correlation length of infiltration is controlled by the typical radius (length) of both grass and shrub canopies (Figure 2). Their spatial analyses also showed that in each

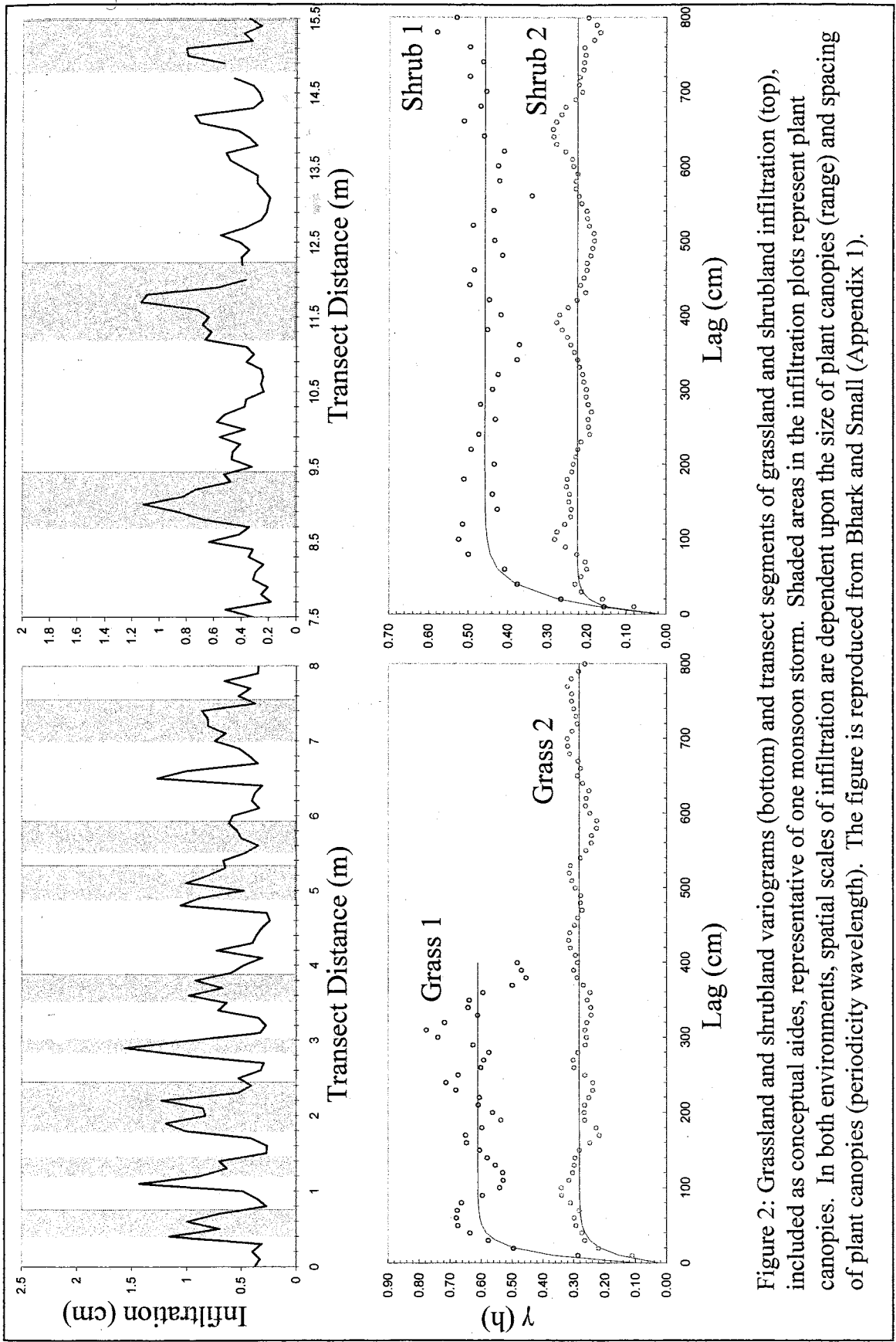


Figure 2: Grassland and shrubland variograms (bottom) and transect segments and infiltration (top), included as conceptual aides, representative of one monsoon storm. Shaded areas in the infiltration plots represent plant canopies. In both environments, spatial scales of infiltration are dependent upon the size of plant canopies (range) and spacing of plant canopies (periodicity wavelength). The figure is reproduced from Bhark and Small (Appendix 1).

environment, second-order stationarity is satisfied with respect to soil-moisture and infiltration within the tens of meters scale, further validating the selection of individual canopy-interspace systems as the spatial scale of measurement in this study. Their results are representative of time intervals immediately following precipitation, intervals at which soil-moisture variability is at a local maximum, and during which water availability to vegetation is greatest.

## **2. Study Area**

Field studies were conducted in grassland and shrubland ecosystems at the McKenzie Flats research area in the Sevilleta National Wildlife Refuge, central New Mexico (Figure 3). Annual precipitation is ~250 mm and more than half of the precipitation falls between July and September. The grass-shrub ecotone is narrow at McKenzie Flats – the shrub and grass sites sampled were within 2 km of each other. The grassland is dominated by black grama and has ~50% plant cover (Figure 4). The shrubland is dominated by creosotebush with ~30% plant cover. According to historical information and repeat photography, the shrubland was dominated by grasses and other herbaceous species in the early 20<sup>th</sup> century. Therefore, we are comparing the soil-water distribution and soil-hydraulic properties in the grassland with those from an area that was recently (~50 yrs) transformed from grassland to shrubland. The slope at all sites is < 2 degrees and the surface soil is a sandy loam that has developed on fan deposits from the Los Pinos Mountains to the west. Kieft et al. (1998) documented soil texture differences between the grassland and shrubland, and they attributed these differences to the shrub invasion process. The entire area has not been grazed since the 1970's.

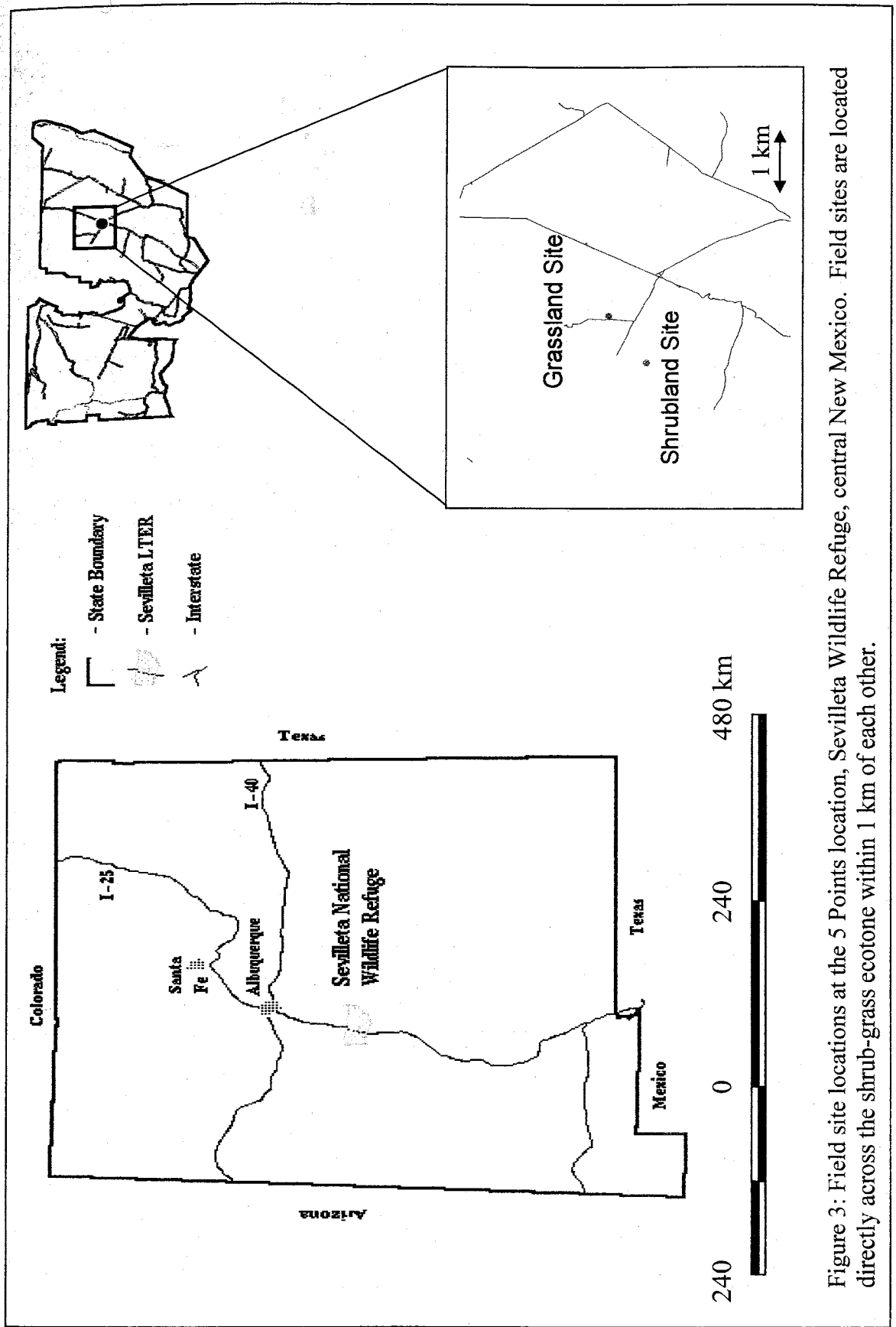


Figure 3: Field site locations at the 5 Points location, Sevilleta Wildlife Refuge, central New Mexico. Field sites are located directly across the shrub-grass ecotone within 1 km of each other.

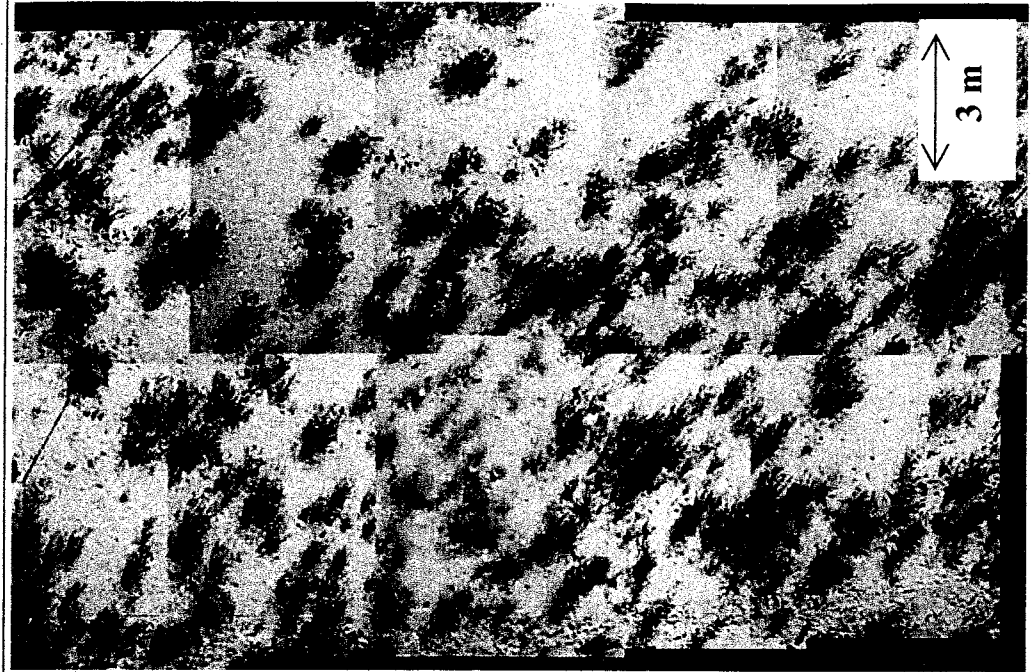
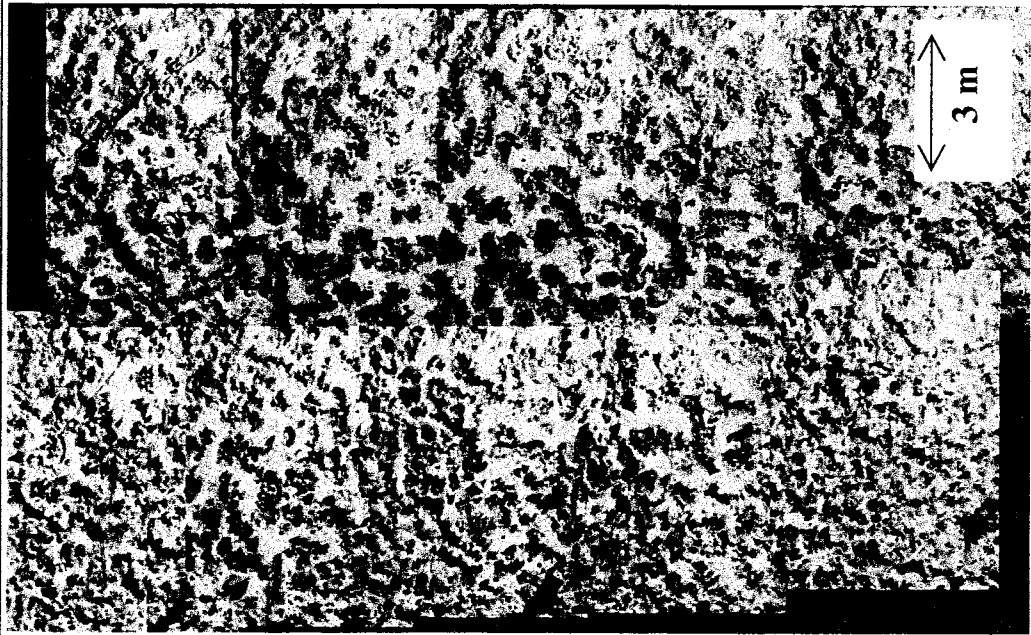


Figure 4: Overhead photo mosaics of representative grassland and shrubland ecosystems. The grassland and shrubland are dominated by black grama (*Prosopis glandulosa*) and creosotebush (*Larrea tridentata*), respectively. Canopies respectively cover approximately 50% and 30% of surface soil in the grassland and shrubland.

### 3. Methods

#### 3.1. Field Data

In the field, we measured precipitation, time series of volumetric soil-water content and soil-matric potential, and infiltration rates at the canopy-interspace (meter) scale. Volumetric soil-water content and matric potential were recorded along sample arrays, designed to measure variations in the spatial and temporal distributions of infiltration, during precipitation and subsequent dry down periods beneath canopies and adjacent bare soil. We additionally measured surface-water infiltration rates beneath a series of canopies and bare soil patches, not according to any spatial sampling scheme, in order to observe general differences in infiltration between the four surface cover types. We define the four surface cover types as the canopy and adjacent bare soil patches at each ecosystem, e.g., shrubland canopy, grassland bare soil.

Beginning with the measurements arrays, soil moisture was measured as volumetric water content ( $\theta$ ) using the Time Domain Reflectometry (TDR) method (Topp, 1980; Schugge et al., 1980). A combination of three-prong 15 cm TDR probes and two-prong 25 cm TDR probes was used. The measurement difference between two and three pronged probes is negligible (Ferre, personal communication). The different probes were used to reduce material cost and construction time, for ease of insertion into various soil samples in the field, and to better control the soil sample volume in the field. All TDR probes were constructed in the laboratory, and both types required calibration.

In theory, the travel time ( $\Delta t$ ) for the pulsed electromagnetic signal along a TDR waveguide (TDR rod) is dependent on the TDR rod length  $L$  and the apparent dielectric constant  $K$  of the insertion (soil) medium. The relationship is expressed as

$$\Delta t = \frac{2L\sqrt{K}}{c}, \quad (1)$$

where  $c$  is the velocity of an electromagnetic signal in free space. Because a change in the volumetric water content of a soil medium is physically expressed as a change in the apparent dielectric constant of the medium, equation (1) is simplified to express the dielectric constant of a soil medium as the ratio of the apparent TDR probe rod length  $La$  to the actual TDR probe rod length  $L$ . The simplified expression has the form

$$\sqrt{K} = \frac{La}{L}, \quad (2)$$

where  $La = c \Delta t/2$ , the value of  $La$  varying with both the medium of insertion and the volumetric water content of the medium. The calibration factor, or probe correction factor  $PC$  [length], is therefore the difference between the measured apparent TDR probe rod length in a medium and the actual, or theoretical, apparent length that should be measured in the medium. The difference between the measured and theoretical apparent rod lengths is an artifact of irregularity in the physical construction of the TDR probes, e.g., cable length, balun thickness, and separation between TDR probe rods. In conjunction with equation (2), the probe correction factor is expressed by the relationship

$$PC = La_{measured} - La_{theoretical} = La - \sqrt{K} * L. \quad (3)$$

For calibration, we used deionized water at a known temperature, and therefore with known  $K$ , as the medium.  $La_{theoretical}$  was then computed from (3) as the product  $\sqrt{K} * L$ ,  $L$  being the actual TDR probe rod length.  $La_{measured}$  was the output from the TDR probe measurement with the probe submerged in the deionized water.

Once  $PC$  is known, the TDR probe is inserted into a soil medium of unknown  $\theta$  and the apparent dielectric constant of the medium (soil and water) is calculated from

$$K = \left( \frac{La - PC}{L} \right)^2, \quad (4)$$

a variation of equation (3). To calculate the volumetric water content of the soil medium, we used Topp's equation, a robust empirical relationship relating  $K$  and  $\theta$  for soil mediums, which has the form

$$\theta = 4.3 * 10^{-6} K^3 - 5.5 * 10^{-4} K^2 + 2.92 * 10^{-2} K - 5.3 * 10^{-2} \quad (5)$$

(Topp, 1980). Laboratory tests with soil samples from the field sites showed Topp's equation to predict the soil-water content to within  $\pm 3\%$  of the actual (gravimetrically measured) (Figure 5)

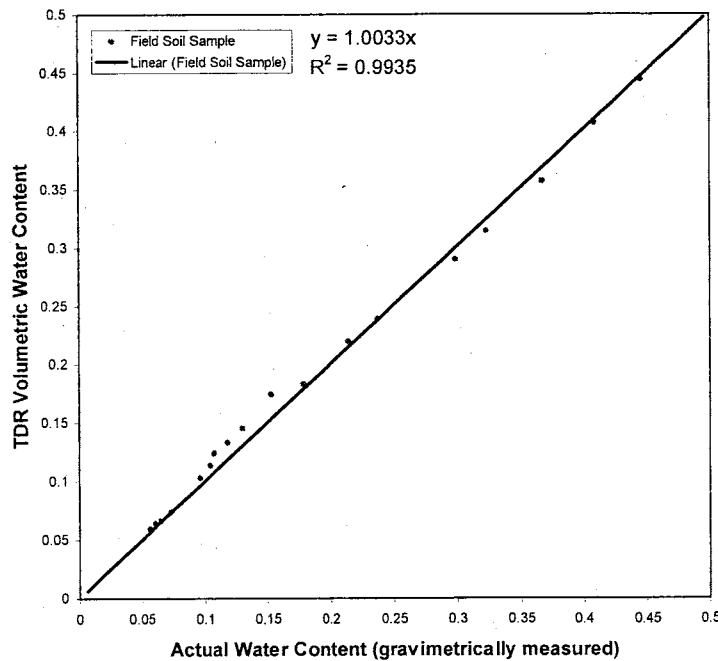


Figure 5: Comparison of soil-water content from gravimetric measurements with TDR measurements in a single field soil column sample through one drydown series from saturation. The TDR is accurate to within  $\pm 3\%$ . A least squares linear model represents 99.35% of the variation in the actual data.

Soil matric potential was measured along the sample arrays using heat dissipation sensors (Phene *et al.*, 1971; Reece, 1996). Heat dissipation sensors were selected over other methods of soil-water potential measurement due to their unique range of measurement, approximately -100 to -10,000 cm (-0.01 to -1.0 MPa). Due to the



variability in heat transfer properties of individual sensors, individual calibration was required, with the sole requirement that the water potential of the medium surrounding the probe was known. The relationship between the natural logarithm of soil water potential and the temperature increase measured by a thermocouple located adjacent to the line heat source within a sensor is shown to be linear (Campbell Scientific, 1998), with form

$$\ln(|\psi|) = \alpha * \Delta T + \beta, \quad (6)$$

where  $\psi$  is soil water potential (-cm),  $\Delta T$  ( $^{\circ}\text{C}$ ) is the temperature increase measured by the thermocouple over a chosen period of time, and  $\alpha$  and  $\beta$  are fitting parameters. We therefore performed a two-point, water potential end-member, calibration of each sensor, using air of known temperature and saturated soil samples of known temperature as the dry and wet end-members, respectively. At each end-member, the dissipation of heat through a constant time interval is recorded for the dry and wet ends, expressed respectively as  $T_d$  and  $T_s$  (in  $^{\circ}\text{C}$ ). We neglect the influence of relative humidity on the dry end-member as air dry conditions correspond to water potentials on the order of  $-10^6$  cm, at least an order of magnitude below (more negative than) those potential observed in the field. In a soil medium of unknown water potential, the dissipation of heat through time is recorded over the same time interval, expressed as  $T$ , and a dimensionless temperature  $T^*$  is computed from

$$T^* = \frac{T - T_d}{T_s - T_d} \quad (6)$$

We then use an empirical relationship relating water potential ( $\psi$ ) [ $\text{J kg}^{-1}$ ] and  $T^*$  of the form

$$\psi = -52.6(T * -2.22)^{-1} \quad (7)$$

(Flint, A. L. and Bilskie, J., personal communication).

The sample arrays were located at designated field sites (Figures 6) in shrubland and grassland (Figure 3), selected to be representative of each environment with respect to canopy coverage per unit area. Note that Figure 3 and Figure 6 do not represent the same area. The slope at each site is  $2^{\circ}$ , so the influence of local topography at each site does not bias the fraction of precipitation that becomes surface runoff when we compare results from each site. A slight slope was necessary such that the effects of runoff during precipitation could be observed. Our results are therefore not relevant to areas that have no slope.

At both shrubland and grassland field sites, a total of five measurement arrays were installed surrounding individual canopies and adjacent interspaces (Figure 6). Precipitation was measured at each site using tipping bucket rain gages with 0.254 mm resolution. TDR probes and heat dissipation sensors were installed along the arrays to measure volumetric soil-water content and soil-water potential, respectively. We designed the arrays to observe spatial and temporal movement of soil-water, at the canopy-interspace scale, during natural precipitation events and subsequent soil drydown. The design further permits observation of soil-water availability to plants as affected by plant structure, microtopography, and soil texture and hydraulic properties.

Four of the measurement arrays were designed as orthogonal transects, oriented parallel to the ground surface, with the intersection of transect midpoints at canopy centers (Figure 7). The four arrays were located at canopies S1 – S4 in the shrubland and G1 – G4 in the grassland (Figure 6). The spacing of TDR probes and heat dissipation

sensors in each array was chosen relative to the radial length,  $r$ , of each canopy in order to remove the influence of canopy size on soil measurements.

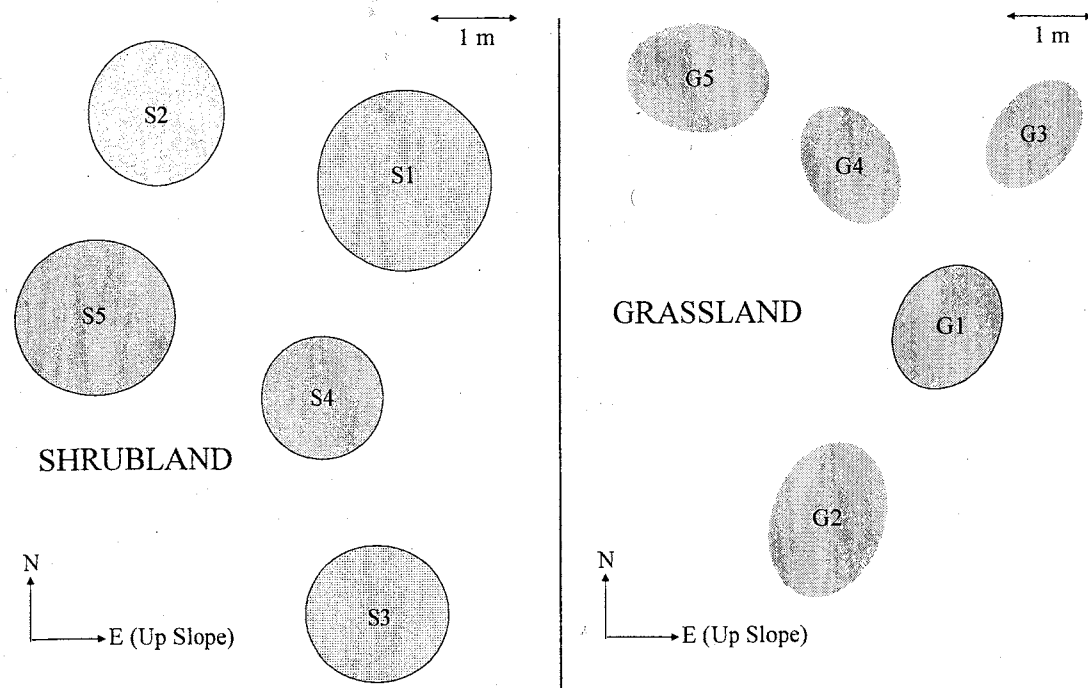


Figure 6: General schematic of shrubland and grassland locations at which probe arrays (Section 3.1) were installed. Shaded areas represent labeled plant canopies. It was necessary to construct all measurement arrays in a small surface area to satisfy cable length requirements for TDR probes and heat dissipation sensors. TDR probe and heat dissipation sensor measurements were recorded at S1 and S2 in shrubland and G1 and G2 in grassland (Figure 7). Only TDR measurements were recorded at S3 and S4 in shrubland, and at G3 and G4 in grassland. At S5 and G5, TDR probe and heat dissipation measurements were recorded with depth at 5, 15, and 25 cm (Figures 8 and 9).

At plant canopies S1 – S4 in shrubland and G1 – G4 in grassland, a total of fifty-two two-prong 25 cm TDR probes were inserted vertically into the ground from the surface at locations equivalent to  $r = 0$  (canopy center),  $r/2$ ,  $r$ ,  $3r/2$ , and  $5r/2$  along each limb of the four arrays. Such spacing ensured that the gradational conversion of soil cover types, from beneath the canopy center to complete bare soil, was sampled. However, we do not present measurements recorded by the two-prong 25 cm TDR probes. Several months following their installation, it was discovered that the vertical

placement of the 25 cm TDR probes into the soil surface created preferential flow paths in the surrounding soil, therefore influencing spatial patterns of soil wetting with depth. When the soil was wetted from the surface, a significant difference in wetting front depth was observed between the soil surrounding the TDR probe rods and the undisturbed adjacent soil; the wetting front beneath the TDR probe was greater than that of the surrounding by at least a factor of two, the difference likely varying with precipitation magnitude.

At plant canopies S1, S2, G1, and G2 (Figure 7), a total of twenty heat dissipation sensors in each ecosystem were inserted at two depths, 5 and 15 cm, adjacent to the vertically inserted TDR probes on the up-slope transect in each array. The pairs of heat dissipation sensors were located at intervals along transects equivalent to  $r = 0$ ,  $r/2$ , and  $5r/2$ , or beneath canopy center (stem in shrubland), canopy, and bare soil, respectively. Each heat dissipation sensor was inserted such that the line heat source lay parallel with the ground surface in order to minimize the affect of a vertical soil temperature gradient on the sensor thermocouple measurements. Note that the entire installation procedure was completed on a temporary, portable platform raised above the ground surface so that the soil was minimally disturbed.

In grassland and shrubland, an additional array, composed of four vertical transects of TDR probes and heat dissipation sensors, was installed at one canopy, S5 in shrubland and G5 in grassland (Figures 6, 8, and 9). The additional arrays were oriented parallel with the direction of maximum topographic relief. In each, twelve three-prong 15 cm TDR probes and twelve heat dissipation sensors were inserted at depths of 5, 15, and 25 cm at four locations, equivalent to radial distances from the canopy center of  $r =$

0,  $r/2$ , and  $5r/2$  (two locations at  $5r/2$ ). In both shrubland and grassland, each probe is provided a location label (Figures 8 and 9, respectively). TDR probes were inserted horizontally into the soil, with probe rods oriented parallel to the ground surface. Here our field method entailed hand-auguring small holes, inserting the probes at a given depth into the soil-wall to measure undisturbed soil, and then backfilling the holes. Adjacent to each TDR probe, a heat dissipation sensor was inserted into the soil wall, again with the line heat source oriented parallel to the ground surface. We make the assumption that the adjacent placement (3 to 5 cm separation distance) of TDR probes and heat dissipation sensors ensured measurement of the same soil sample.

The arrays were installed prior to the summer monsoon season of 2001. All measurements were automated and recorded hourly through the season.

Separate from the spatially designed measurement systems, we measured surface infiltration rates at the four representative surface cover types (e.g., grass canopy, shrubland bare soil) using single ring infiltrometers with a constant ponded head of 10 cm and insertion depth of 5 cm. The constant head was applied using a Mariotte siphon. For each soil cover type, measurements were made at five representative locations. At canopies, the ring infiltrometer was placed at a location approximately half-way between the canopy center and canopy-bare soil border. At bare soil, ring infiltrometers were located approximately in the center of the bare soil area. All sample locations were selected haphazardly, where we did not consider the influence of slope, microtopography, or canopy and bare soil patch size. We used the corresponding results primarily to observe any effects of surface soil crusts, or soil seals, on infiltration in undisturbed soil samples. In both grassland and shrubland, thin soil seals, on the order of millimeters,

## SHRUBLAND and GRASSLAND: PLAN VIEW

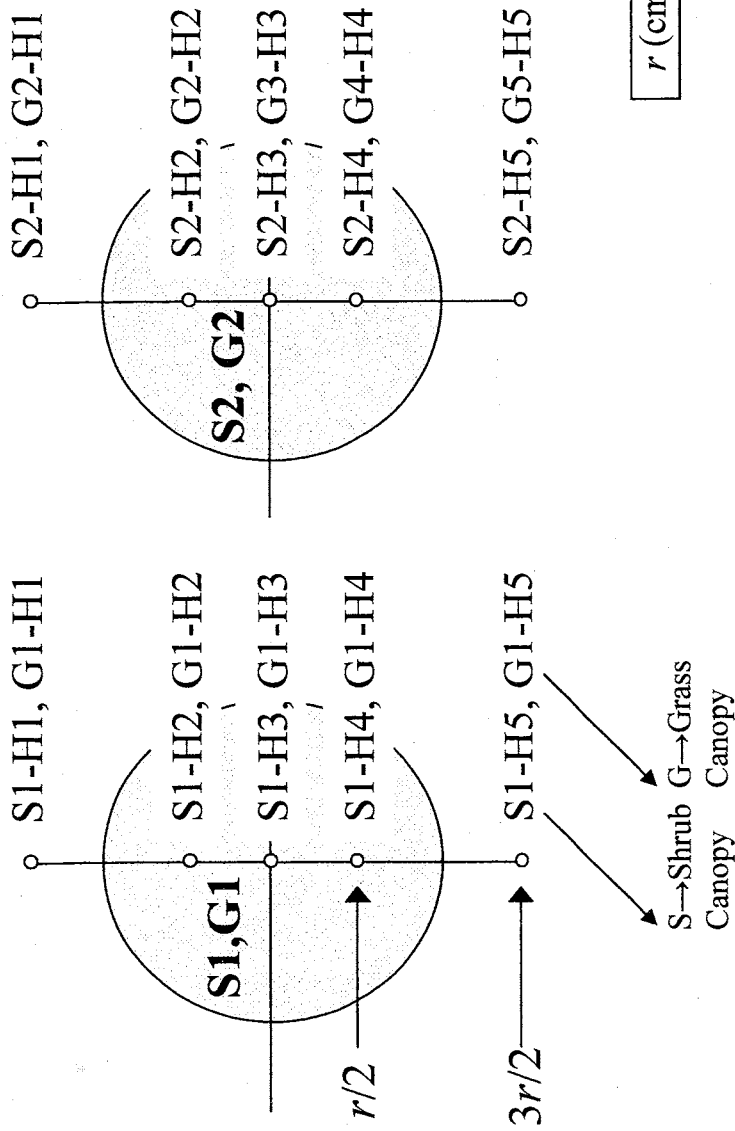


Figure 7: Schematic of heat dissipation sensor arrays in shrubland and grassland with corresponding sensor location labels. In both shrubland and grassland, there are two arrays as depicted in the plan view, located at shrub canopies S1 and S2 and grass canopies G1 and G2 (Figure 6). At each measurements location, heat dissipation sensors are inserted at depths of 5 and 15 cm, with the line heat source oriented parallel to the ground surface. The location of all probes is relative to the individual canopy radius,  $r$  (see table above). A total of 20 heat dissipation sensors are used across two measurement arrays.

# SHRUBLAND: CROSS - SECTIONAL VIEW

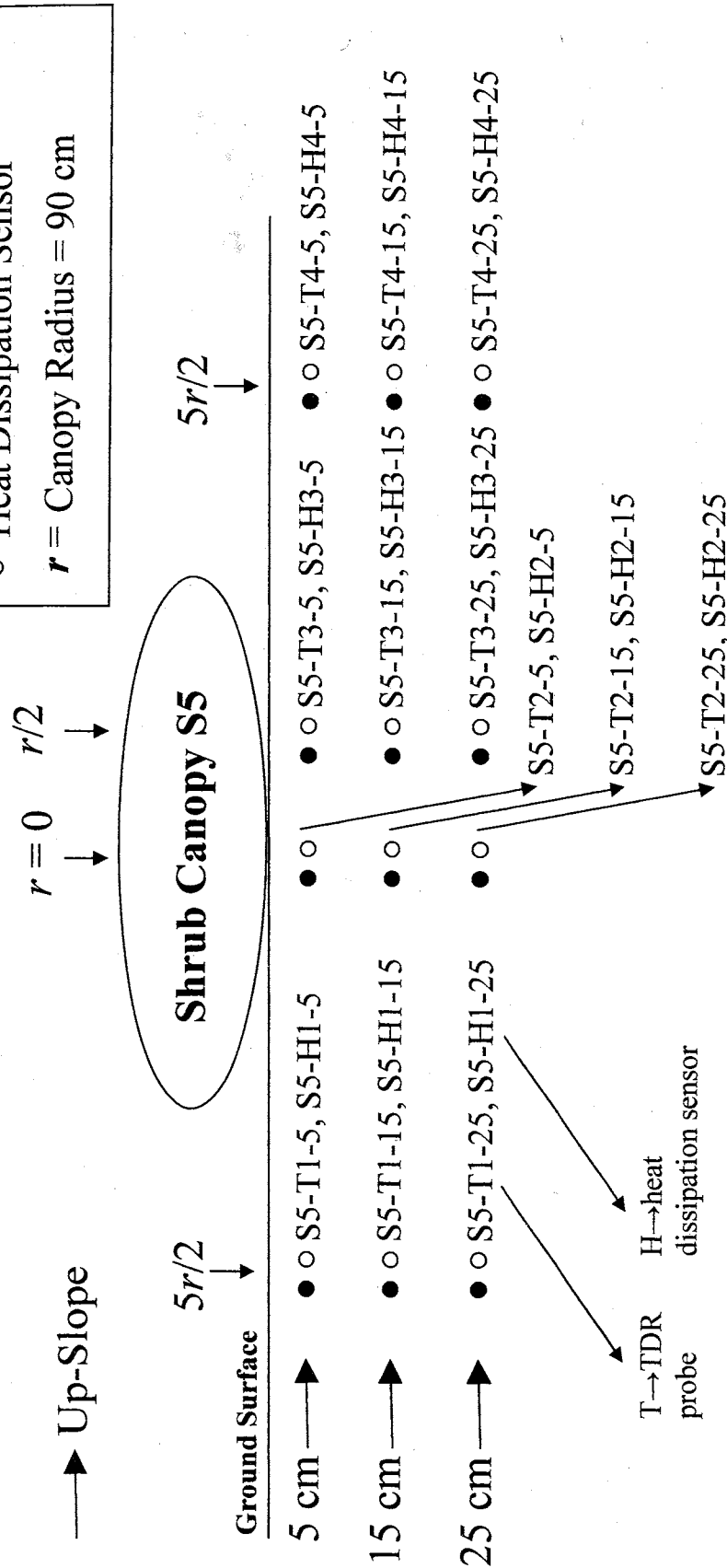


Figure 8: Schematic of shrubland field probe array, with corresponding probe location labels, where volumetric soil-water content and matrix potential are measured along vertical transects. Pairs of three-prong 15 cm TDR probes and heat dissipation sensors are inserted horizontally (**parallel to ground surface**) at 5, 15, and 25 cm depth along each vertical transect. Each probe-sensor pair has a 3 to 5 cm separation distance between instruments. The horizontal spacing between all probes is relative to the individual canopy radius, where  $r = 90 \text{ cm}$ .

# GRASSLAND: CROSS - SECTIONAL VIEW

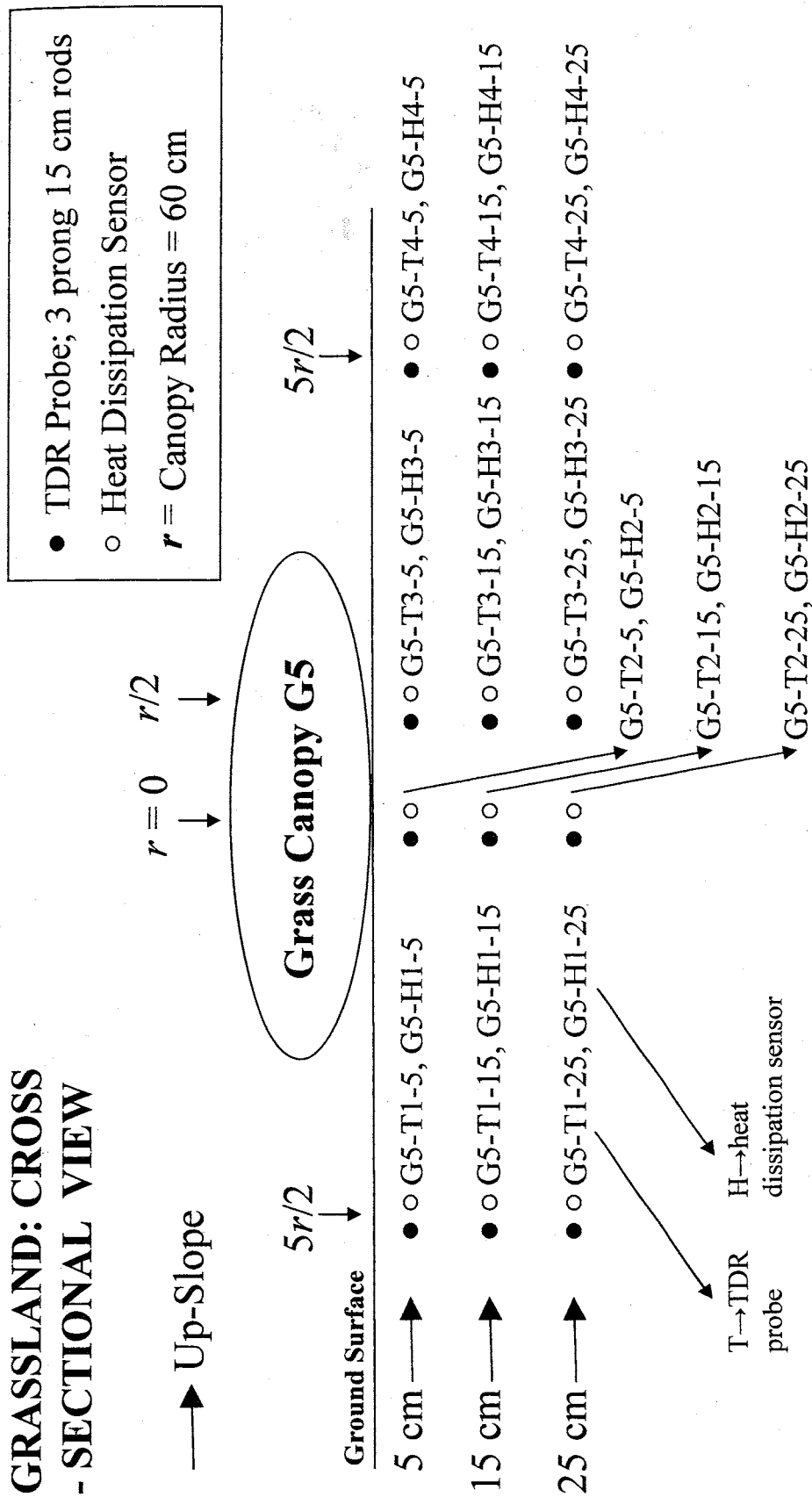


Figure 9: Schematic of grassland field probe array, with corresponding probe location labels, where volumetric soil-water content and matrix potential are measured along vertical transects. Pairs of three-prong 15 cm TDR probes and heat dissipation sensors are inserted horizontally (**parallel to ground surface**) at 5, 15, and 25 cm depth along each vertical transect. Each probe-sensor pair has a 3 to 5 cm separation distance between instruments. The horizontal spacing between all probes is relative to the individual canopy radius, where  $r = 60$  cm.



form on bare soil patches as a result of rainsplash compaction during precipitation. The influence of seals on soil permeability could not be recorded from similar laboratory measurements made on surface soils, discussed in the following section.

It is important to note that the surface soil infiltration measurements measured in the field are different from the saturated hydraulic conductivity of the surface soil layer. Although methods are available for estimation of field saturated hydraulic conductivity using the single ring infiltrometer, e.g., Elrick et al. (1995), our measurements record the effects of three dimensional flow, or soil-water potential gradient driven flow as the wetting front progresses into dry soil below and to the sides of the infiltrometer. Our field measurements would therefore overestimate the actual field saturated hydraulic conductivity. When the saturated hydraulic conductivity of an intact soil sample is measured, traditionally via the constant or falling head method, soil-water flow is gravity driven.

### **3.2. Laboratory Data**

Soil samples were collected from the shrub and grass field sites and their soil hydraulic properties were measured. The primary purpose of these measurements was to establish standards with which to compare the field data to, particularly the soil-water potential measurements. The heat dissipation sensors used in the field provided a relatively new and therefore uncertain means of indirectly measuring soil-water potential. It was necessary to check their measurements with those derived from methods more rigorously tested. We derived such standards via two methods. First, soil hydraulic properties of intact soil column samples were measured using a combination of TDR probes, tensiometers, and thermocouple psychrometers. Second, a particle size analysis

was completed for each soil column sample, the results of which were used in conjunction with a pedotransfer function to estimate soil hydraulic properties. Results from the pedotransfer function provided our most fundamental and confident standards. The details of both methods are explained below.

In order to estimate soil hydraulic properties of intact soil samples, column soil samples were collected at two depth intervals, 0-10 cm and 10-35 cm, at locations characteristic of the four soil cover types, e.g., shrub canopy, grassland bare soil. These locations were selected haphazardly, where we did not consider the influence of slope, microtopography, or canopy and bare soil patch size. The depth intervals were selected to represent the A and B soil horizons, respectively (Kieft et al., 1998). The A horizon, its thickness varying between 5 and 10 cm, is characterized by its high sand content, low calcium carbonate concentration (< 10% dry mass), and loose texture, probably attributed to daily cycles of wetting and drying (nightly condensation and subsequent evaporation). The B horizon, located directly beneath the A horizon, has a more variable thickness due to the spatially varying elevation of a caliche layer that bounds it from below, first appearing at a depth anywhere between ~30 and 100 cm. The B horizon is similar in particle size distribution to the A, however calcium carbonate concentrations are higher, between approximately 20 and 40% by mass, and the soil texture is compact. Soil bulk density differences were not measured in the two horizons. Samples were collected in acrylic columns, each with radial surface area of  $184 \text{ cm}^2$  (inner diameter = 15.3 cm) (Figure 10). A total of four pairs (eight total) of samples were taken.

In the lab, soil columns were saturated through capillary rise and the saturated hydraulic conductivity ( $K_{sat}$ ) of each sample was measured using the constant head method under 5 cm ponded head. Note that we used the  $K_{sat}$  values measured in the laboratory to represent field saturated hydraulic conductivity corresponding to the field soil measurements;  $K_{sat}$  was not measured in the field. We then measured soil  $\theta$  [-] and  $\psi$  [-cm] through a drydown series using three-prong 15 cm TDR probes, tensiometers, and thermocouple psychrometers. Each set of instruments was inserted into the columns at the same height, one set of instruments in the 0 – 10 cm sample at 5 cm depth, and three sets in the 10 – 35 cm sample at 16.5, 22.5, and 29.5 cm depth (Figure 10).

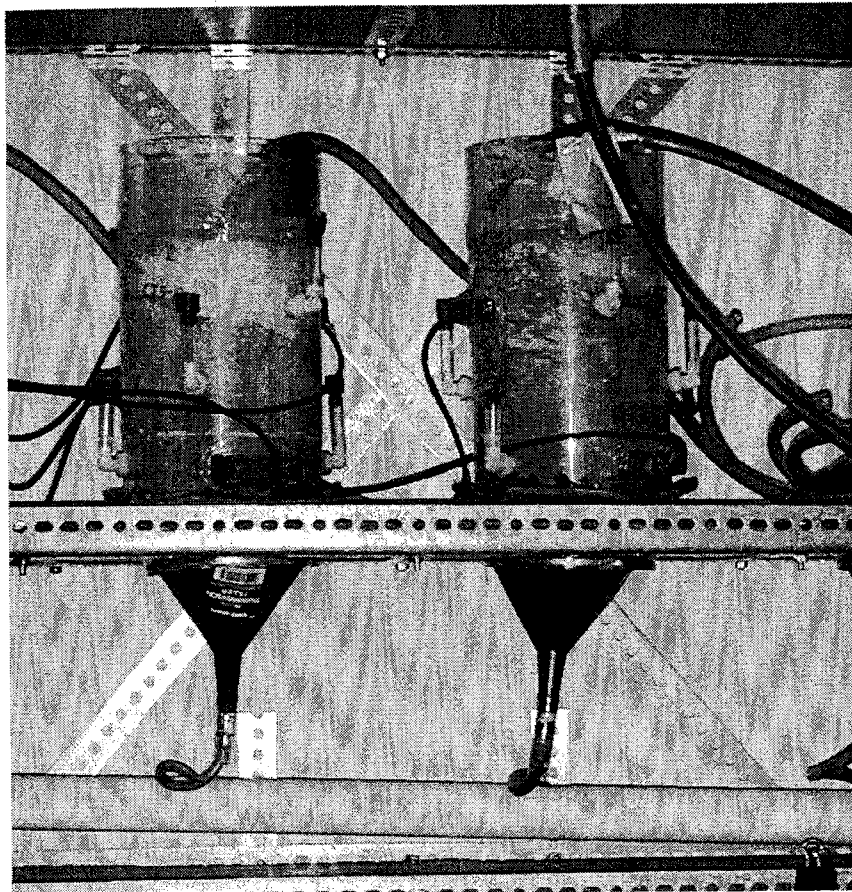


Figure 10: 25 cm acrylic column field soil samples, used to sample soil from 10 – 35 cm depth. At three depths (relative to the column length) of 6.5, 12.5 and 19.5 cm, volumetric soil-water content is measured by 15 cm TDR probes that are horizontally inserted into the column. Soil-water potential is measured by two tensiometers that are inserted adjacent to each TDR probe.

We used tensiometers constructed in the laboratory and Wescor peltier cooled thermocouple psychrometers to measure the soil-matric potential in soil columns. The

use of both instruments was necessary to capture the full range of soil-water potential through a drydown series. The tensiometers sampled a small soil volume of  $\sim 15 \text{ cm}^3$  and were useful to a potential of -600 cm, pressures below which exceeded the air-entry pressure of the ceramic tensiometer cup that was in contact with the soil volume.

At matric potentials greater (more negative) than the tensiometer threshold we used peltier thermocouple psychrometers. Psychrometers estimate soil matric and osmotic (if salts are presents) potential by measuring a temperature differential between fine-wire junctions (thermocouples), both located in the soil medium at thermal and potential equilibrium with the medium. The temperature differential can be expressed as a voltage differential when an electrical current is passed across the junctions. To estimate soil-water potential, one of the junctions (the wet-bulb junction) is cooled to the point of condensation where a water droplet condenses on the junction. Once formed, cooling is then ceased and the droplet re-evaporates at a rate proportional to the relative humidity of the soil medium. As the droplet evaporates, a voltage differential between the wet-bulb and dry-bulb junction is measured. The rate at which the differential voltage measurement decreases is related to a voltage differential calibration factor previously established for each instrument using an aqueous salt solution of known osmotic potential. We found the Wescor psychrometers effective from approximately -100 to -100,000 cm (-0.10 to -10 MPa), although -100,000 cm (-10 MPa) is below the standard range (-50,000 cm; -5 MPa). Regardless, we found that soil-water content decreased less than 1% when  $\psi < -50,000 \text{ cm}$ .

Experimental water retention curves were constructed from the drydown measurements and we used the van Genuchten water retention model to characterize the experimental curves (van Genuchten, 1980). The model has the form

$$S_e = \frac{\theta - \theta_r}{\theta_s - \theta_r} = \frac{1}{[1 + (\alpha h)^n]^m}, \quad m = 1 - \frac{1}{n}, \quad (8)$$

where  $\theta$ ,  $\theta_r$ , and  $\theta_s$  are the measured volumetric water content, residual water content and saturated water content, respectively,  $\alpha$  and  $n$  are fitting parameters, and  $h$  is water potential (in cm). We then characterized the unsaturated hydraulic conductivity of each soil sample using Mualem's model (Mualem, 1976), as simplified by van Genuchten (van Genuchten, 1980), of form

$$K(\theta) = K_s S_e^{1/2} [1 - (1 - S_e^{1/m})^m]^2, \quad (9)$$

where  $K_s$  is the sample saturated hydraulic conductivity. Again, we used these relationships primarily as a check for the field measurements and also to confirm results derived from field measurements.

As a second standard, used for comparison against soil hydraulic properties and relationships derived from field measurements, we constructed water retention and unsaturated hydraulic conductivity curves for each soil sample via an indirect method using a pedotransfer function. After completion of soil drying in the eight column samples, a particle size analysis was performed on each column soil sample in which sand, silt and clay percentages were evaluated. These results were used to estimate the van Genuchten water retention model parameters for each soil sample via the Rosetta Lite v. 1.0 pedotransfer function, a program built into Hydrus 2D, a finite element code used for simulating the movement of water, heat, and multiple solutes in variably

saturated media. Water retention and unsaturated hydraulic conductivity curves were then constructed for each field soil sample using the van Genuchten models.

## 4. Results

### 4.1. Soil Texture and Hydraulic Properties

#### 4.1.1. Soil Particle Size Analysis

Results from the soil particle size analyses, and the corresponding soil hydraulic parameters estimated using the Rosetta Lite v. 1.0 pedotransfer function, provide the most fundamental assessment of the differences in soil hydraulic properties at the field measurement locations. We use these results primarily as a check against field measurements, discussed in section 4.1.2. Further, results based upon the soil column samples (8 total) capture neither spatial nor temporal variability of soil properties, thus their use as data is limited to this basic role.

A percent sand, silt and clay particle size analysis was completed for the column soil samples representative of the four surface cover types, e.g., shrubland bare soil, at two depth intervals, 0 – 10 cm and 10 – 35 cm (see Section 3.2). Results are shown in Table 1. From comparison of results with a texture triangle (Hillel, 1998), all soils are classified as sandy loams, with the exception of the 10 – 35 cm grass canopy sample, classified as a sandy clay loam. The source of the particularly high clay content of this sample, 25.6%, is probably due to spatial variability in soil texture, and is not strictly representative of the sample location. Kieft *et al.* (1998), at a similar Sevilleta grassland field site, found that the average clay percentage beneath grass canopies in a 0 – 20 cm

depth interval was 9.2%, a value that better agrees with results from the other sample locations.

	0 – 10 cm			10 – 35 cm		
	% Sand	% Silt	% Clay	% Sand	% Silt	% Clay
Shrub Canopy	67.7	21.2	11.1	53.8	36.0	10.2
Grass Canopy	79.0	14.3	6.7	47.4	26.0	25.6
Shrub Bare	61.1	23.3	15.6	54.7	34.0	11.3
Grass Bare	56.3	23.7	20.0	67.0	16.1	15.9

Table 1: Field soil particle size. From comparison with a texture triangle (Hillel, 1998), all soils are classified as a sandy loam with the exception of the grass canopy sample at the 10 – 35 cm sample interval (shaded gray) that is classified as a sandy clay loam. Values are derived from soil column samples ( Section 3.2) and represent one cover type location.

We used the Rosetta Lite v. 1.0 pedotransfer function to estimate the van Genuchten parameters  $\alpha$ ,  $n$ ,  $K_{sat}$ ,  $\theta_r$  and  $\theta_s$  for each soil sample (Tables 2 and 3). We then constructed water retention curves (Figures 11 and 12) for each sample using the van Genuchten water retention model discussed above. The data suggests two results. First, the soil hydraulic properties do not appreciably vary between the four sample locations at either depth interval with the exception of the grassland 0 – 10 cm canopy sample. The grassland 0 – 10 cm canopy soil has a particularly high percent sand content (Table 1), therefore its water retention curve shows both the highest (least negative) air-entry pressure (largest  $\alpha$  - parameter, Table 2) and smallest pore size distribution (largest  $n$  - parameter) (Russo, 1988). Appropriately, the water retention curve shows volumetric water contents up to 15% below those of the other samples during the primary dewatering phase of the curve, represented by the segment of steepest slope. At all other sample locations and at both depths, air-entry pressures are similar, indicated by the small range of the  $\alpha$  - parameter (0.011 to 0.040  $\text{cm}^{-1}$ ). Likewise, the small range of the  $n$  - parameter (1.371 to 1.62) indicates a similar width of pore-size distributions for each

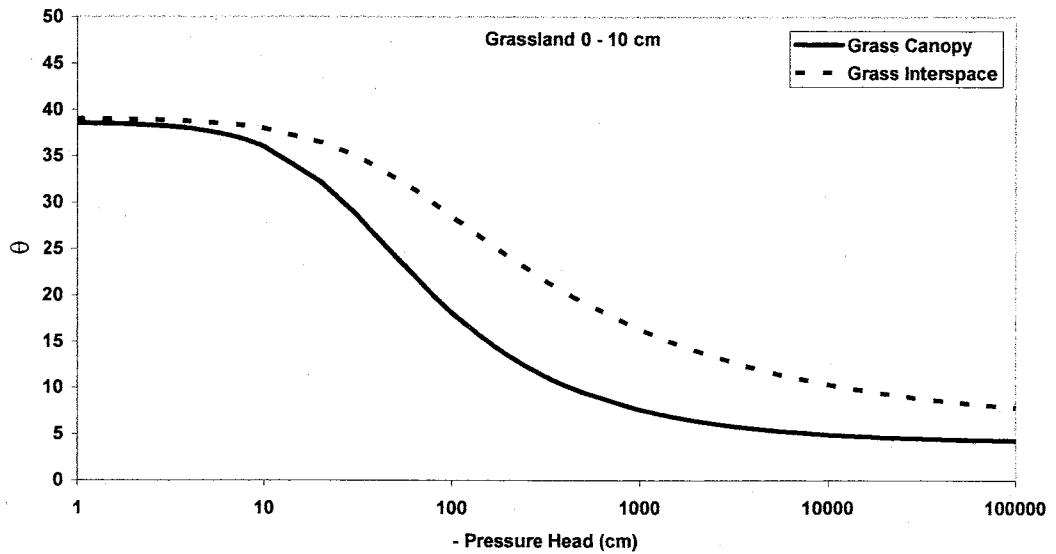
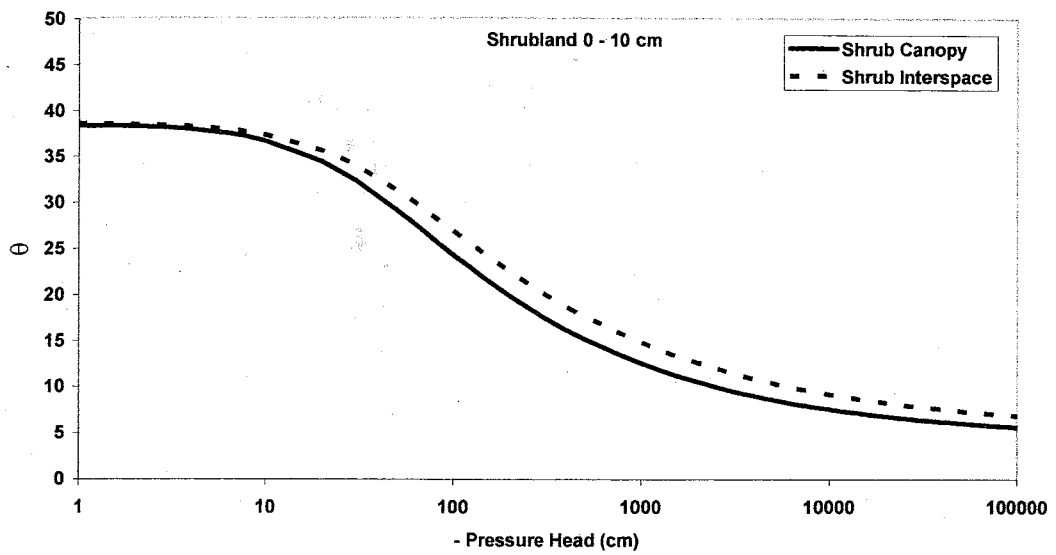


Figure 11: Water retention curves (van Genuchten water retention model) for the four surface cover type soils (e.g., shrub canopy) representative of the surface 0 – 10 cm soil. Model parameters (Tables 2 and 3) were estimated using the Rosetta Lite v. 1.0 pedotransfer function in conjunction with field soil particle size analyses (percent sand, silt, clay; Table 1) completed for the 0 – 10 cm column soil samples (Section 3.2). All water retention curves represent one field sample location.



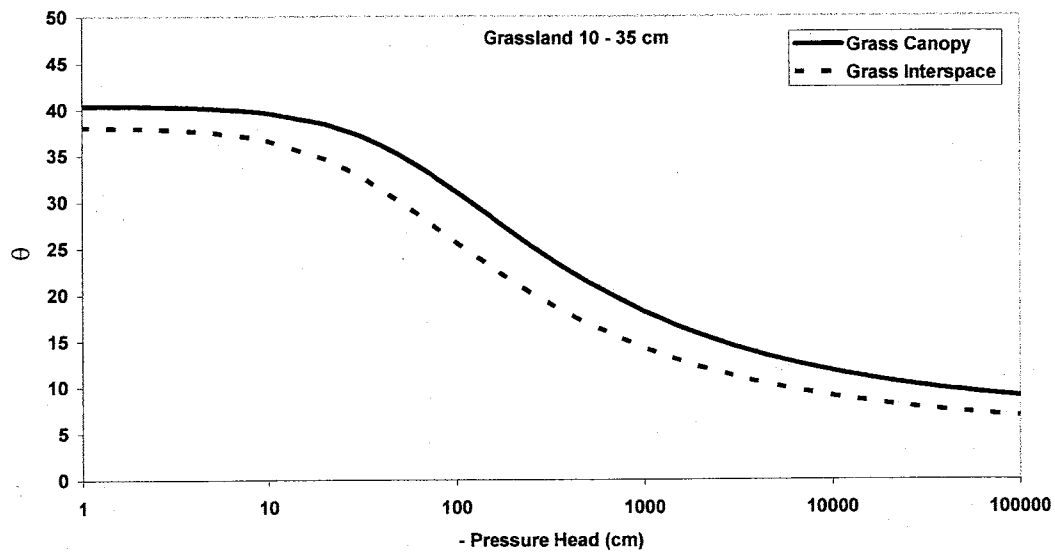
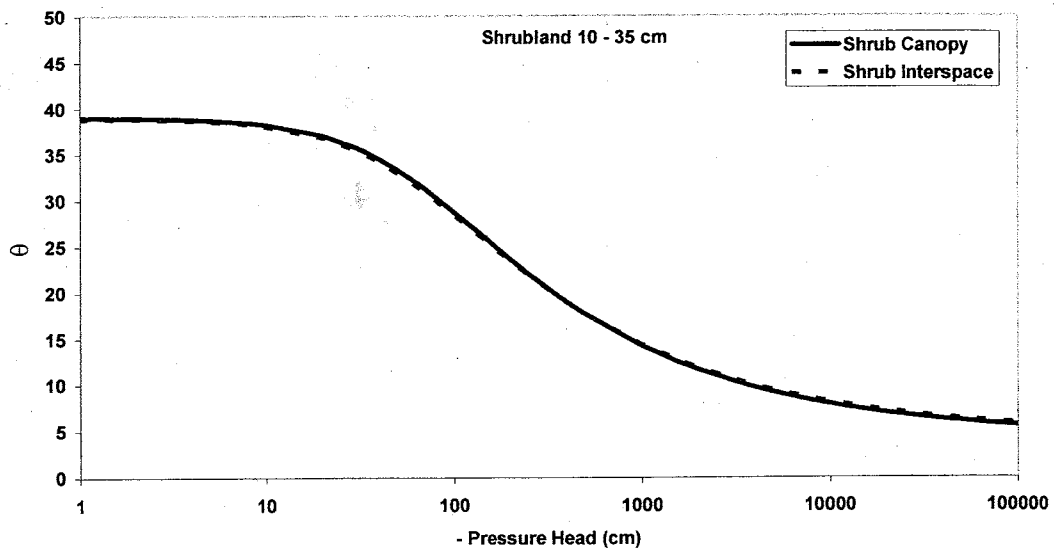


Figure 12: Water retention curves (van Genuchten water retention model) for the four surface cover type soils (e.g., shrub canopy) representative of the surface 10 – 35 cm soil. Model parameters (Tables 2 and 3) were estimated using the Rosetta Lite v. 1.0 pedotransfer function in conjunction with field soil particle size analyses (percent sand, silt, clay; Table 1) completed for the 10 – 35 cm column soil samples (Section 3.2). All water retention curves represent one field sample location.

sample. We observe these results with prudence however, as the particle size analyses and subsequent use of the pedotransfer function do not capture the actual soil/pore structure of the soil medium. The air-entry pressure of the soil samples that would be measured from a sample that has retained its in situ pore structure, controlled by the largest soil pores, is not represented in these results.

A second result from the soil texture analysis is that the soil hydraulic properties at different locations are more similar in the 10 – 35 cm interval. The ranges of the  $\alpha$  and  $n$  – parameters is smaller in the lower depth interval, which is visually apparent in a comparison of water retention curves representing the two depth intervals. This result would indicate that soil hydraulic properties may have a greater influence in the redistribution of soil water in soils nearer to the surface, and less so with depth. This result is discussed further in the following section.

	Soil Type	$\theta_r$ [%]	$\theta_s$ [%]	Air-entry pressure [cm]	$\alpha$ [cm <sup>-1</sup> ]	Dewateri- ng slope [ $d\theta/d\psi$ ]	$n$ [-]
Particle Size Analysis	Shrub Canopy	4.39	38.47	-10	0.0327	-0.08	1.4081
	Grass Canopy	4.09	38.66	-10	0.0407	-0.16	1.6154
	Shrub Bare	5.19	38.63	-10	0.0264	-0.07	1.3807
	Grass Bare	5.98	39.08	-20	0.0231	-0.04	1.3706
Soil Column (Laboratory) Analysis	Shrub Canopy	8.25	44.54	-30	0.0142	-0.30	3.5357
	Grass Canopy	9.80	44.42	-40	0.0106	-0.33	4.0000
	Shrub Bare	10.75	42.23	-20	0.0113	-0.21	3.1702
	Grass Bare	7.08	43.00	-10	0.0194	-0.16	1.9334
Field Analysis	Shrub Stem	4.93	36.41	> -10	0.0583	-0.07	1.3506
	Shrub Canopy	3.88	40.42	-10	0.0177	-0.12	1.9336
	Grass Canopy	4.84	43.23	-10	0.0332	-0.21	1.9480
	Shrub Bare	3.37	39.85	-30	0.0105	-0.11	1.9445
	Grass Bare	3.56	44.98	-10	0.0243	-0.19	1.9868

Table 2: van Genuchten water retention model parameters. Soil column results are derived from soil-volume measurements that represent the surface 0 – 10 cm soil interval. Field measurements are derived from individual pairs of TDR probes and heat dissipation sensors at 5 cm at a given location, i.e., one cover type location is represented. Dewatering slopes are representative of soil matric potential between -50 and -500 cm.

	Soil Type	$\theta_r$ [%]	$\theta_s$ [%]	Air-entry pressure [cm]	$\alpha$ [cm <sup>-1</sup> ]	Dewater- ing slope [ $d\theta/d\psi$ ]	$n$ [-]
Particle Size Analysis	Shrub Canopy	4.26	39.01	-20	0.0172	-0.06	1.4369
	Grass Canopy	7.00	40.43	-10	0.0186	-0.03	1.3734
	Shrub Bare	4.44	38.91	-20	0.0184	-0.06	1.4272
	Grass Bare	5.29	38.15	-30	0.0308	-0.05	1.3801
Soil Column (Laboratory) Analysis	Shrub Canopy	8.33	40.21	-10	0.0259	-0.17	2.1573
	Grass Canopy	10.75	43.70	-10	0.0212	-0.16	2.4217
	Shrub Bare	8.84	42.46	-10	0.0179	-0.15	2.1370
	Grass Bare	7.08	37.63	-10	0.0174	-0.15	2.1663
Field Analysis	Shrub Stem	6.82	40.21	-5	0.039	-0.07	1.424
	Shrub Canopy	6.89	40.21	-20	0.014	-0.05	1.565
	Grass Canopy	8.97	40.70	-10	0.038	-0.06	1.531
	Shrub Bare	8.34	42.46	-20	0.022	-0.08	1.570
	Grass Bare	8.97	40.62	-20	0.015	-0.11	1.992

Table 3: van Genuchten water retention model parameters. van Genuchten water retention model parameters. Soil column results are derived from soil-volume measurements that represent the surface 10 – 35 cm soil interval. Field measurements are derived from individual pairs of TDR probes and heat dissipation sensors at 15 cm at a given location, i.e., one cover type location is represented. Dewatering slopes are representative of soil matric potential between -50 and -500 cm.

Note again that we use the soil particle size analyses and pedotransfer function results as a general introduction to the texture and hydraulic properties of the soil types observed in this study. Due to the indirect nature of the other methods that we use to measure soil hydraulic properties, and to the general difficulty encountered when measuring any soil hydraulic property, results from particle size analyses and the pedotransfer function serve as a standard that we refer back to throughout this study.

#### 4.1.2. Field Results

Figures 13 and 14 show water retention curves constructed from field measurements of volumetric soil-water content and matric potential made at both 5 cm and 15 cm depth, as discussed in section 3.1. Each water retention curves is constructed from the measurements of individual pairs of three-prong 15 cm TDR probes and heat

dissipation sensors, therefore one canopy and adjacent bare soil patch in each ecosystem are represented. In addition to constructing water retention curves representative of soils beneath the four cover-types (previously defined), these were constructed for soil samples adjacent to the shrub stem at 5 and 15 cm depth as well. In the shrubland, at 5 cm depth we use the pairs (TDR probe : heat dissipation sensor) S5-T2-5:S5-H3-5 beneath stem, S5-T3-5:S5-H3-5 beneath canopy, and S5-T4-5:S5-H4-5 beneath bare soil (Figure 8). At 15 cm depth, we use the pairs S5-T2-15:S5-H2-15 beneath stem, S5-T3-15:S5-H3-15 beneath canopy, and S5-T4-15:S5-H4-15 beneath bare soil. In the grassland, we use pairs of TDR probes and heat dissipation sensors at exactly the same respective locations as in the shrubland (Figure 9). The van Genuchten water retention model was subsequently used to characterize the experimental curves.

At 5 cm depth, there is little difference between water retention curves for the four representative soil cover types (Table 2); this excludes measurements made adjacent to the shrub stem. Saturated and residual water contents range from 40 to 45% and 3 to 5%, respectively. Air-entry pressures range from -10 to -30 cm, a relatively small range. The slopes ( $d\theta / d\psi$ ) of the primary dewatering phase for each sample, represented by the water retention curve section of steepest slope (corresponding to matric potentials between -50 and -500 cm), vary by only  $0.10 \text{ cm}^{-1}$ , a small difference as confirmed by  $n$ , which varies from 1.934 to 1.986. Such observations imply a definite similarity in the magnitude and spread of the pore size distribution between the measurement locations. With respect to estimated values of  $\alpha$  and  $n$ , the soil samples fall between the classifications of a sandy loam and silt (Table 2) and are consistent with particle size analyses.

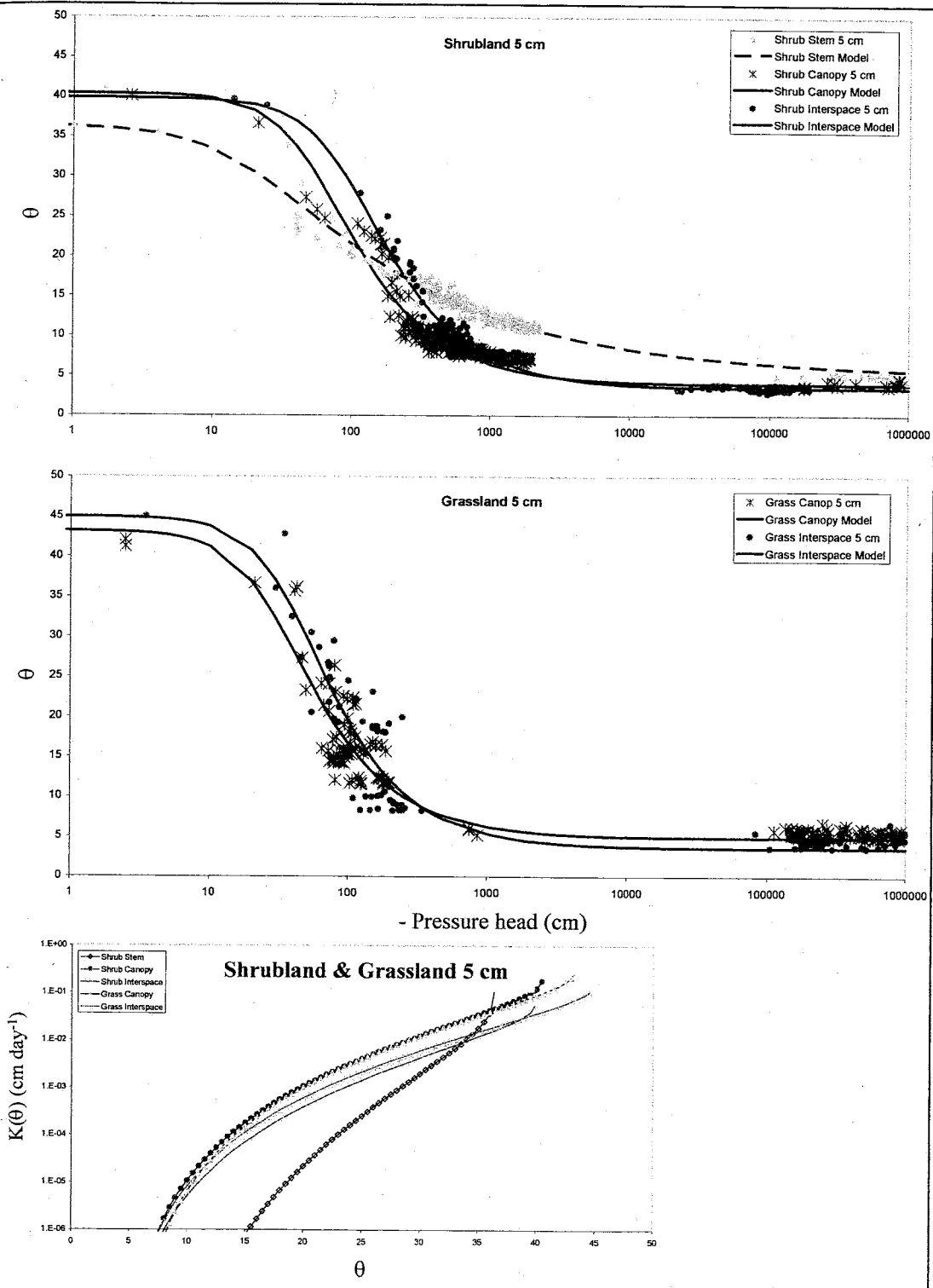


Figure 13: Water retention and  $K(\theta)$  (bottom) curves representative of the five surface cover type soils (including shrub stem). The data corresponds to field measurements of soil-water content and matric potential measured at one location using adjacently placed TDR probes and heat dissipation sensors, respectively, at 5 cm depth (see Section 4.1.2 and Figures 8 and 9). The van Genuchten water retention and unsaturated hydraulic conductivity model is used to fit the experimental data. Corresponding model parameters are shown in Tables 2 and 3.

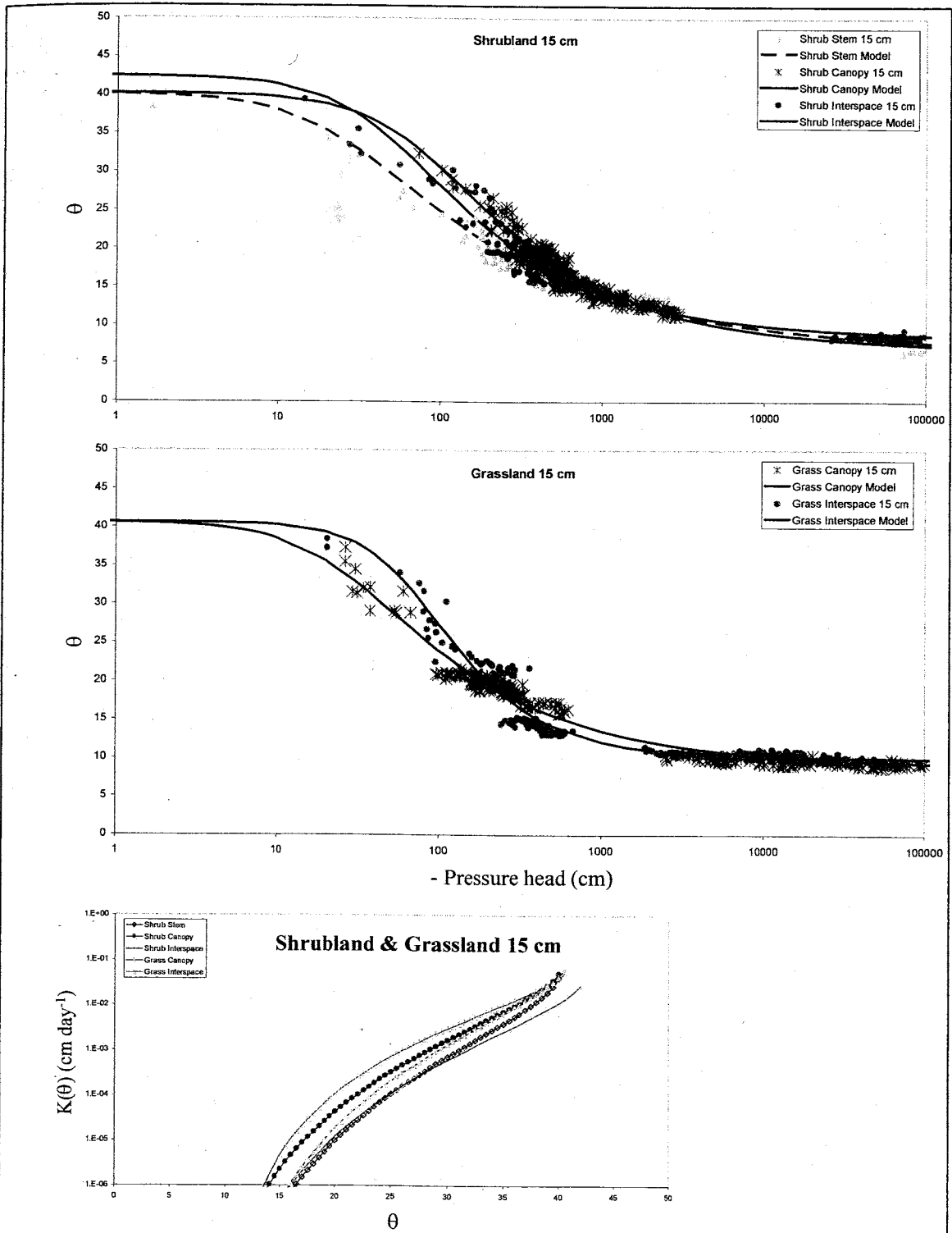


Figure 14: Water retention and  $K(\theta)$  (bottom) curves representative of the five surface cover type soils (including shrub stem). The data corresponds to field measurements of soil-water content and matric potential measured at one location using adjacently placed TDR probes and heat dissipation sensors, respectively, at 15 cm depth (see Section 4.1.2 and Figures 8 and 9). The van Genuchten water retention and unsaturated hydraulic conductivity model is used to fit the experimental data. Corresponding model parameters are shown in Tables 2 and 3.

Notably dissimilar, however, is the water retention curve representative of the soil sample at the shrub stem, the greatest differences being the lower saturated water content (36%), the higher air-entry pressure (-5 cm) and the low slope ( $n = 1.350$ ) of the primary dewatering phase. Again, with respect to estimated values of  $\alpha$  and  $n$ , the shrub stem soil sample can be approximately classified as a sandy loam (Table 2).

Such contrasts are more perceptible in the corresponding unsaturated hydraulic conductivity profiles (Figure 13). All soil samples with the exception of the shrub stem display approximately equivalent  $K(\theta)$  relationships, values falling within the same order of magnitude at a given water content. The shrub canopy sample maintains the highest  $K(\theta)$  for all  $\theta$ , the shrub interspace the lowest  $K(\theta)$ , and the grass canopy and interspace sample conductivities overlap each other, falling between the shrub canopy and interspace curves.  $K(\theta)$  for the shrub stem soil sample falls within three orders of magnitude below those of the four other soil samples at low  $\theta$ . As  $\theta$  increases, the stem soil conductivity rapidly approaches and surpasses those of the other samples when  $33\% < \theta < 36\%$ . Although the saturated hydraulic conductivity is not greatest at the stem (the grass and shrub canopy soils retain higher  $K_{sat}$  values (Table 4)), the stem soil sample is saturated at a soil-water content 5-10% less than those of the other samples. Less soil-water is therefore required to attain saturated hydraulic conductivity beneath the stem. This result seems appropriate given the wide pore-size distribution beneath the shrub stem, as indicated by the van Genuchten parameter  $n$  (Table 2), and is a likely result of large pores surrounding shrub stems. The reader may however note that large pores, and possibly macropores, surrounding the shrub stem would suggest a higher saturated hydraulic conductivity measured at the stem rather than at an adjacent canopy soil.

Remember now that we used  $K_{sat}$  measured in the laboratory (presented further below) to represent that of the field soils. It is proposed that reconfiguration of the soil matrix structure and closure of larger pores during the field sampling method is the source of the contradiction.

	$\theta_r$ [ - ]	$\theta_s$ [ - ]	$\alpha$ [ $\text{cm}^{-1}$ ]	$n$ [ - ]
Sand	0.045	0.43	0.145	2.68
Sandy Loam	0.065	0.41	0.075	1.89
Silt	0.034	0.46	0.016	1.37
Sandy Clay	0.10	0.38	0.027	1.23
Clay	0.68	0.38	0.008	1.09

Table 4: van Genuchten water retention model parameters for five soil classes derived from standards defined in the Rosetta Lite v. 1.0 pedotransfer function.

At the deeper sampling location, 15 cm, differences between soil hydraulic properties between sample locations become less apparent. Water retention curves representative of each sample interval are shown in Figure 14 and a description of hydraulic parameters in Table 3. With few exceptions, all sample locations, including that beneath the shrub stem, display approximately equivalent residual and saturated water contents, air-entry pressures and pore-size distributions. The exception, however, is that the air-entry pressure beneath the shrub stem remains higher (less negative) than for the other sample locations, again a likely result of large pores. Although the stem location does appropriately imply the widest pore-size distribution (Table 3), at this depth the other sample locations also display large pore-size distributions, with the exception of the sample beneath the grass interspace. Such broadening of distributions is probably due to the presence of finer grains (e.g., clays) that result from weathering.



In summary, soil texture and hydraulic properties are more uniform at 15 cm than at 5 cm. A similar result was concluded from the particle size analyses. Differences apparent at the surface become less so at 15 cm depth, implying that observed differences in water availability to plants that result from soil hydraulic properties are probably controlled by differences in the surface soils.

It is important to note here that spatial variability of soil texture and hydraulic properties is not investigated. Results are based upon measurements of soil samples at individual locations, thus it is possible that observed differences are a result of spatial variability that overwhelm the influence of location and canopy cover. Two lines of reasoning, however, suggest that this is not the case. First, the abovementioned results derived from soil particle size analyses and field measurements correspond well, which is unlikely if measurements are controlled by spatial variability, and therefore by some component of randomness, alone. Second, at the 5 Points Sevilleta location, Kieft et al. (1998) found that differences in soil texture from 0 – 20 cm beneath canopies and bare soil were often significantly different ( $P < 0.05$ ) in shrubland but never different in grassland. Therefore, differences in soil texture, and therefore soil hydraulic properties, are not likely controlled by spatial variability in the shrubland. However, spatial variability of soil properties in the grassland may have had a greater influence on our measurements due to the similarity of canopy and interspace soils.

In the field, we also measured surface soil infiltration rates using single ring infiltrometers under a constant ponded head of 10 cm, the rings inserted to 5 cm depth. Five measurements were recorded beneath each of the four surface soil cover types, e.g, grassland bare soil, shrub canopy. Infiltration rates were not measured at shrub stems

because of physical impracticalities in placing the infiltrometer around the stem.

Infiltration rates are shown in Table 5. Bare soil infiltration rates are 2 to 4 times lower than their respective canopy soil infiltration rates, with standard deviations at all locations approximately equal. The difference in grassland and shrubland is attributed to thin soil crusts (soil seals), on the order of millimeters thick, that form principally on bare soil surfaces in both ecosystems. Soil seal formation is a result of rainsplash compaction during precipitation, thus above-ground shading from plant canopies protects sub-canopy soils from forming seals. The influence of bare soil crust formation on the redistribution of precipitation as surface water is later discussed.

		Shrub Stem	Shrub Canopy	Grass Canopy	Shrub Bare	Grass Bare
Lab 0 – 10 cm	<b>Mean</b>	$1.30 \times 10^{-1}$	$1.91 \times 10^{-1}$	$2.77 \times 10^{-1}$	$8.07 \times 10^{-2}$	$1.01 \times 10^{-1}$
	<b>Stdev</b>	$1.03 \times 10^{-2}$	$5.76 \times 10^{-2}$	$5.02 \times 10^{-2}$	$2.53 \times 10^{-2}$	$1.72 \times 10^{-2}$
Lab 10 – 35 cm	<b>Mean</b>	---	$8.77 \times 10^{-2}$	$1.14 \times 10^{-2}$	$5.67 \times 10^{-2}$	$6.32 \times 10^{-2}$
	<b>Stdev</b>	---	$2.98 \times 10^{-3}$	$6.98 \times 10^{-3}$	$2.63 \times 10^{-3}$	$1.44 \times 10^{-3}$
Field 0 – 5 cm	<b>Mean</b>	---	$5.96 \times 10^{-1}$	$5.81 \times 10^{-1}$	$1.50 \times 10^{-1}$	$2.76 \times 10^{-1}$
	<b>Stdev</b>	---	$1.27 \times 10^{-1}$	$1.07 \times 10^{-1}$	$6.12 \times 10^{-2}$	$9.29 \times 10^{-2}$

Table 5: Effective saturated hydraulic conductivity [ $\text{cm min}^{-1}$ ] measured in the lab (constant head method) and infiltration rates measured in the field (single ring infiltrometer). Lab measurements were conducted using one soil column sample (Section 3.2) per representative area; five (5) conductivity measurements were completed per sample. Field results represent measurements made at five (5) different locations for each of the soil cover types. Both sets of measurements use cylinders of surface area  $122.72 \text{ cm}^2$  ( $183.85 \text{ cm}^2$  for the shrub stem sample).

#### 4.1.3. Laboratory Results

Similar to results based upon soil texture and particle size discussed in 4.1.1, soil hydraulic properties measured in the laboratory are primarily used as standards against which we check field measurements. The following results are from soil-water potential and water content measurements made in the intact soil column samples (0 – 10 cm, 10 –

35 cm) collected at the field sites (Section 3.2). The following results therefore represent one plant canopy and adjacent bare soil patch in each ecosystem. As discussed above, the column samples were saturated through capillary rise in the laboratory, and the hydraulic measurements were subsequently recorded during one soil dry-down series.

We first consider soil samples representative of the surface 0 – 10 cm interval. Figure 15 shows water retention curves for these surface samples. The saturated water content (42 – 45%) and air-entry pressure are approximately equal for all soils (-20 – -40 cm). At matric potentials below (more negative than) the air-entry pressure, the slope ( $d\theta/d\psi$ ) of the primary dewatering phase is greater in magnitude in canopy than interspace soil samples, indicating smaller pore size distributions. This is appropriate for the given differences in particle size (Table 1), the canopy soils having greater and smaller percentages of sand and clay, respectively, than bare soil. In each sample, actual residual water contents of 2-3%, as observed in the field, are not reached due to the controlled conditions in the laboratory. Drying to such a degree indoors would take months.

Due to a soil-columns inability to achieve a residual water content that would be observed under field conditions (2-3%), we observe irregularly high values of the van Genuchten water retention fitting parameter  $\theta_r$  (Tables 3). The high values have an ensuing affect on estimation of the van Genuchten water retention parameters  $\alpha$  and  $n$ ; there are less data points available to constrain estimates of  $\alpha$  and  $n$ , predominantly at the low (more negative) matric potential end. Values of  $\alpha$  range from 0.0113 to 0.0194  $\text{cm}^{-1}$ , indicative of silts. Values of  $n$  range from 1.93 to 4.00, indicative of a sandy loam or sand. In addition to such a contradiction, a typical  $n$ -parameter value for a sand is 2.68,

well below the maximum value of  $n = 4.00$  estimated from the grass canopy column sample. We therefore use results concerning soil hydraulic parameters inferred from soil column analyses with careful consideration in later discussions.

Unsaturated hydraulic conductivity ( $K(\theta)$ ) is shown in Figure 15. The van Genuchten parameters (Table 3) and saturated hydraulic conductivities (Table 5) were used for these calculations. Soil samples beneath both shrub and grass canopies display nearly identical relationships between  $\theta$  and  $K(\theta)$ .  $K(\theta)$  for the interspace soils predominantly fall within 3 orders of magnitude below those of soils representative of the canopies. Under dry conditions, 5 – 15% water content,  $K(\theta)$  for the shrub interspace sample is one-to-two orders of magnitude greater than for the grass interspace. As the interspace soil-water content increases, this difference decreases, until at  $\theta \approx 35\%$  the conductivity curves intersect. As conditions tend toward saturation, the grass interspace conductivity increases at a greater rate than that for the shrub sample, until at saturation the grass interspace conductivity equals that of the canopies. Under the Green-Ampt assumption of equivalent vertical potential gradients across the wetting front, surface infiltration beneath grass interspaces, grass canopies and shrub canopies would therefore become equal at field saturation.

At the deeper sample interval, 10 – 35 cm, soil hydraulic properties differ less than those between the overlying soils (Table 3). Figure 16 shows soil-water retention curves representative of these sample locations. The air-entry pressure at each location is  $\sim -10$  cm, and corresponding  $\alpha$  – parameters suggest soil-textural classifications between a silt and sandy loam. Upon drying from a saturated state, the rate of primary pore dewatering, again represented by the steepest section of the water-retention slope

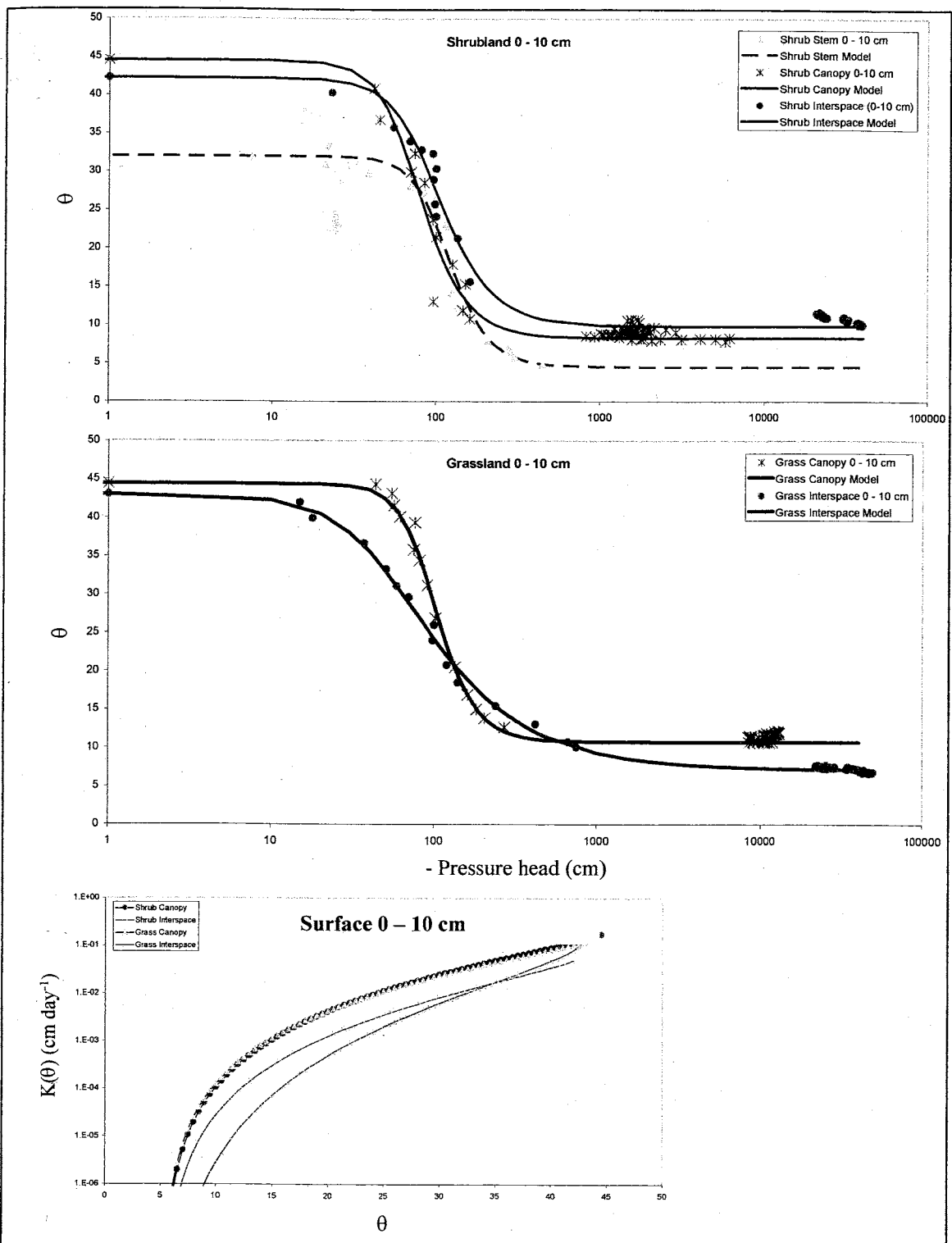


Figure 15: Water retention and  $K(\theta)$  (bottom) curves representative of the four surface cover type soils. Measurements correspond to soil-water content (TDR) and matric potential (tensiometer) measured in the 0 – 10 cm soil column samples (see Section 3.2) during one soil dry-down from saturation. Each curve represents one field sample location. The van Genuchten water retention and unsaturated hydraulic conductivity model is used to fit the experimental data, and corresponding model parameters are shown in Tables 2 and 3.

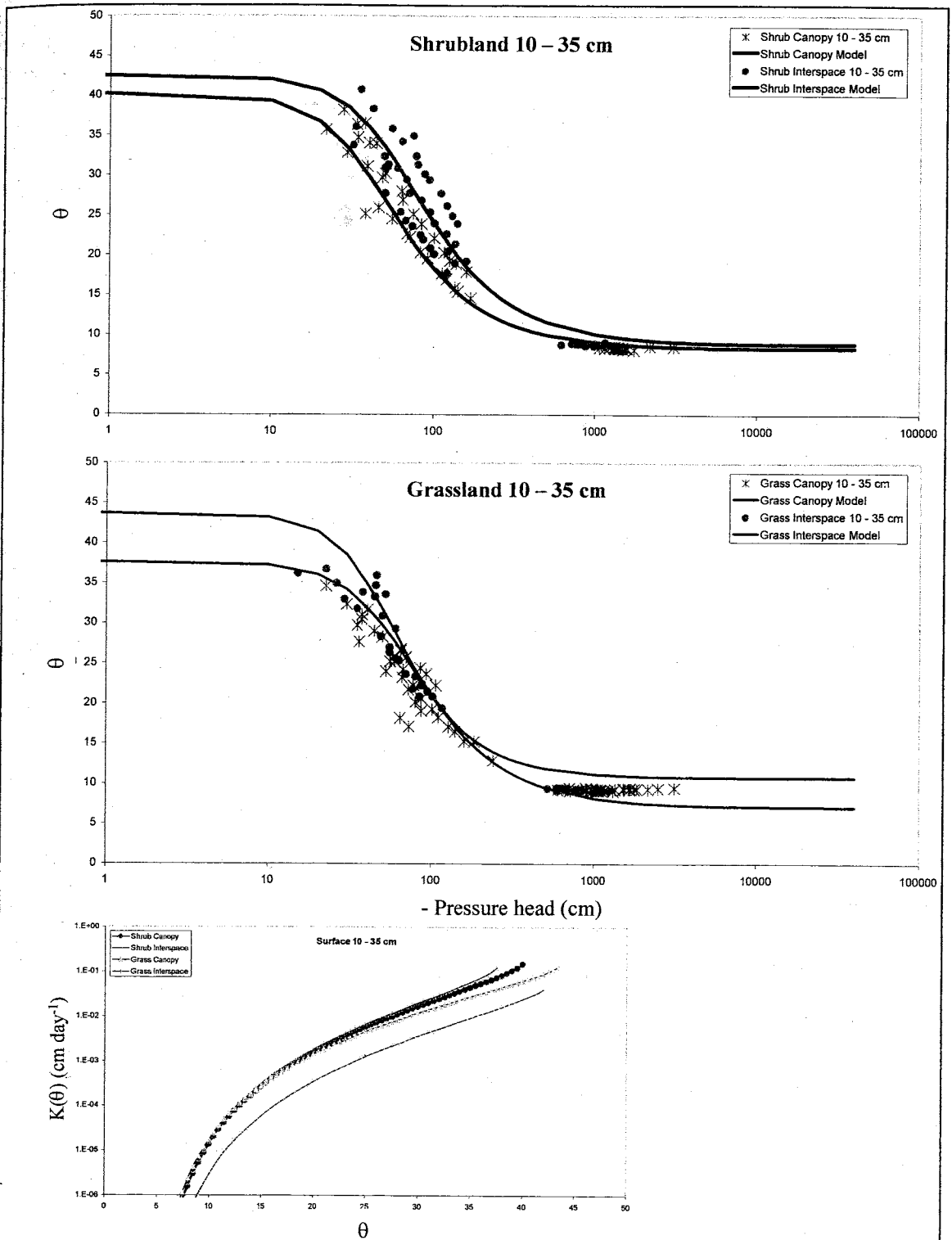


Figure 16: Water retention and  $K(\theta)$  (bottom) curves representative of the four surface cover type soils. Measurements correspond to soil-water content (TDR) and matric potential (tensiometer) measured in the 10 - 35 cm soil column samples (see Section 3.2) during one soil dry-down from saturation. Each curve represents one field sample location. The van Genuchten water retention and unsaturated hydraulic conductivity model is used to fit the experimental data, and corresponding model parameters are shown in Tables 2 and 3.

(corresponding to matric potentials between -50 and -500 cm), ranges from  $d\theta / d\psi = -0.21$  to  $-0.29$ . Such relatively large slopes agree well with corresponding  $n$ -parameter values that have a range from 2.14 to 2.42, indicating sandy loam or sand soil-texture classifications. Similarly, the residual water content is first reached at a matric potential of  $\sim -1000$  cm in all samples. All such observations imply consistent distributions of grain and pore-size throughout the different sampling locations, and are consistent with particle size analysis results (Table 1), with the exception of the grass canopy sample that has a particularly high clay content.

In summary, when we compare the vertically adjacent soil samples at a given location, the principal difference observed involves the width of the soil pore size distribution between samples. The distribution size is related to the slope of the primary soil dewatering interval of the water retention curve, steeper slopes representing smaller distributions. When we measure this slope between -50 and -500 cm matric potential, surface (0 – 10 cm) canopy soils have a slope with magnitude greater than two times that observed in any other soil sample. For example, during soil drydown following saturation, for every cm that matric potential decreases in this range, volumetric soil-water content decreases 0.33% in the grass canopy sample and 0.16% in the grass interspace soil. Such results indicate a less compacted soil structure and/or a larger average pore size in canopy surface soils. On the contrary, the water retention slopes during the primary dewatering phase for the surface interspace soils and all 10 – 35 cm soil samples are approximately equal. The ability of these soils to retain soil-water at more negative soil-water potentials is probably a result of the smaller mean particle size and high (relative to surface canopy soil) clay percentage (Table 1).

In following discussions, however, we do not focus on results derived from the soil column analyses in the lab, but focus on field results. The aforementioned contradiction between van Genuchten parameters within individual column samples indicate that results derived from the soil columns have error, error that was not quantified.

## 4.2. Water Availability

In this section we address the water availability to plants through observation of infiltration during precipitation and subsequent redistribution. By water availability, we mean the occurrence of liquid soil-water flow and neglect periods of vapor dominated flow. Bhark and Small (Appendix 1) showed that under dry conditions, defined as periods without precipitation for more than two weeks, the average near surface (0 – 5 cm) volumetric soil-water content over all locations is  $2.4 \pm 0.6\%$ . At this residual soil-water content, soil-water transport is dominated by vapor flow; we assume liquid flow negligible. Although soil-water remains available to plants up to  $\psi = -8.0$  MPa, substantial liquid soil-water flow does not occur when  $\psi < \sim -1.0$  MPa, a subject later discussed. The question of water availability to plants becomes one governed by a different hydrologic flow system as well as by plant physiology. We therefore ignore time periods of vapor dominated soil-water flow and focus on periods during and directly following (on the order of hours) precipitation.

### 4.2.1. *Volumetric Soil-Water Content beneath Canopies and Interspaces*

In Figure 17 we show time series of volumetric soil-water content measured beneath one shrub stem, canopy, and bare soil patch along one transect, therefore sampling one canopy, S5 (Figure 6). Measurements at each location were recorded



hourly at 5, 15, and 25 cm depth. Beneath the stem, we used TDR probes S5-T2-5, 15, 25 at 5, 15, and 25 cm, respectively (Figure 8). Beneath the canopy, we used TDR probes S5-T3-5, 15, 25, and beneath bare soil we used TDR probes S5-T4-5, 15, 25.

Beneath the stem, there is an immediate sharp response in soil moisture to precipitation events. Such responses occur at all measurement depths with the exception of 25 cm when precipitation is less than ~6 mm. The magnitude of the response usually decreases with depth. In the exceptional case where the soil at 15 cm is wetter than at 5 cm during precipitation, e.g., day 228, this can be attributed to soil-water accumulation near 15 cm, probably due to soil-texture differences. Beneath the shrub canopy (not stem), patterns of infiltration during precipitation are similar to those beneath the stem with the exception of wetting at 25 cm. Following no storm event is a wetting front observed at 25 cm depth. Beneath the shrub interspace, the soil moisture response to precipitation is even less pronounced than beneath the canopy. Only following large storms, greater than ~10 mm, does wetting reach 15 cm depth, and at no time does the wetting front reach 25 cm depth.

Figure 17 shows plots of the difference in soil-water content between the shrub stem and interspace, and between the shrub canopy and interspace, at three depths. Following all precipitation events, the difference is typically positive at all depths, where the canopy soil is up to 25% wetter than the interspace soil. The difference is clearly greater between stem and interspace than between canopy and interspace. As the soils dry to residual values, the differential water contents at all locations have a range of  $\pm 3\%$ , a negligible difference given a TDR probe error of  $\pm 3\%$ .

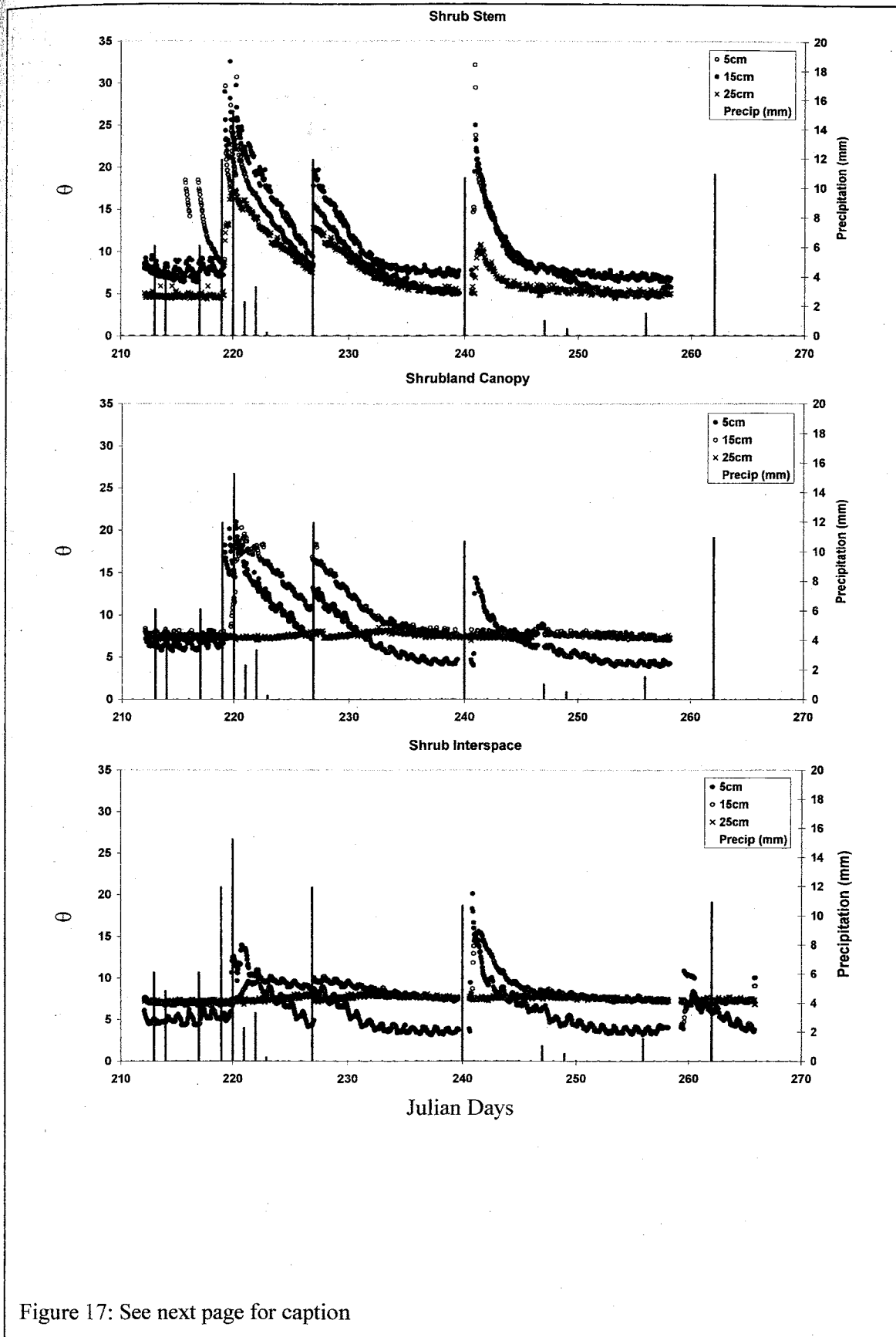
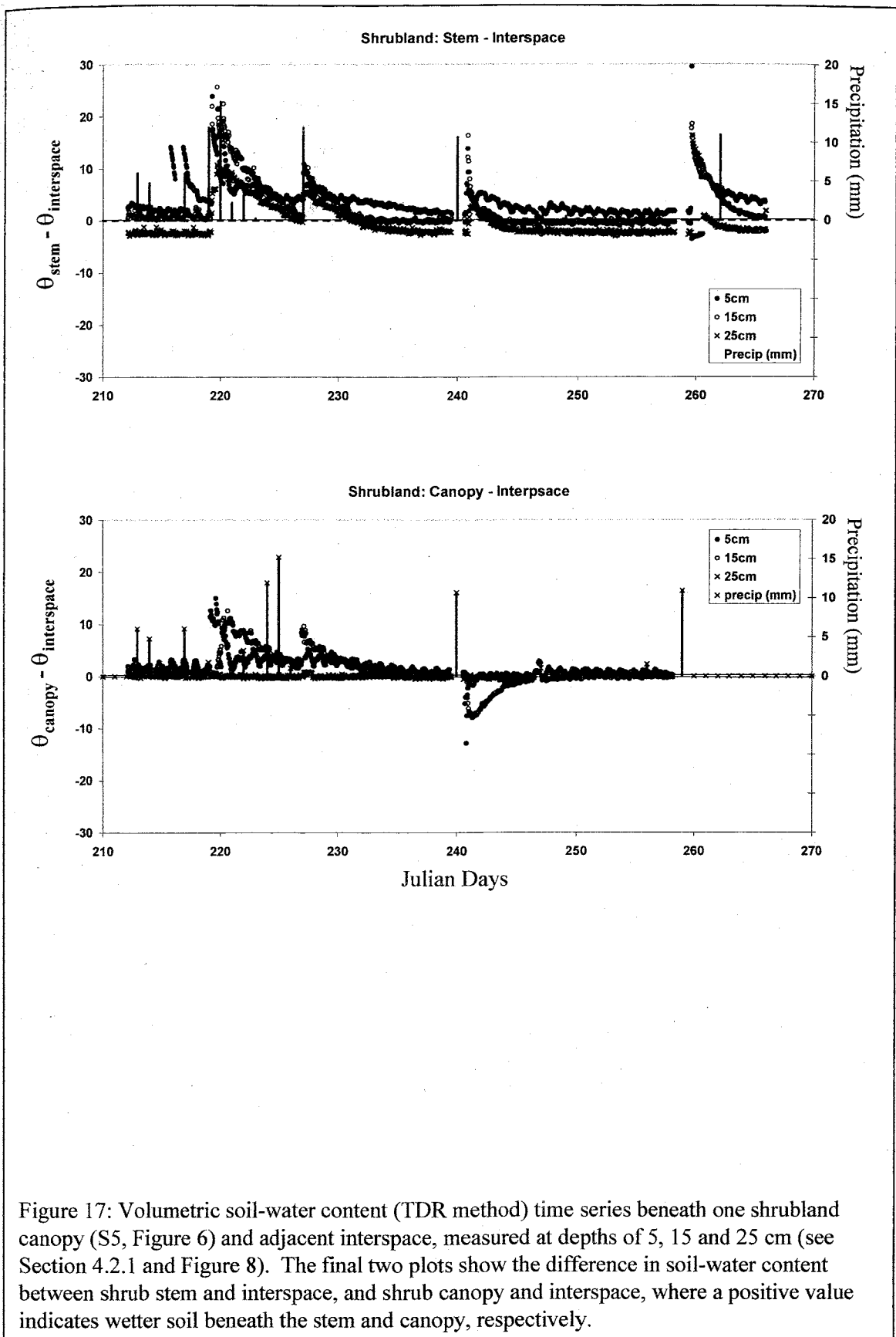


Figure 17: See next page for caption



In Figure 18 we reproduce shrubland soil moisture time series plots for grassland soil moisture beneath one grass canopy, G5 (Figure 6). The field setup is identical to that described for the shrubland (see Figures 8 and 9). The time series show that there is a smaller difference between grassland canopy and interspace infiltration than between that observed in the shrubland. Within the surface 15 cm, the soil-water content response to precipitation varies little between canopy and interspace. At 5 cm, the response to precipitation beneath both canopy and interspace is identical through time, with the exception that the canopy water content is on average 5% higher than that of the interspace. The higher water content is probably a collective effect of the higher organic content and macropores surrounding grass stalks. At 15 cm, a wetting front is observed at both locations only once, following a series of large precipitation events (days 224-5). Although the magnitude of wetting is approximately equal at this depth beneath canopy and interspace, the interspace soil moisture response is delayed several hours relative to the canopy. As the soils at 15 cm dry, the interspace soil approaches a residual value of ~10% while the canopy soil approaches ~5%. Therefore, although the soil-water content is up to 10% higher beneath the canopy at 5 and 15 cm following precipitation, through time the soil-water content difference is not always positive. At 25 cm, wetting is observed only once beneath the canopy, following the same series of large storms, and is at no time observed beneath the interspace.

Note that the above results represent measurements recorded beneath one plant canopy and adjacent bare soil patch in each ecosystem. Although the results lack consideration of spatial variability of soil-moisture wetting, soil-water potential gradients

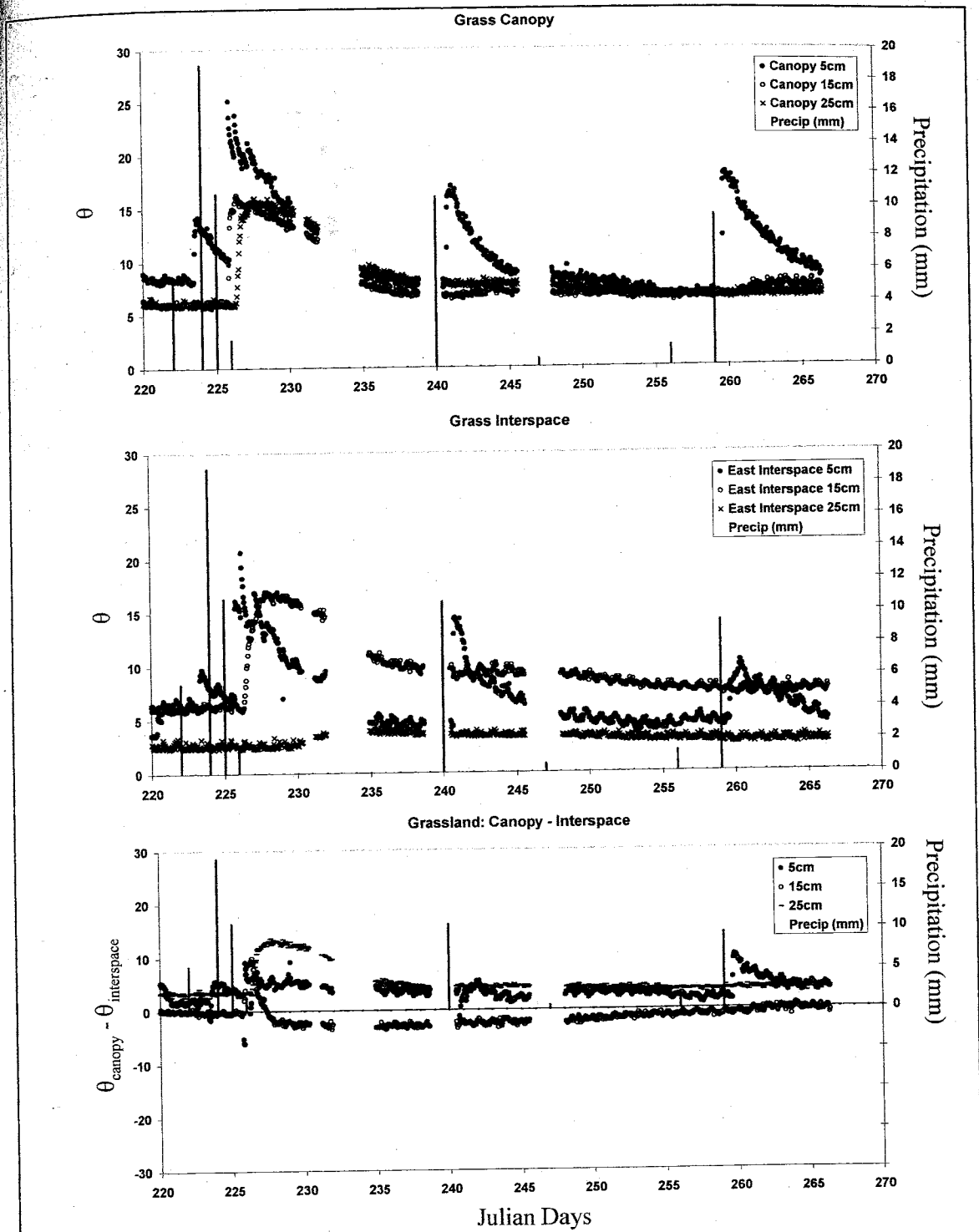


Figure 18: Volumetric soil-water content (TDR method) time series beneath one grassland canopy (G5, Figure 6) and adjacent interspace, measured at depths of 5, 15, and 25 cm (see Section 4.2.1 and Figure 9). The bottom plot shows the difference in soil-water content between grass canopy and interspace, where a positive value indicates wetter soil beneath canopy.

(section 4.3), measured at spatially varying locations that include those locations represented above, support the preceding soil-water content time series results.

#### *4.2.2. Comparison of Soil-Water Content beneath Shrub and Grass Canopies*

The difference in availability of soil-water to plants can be summarized by three points. First, shrub canopies are infiltration sinks during and following precipitation. Although grass canopies are infiltration sinks to a lesser degree, the difference between grass canopy and interspace soil-water content does not always favor the canopy. Second, the difference between the shrub canopy and interspace wetting depth is up to three times greater than that difference observed in the grassland. Third, the wetting depth beneath shrub canopies is greater than beneath grass canopies and occurs more frequently than beneath grasses. This effect is displayed most clearly following small precipitation events ( $< 10$  mm) where wetting is observed at 5 cm depth beneath the stem, a response not observed at this depth beneath the grass canopy. We attribute all such contrasts to soil type, interspace size and plant structure, and address these below.

### **4.3. The Influence of Precipitation on Soil-Water Potential**

We observe spatial and temporal variations in soil-water potential at the shrub and grassland field sites throughout the 2001 summer monsoon season. Water potential measurements were collected through time via the heat dissipation method, in spatial arrays previously described (Section 3.1). Rather than observing soil-water potential at individual canopy and interspace locations, we evaluate soil-water potential gradients between locations in both vertical and horizontal orientations. In the vertical, potential gradients are evaluated between depth intervals of 5-to-15 cm and 15-to-25 cm, beneath canopy and interspace locations in both ecosystems. In the horizontal, or lateral,

orientation, water potential gradients are evaluated between canopy and interspace locations at three depths, 5, 15, and 25 cm. In the shrub, we are able to reproduce such gradients between the shrub stem and canopy as well. Gradients calculated at 5 and 15 cm depth represent averages over five pairs of heat dissipation sensors, discussed below. Gradients at 25 cm however represent only one pair of heat dissipation sensors, also discussed below.

Vertical soil-water potential gradients ( $dh/dz$ ) are constructed from, and therefore represent, individual pairs of heat dissipation sensors. In the shrubland, we used heat dissipation sensors beneath one shrub canopy, S5 (Figure 6). At 5, 15, and 25 cm, the sensors used were labeled S5-H2, S5-H3, and S5-H4; we did not use sensors labeled S5-H1 (Figure 8). In the grassland, we used heat dissipation sensors beneath one grass canopy, G5 (Figure 6). At 5, 15, and 25 cm, the sensors used were labeled G5-H2, G5-H3, and G5-H4; we did not use sensors labeled G5-H1 (Figure 9). Between a given depth interval, either 5-to-15 cm or 15-to-25 cm, the gradient is calculated as

$$dh / dz = [(\psi + z)_{top} - (\psi + z)_{bottom}] / dz \quad (8)$$

where  $\psi$  is matric potential [cm],  $dz$  is the vertical distance between heat dissipation sensors (10 cm), and the datum is the ground surface. A positive water-potential gradient indicates soil-water flux in the downward direction.

Lateral soil-water potential gradients ( $dh/dx$ ) at 5 and 15 cm are constructed from measurement averages over five pairs of heat dissipation sensors. In the shrubland, gradients represent matric potential measurements beneath canopies S1, S2, and S5 (Figure 6). At 5 and 15 cm between canopy and bare soil, we use heat dissipation sensor pairs S1-2:S1-1, S1-4:S1-5, S2-2:S2-1, S2-4:S2-5 (Figure 7) and S5-H3:S5-H4 (Figure

8). At 25 cm, we use only one pair S5-H3-25:S5-H4-25, as this is the only pair at this depth (Figure 8). At 5 and 15 cm between stem and canopy soil, we use heat dissipation sensor pairs S1-3:S1-3, S1-3:S1-4, S2-3:S2-2, S2-3:S2-4 (Figure 7) and S5-H2:S5-H3 (Figure 8). At 25 cm between stem and canopy soil, we use again only one pair, S5-H2-25:S5-H3-25. In the grassland, soil-water potential gradients represent measurements beneath canopies G1, G2, and G3 (Figure 6). The heat dissipation sensors used in the grassland (Figure 9) have locations identical to those sensors used in the shrubland (Figure 8) between canopy and bare soil, as described above. Similar to the vertical orientation, the gradients are calculated as

$$dh / dx = [(\psi + z)_{canopy} - (\psi + z)_{bare}] / dx = (\psi_{canopy} - \psi_{bare}) / dx \quad (9)$$

where a positive gradient indicates a soil-water flux out from the canopy towards the interspace. The distance  $dx$ , however, varies with location and is equal to the average distance between adjacent heat dissipation sensors used for a gradient calculation. In the shrubland and grassland, the average distance between canopy and interspace sensor locations ( $dx$ ) is 115 cm and 75 cm, respectively. Also in the shrubland, the average distance between stem and canopy sensor locations ( $dx$ ) is 35 cm.

Once more we assume that periods of water availability to plants are limited to those during and after precipitation when soil-water flux is dominated by the liquid phase, and therefore neglect soil-water vapor flow. To determine the soil-water content at which vapor flow becomes the dominant transport mechanism as a soil sample dries after precipitation, the hydraulic diffusivity as a function of soil-water content  $D(\theta)$  is estimated for the soil samples. Hydraulic diffusivity is calculated as

$$D(\theta) = K(\theta) * \left( \frac{d\psi}{d\theta} \right) \quad (10)$$



(Hillel, 1998). Philip (1955) showed that as the liquid hydraulic diffusivity exponentially decreases with a decrease in soil-water content, the vapor diffusivity increases, thereby indicating the threshold soil-water content at which vapor flow becomes dominant.

Figure 19 shows plots of liquid hydraulic diffusivity for grass and shrub canopy soils, selected because these usually have higher soil-water contents than interspace soils and therefore control soil-water flux. For both soils, the diffusivity begins to exponentially decrease when the soil-water content is between 5 and 10%, signifying the liquid-vapor transition zone. Water release curves for these soil samples (Figure 13) show that the corresponding soil-water potentials fall within the approximate range -5,000 to -10,000 cm (~0.5 to 1.0 MPa). We therefore ignore (and do not plot) all soil-water potential gradients if the soil-water potential is less (more negative) than -10,000 cm (1.0 MPa) at both measurement locations.

The concept of hydraulic diffusivity is valid only when soil-water flux is driven by a soil-water matric potential gradient. Gravity driven flow, induced by a potential energy gradient, can be significant in the field when precipitation ponds at the surface. Under dry conditions when soil-water flux is vapor controlled, thermal gradients dominate matric potential gradients. We therefore use hydraulic diffusivity only as a rudimentary method to determine the approximate water content (and soil-water potential) at which liquid flow ceases.

As a final note, Figure 20 provides a general simplification of the following discussion, showing the direction of vertical and lateral soil-water flux during periods of precipitation and during subsequent drydown periods. The reader should refer to this figure as the text below is read.

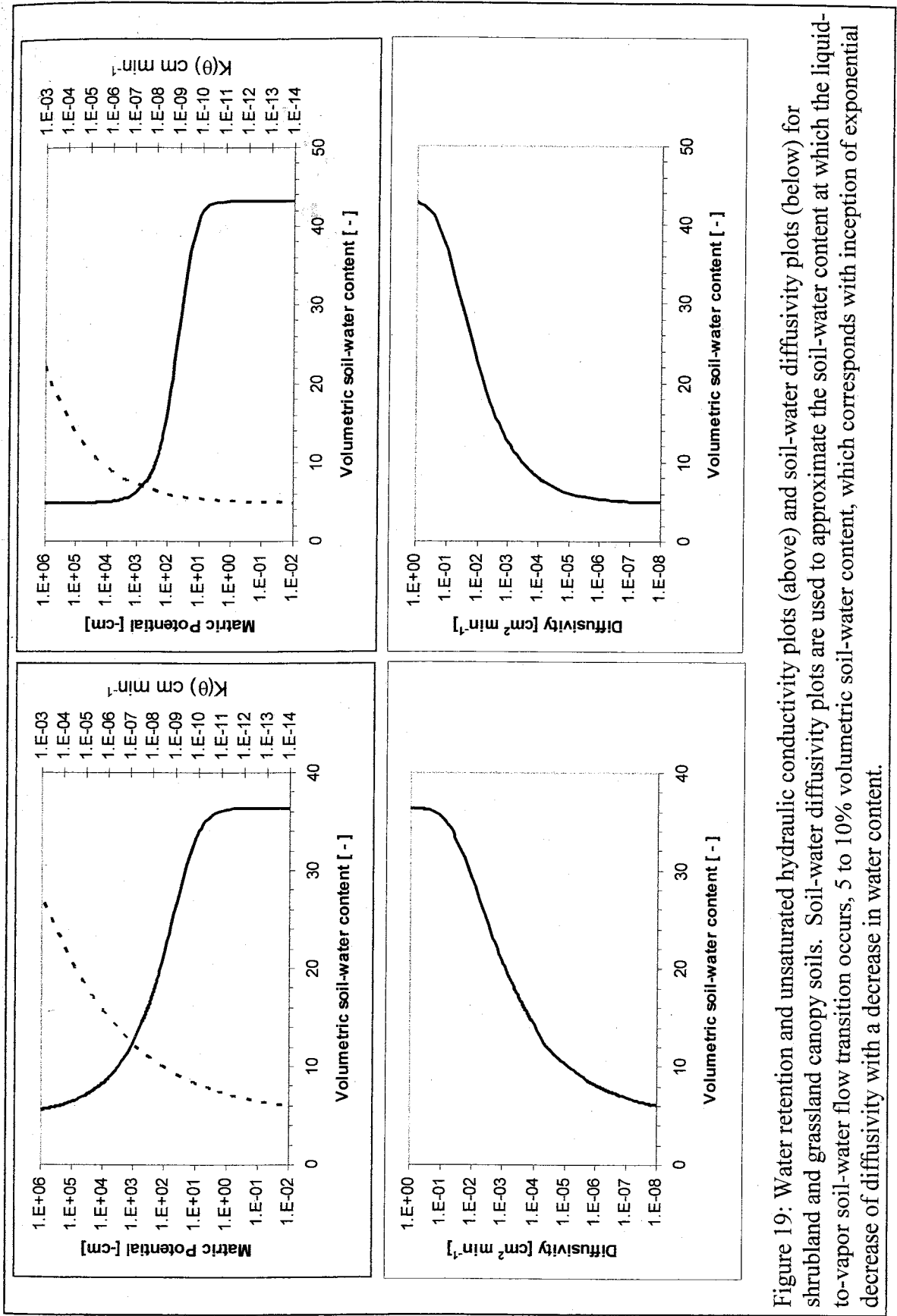


Figure 19: Water retention and unsaturated hydraulic conductivity plots (above) and soil-water diffusivity plots (below) for shrubland and grassland canopy soils. Soil-water diffusivity plots are used to approximate the soil-water content at which the liquid-to-vapor soil-water flow transition occurs, 5 to 10% volumetric soil-water content, which corresponds with inception of exponential decrease of diffusivity with a decrease in water content.

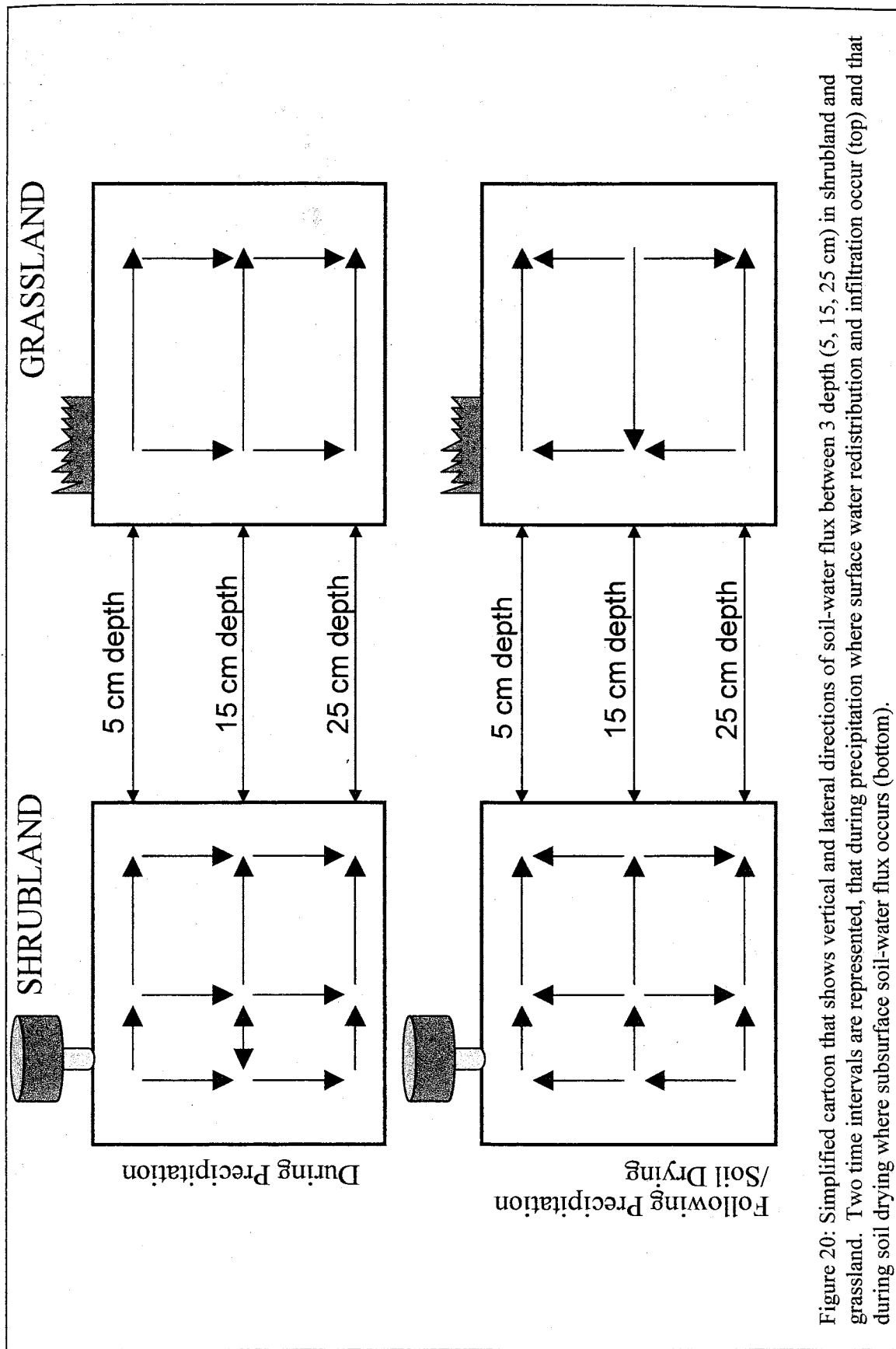


Figure 20: Simplified cartoon that shows vertical and lateral directions of soil-water flux between 3 depth (5, 15, 25 cm) in shrubland and grassland. Two time intervals are represented, that during precipitation where surface water redistribution and infiltration occur (top) and that during soil drying where subsurface soil-water flux occurs (bottom).

#### *4.3.1. Vertical Soil-Water Potential Gradients*

In the shrubland, there is little discrepancy between both the magnitude and sign of the vertical potential gradients beneath canopy (not stem) and interspace locations through time (Figure 21). During precipitation, the soil-water flux is always directed downwards as the wetting front progresses into dry soil below. Between 5 and 15 cm depth, the flux direction reverses within days of the event as soils near the surface dry from evaporation at a faster rate than those at depth. Between 15 and 25 cm, however, the soil-water flux retains its downward direction, primarily due to the absence of wetting at 25 cm beneath both canopy and interspace following the majority of storms. Such similarity at both locations between gradient direction and magnitude through time suggest an important result. If neither soil-texture (Tables 1, 2) nor vertical potential gradients (Figure 21) are considerably different beneath canopy and interspace locations, then the high soil-water content measured beneath shrub canopies (relative to the interspace) following precipitation must result from interspace runoff into canopies and/or canopy interception and stemflow.

Beneath the shrub stem, we observe similar potential gradients in space and through time with the exception of one key feature. Following precipitation, the downward flux direction for both 5 – 15 cm and 15 – 25 cm depth intervals reverses at an approximately equal time. This indicates either equal rates of drying (Figure 17) and/or soil-water redistribution below 25 cm depth. Following this reversal, the soil-water flux is directed upwards from 25 to 5 cm beneath a shrub stem. In contrast, beneath the canopy and interspace the soil-water flux diverges from 15 cm, directed both upwards

and downwards. The depth at which such a divergence may exist beneath the shrub stem is therefore below our range of measurement.

In the grassland, we observe distinct differences in temporal patterns of vertical soil-water potential gradients from those in the shrubland. Beneath grass interspaces, we similarly see a net soil-water flux directed downwards between 5 and 25 cm following precipitation. The gradient magnitude is consistently larger at the lower depth interval due to lack of significant wetting at 25 cm (Figure 18). Therefore, at all times the soil-water flux is directed downwards from 15 cm. Within days following precipitation, the interspace flux direction between 5 and 15 cm reverses, such that there is a divergence in soil-water flux from 15 cm similar to that observed beneath the shrub canopy and interspace. However, at the inception of the flux divergence in the grassland interspace, the gradient magnitude in the lower 15 – 25 cm interval begins to decrease through time, an inferred effect of gradual downward soil-water flow from 15 cm through time. This inference is supported by the soil moisture time series (Figure 18), where a distinct decrease in soil-water content at 15 cm corresponds with a soil moisture increase at 25 cm. Such a flux and corresponding gradient reduction are neither observed beneath the shrub canopy or interspace, and imply the advantageous ability of grassland interspaces to retain soil moisture at depth through time.

Time series of potential gradients beneath grass canopies more resemble those beneath the shrub stem, however there remain key deviations between the two. Following precipitation, we make the now standard observation of a net downward soil-water flux between 5 and 25 cm, and the subsequent complete reversal of gradient direction after days of soil drying. Beneath the grass canopy, however, the flux direction

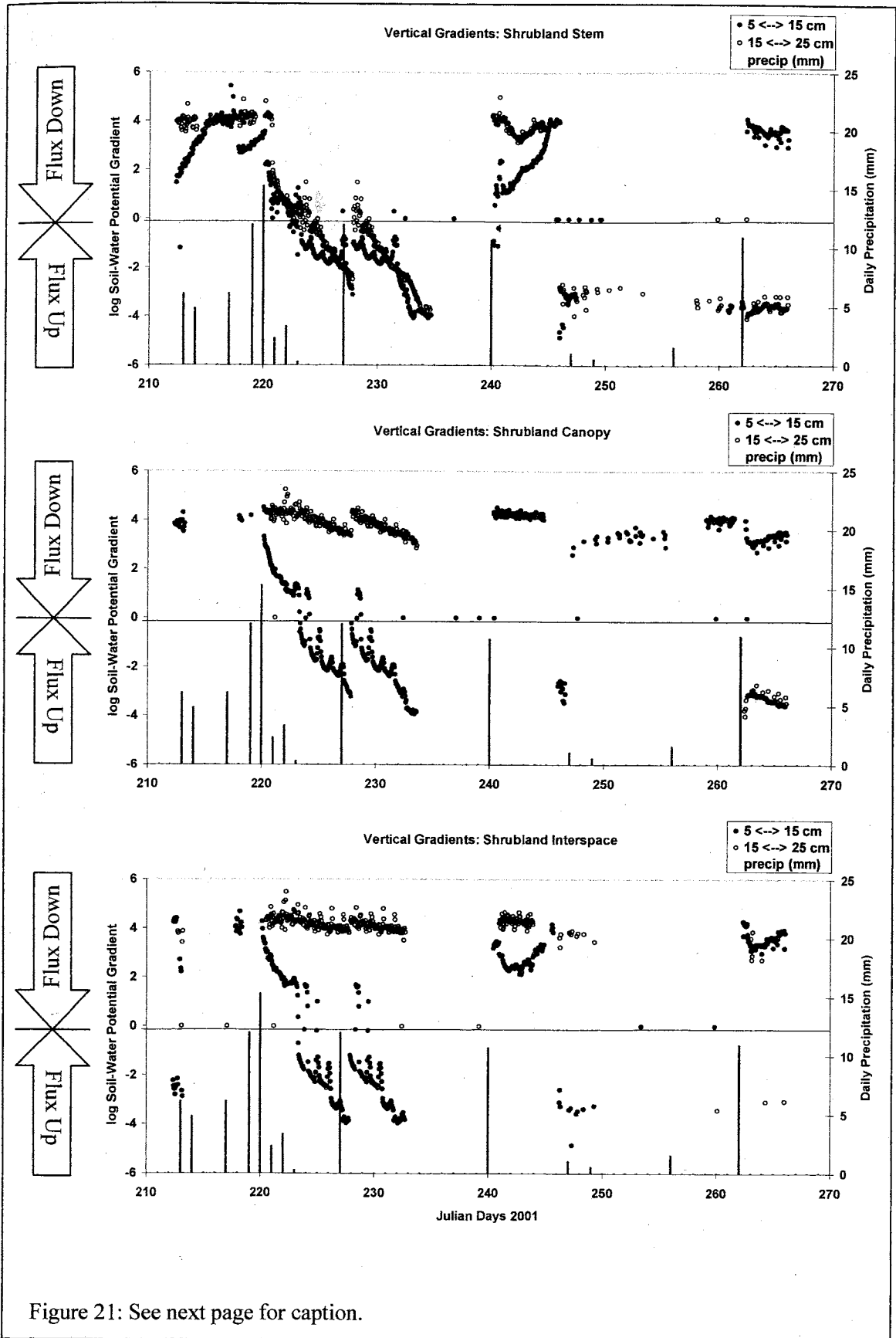


Figure 21: See next page for caption.

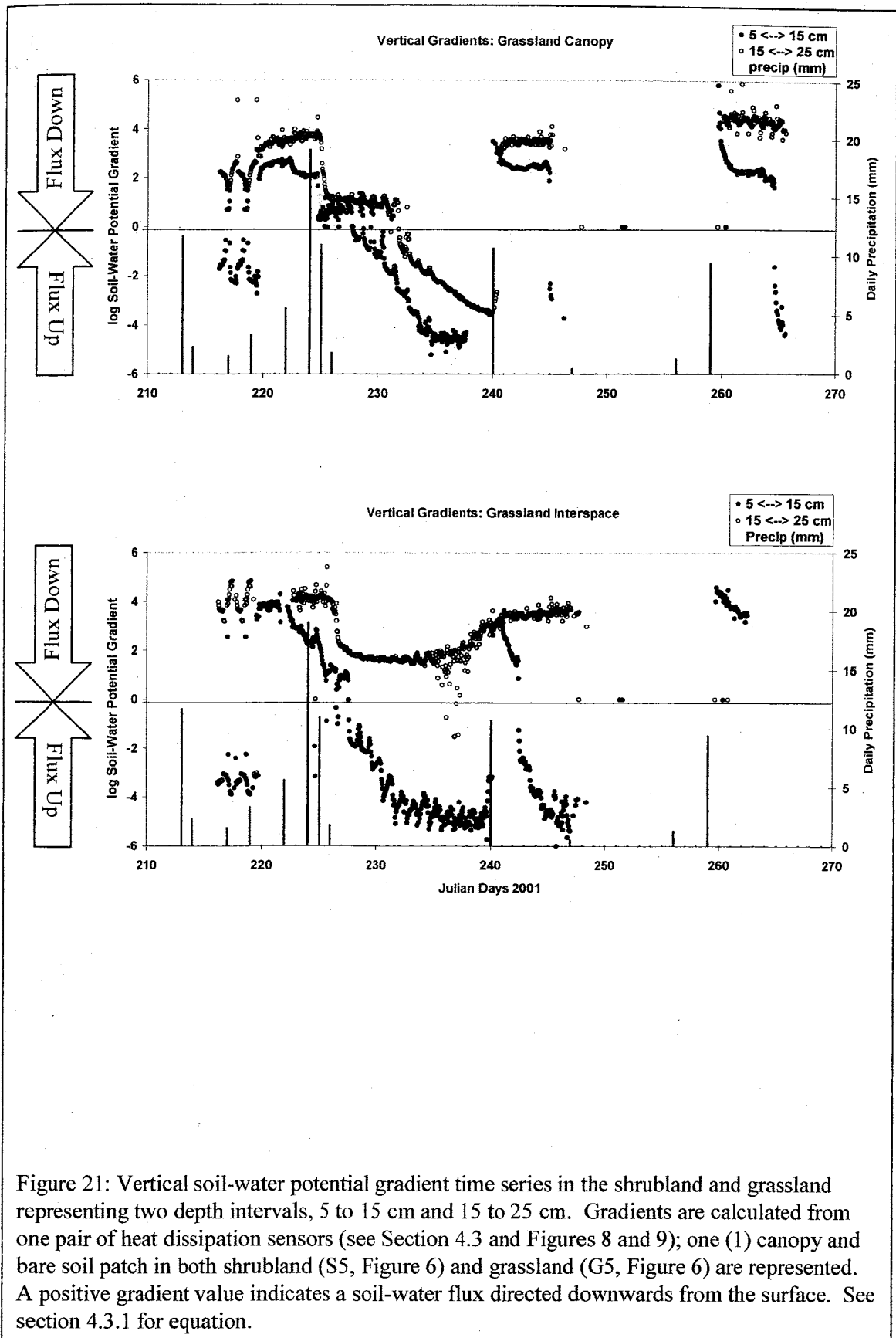


Figure 21: Vertical soil-water potential gradient time series in the shrubland and grassland representing two depth intervals, 5 to 15 cm and 15 to 25 cm. Gradients are calculated from one pair of heat dissipation sensors (see Section 4.3 and Figures 8 and 9); one (1) canopy and bare soil patch in both shrubland (S5, Figure 6) and grassland (G5, Figure 6) are represented. A positive gradient value indicates a soil-water flux directed downwards from the surface. See section 4.3.1 for equation.

reversal occurs at the lower depth interval days after the occurrence of that between the upper 5 – 15 cm depth interval. Remember that beneath the shrub stem, such reversals between depth intervals occur at approximately equal times. Soil-moisture beneath grass canopies is therefore retained at shallower depths for longer periods of time than beneath shrubs. A depth of 15 cm corresponds well with the depth of maximum root density in the grassland (Figure 1). If a link exists between soil moisture retention and root density, where roots possibly exert a soil-water potential below that of the surrounding soil, then we are not able to make the appropriate observations in the shrub ecosystem as the maximum root density occurs at 40 cm, a depth below our measurement range.

However, in support of such a conjecture, observe that the flux direction between 5 – 15 cm reverses at an equivalent time beneath both grassland canopy and interspace. On the contrary, between 15 – 25 cm, the flux direction reverses beneath the canopy several days after that of the upper 5 – 15 cm interval, but does not at any time reverse beneath the interspace. This indicates significant soil-water depletion beneath the shaded canopy but not beneath the un-shaded interspace. Further, the soil at 25 cm is wet beneath the canopy but not beneath the interspace (Figure 18), so the soil-water depletion beneath the grass canopy at 15 cm is probably attributed to root-water uptake.

#### *4.3.2. Lateral Soil-Water Potential Gradients*

In the shrubland, water potential gradients from stem-to-canopy and from canopy-to-interspace follow similar patterns through time. Following precipitation, the soil-water flux is directed out from the stem-to-canopy, and out from the canopy-to-interspace, indicating a gradational net soil-water flux directed out from the stem into surrounding interspace. The magnitude of these gradients increases with both time and depth.



Through time, a gradient increase is the primary result of soil drying such that the matric potential at the outer location (relative to the stem) tends toward a value of extremely large magnitude, on the order of MPa's (or tens of thousands of cm). A slight difference in soil-water content at this measurement point therefore yields a potential gradient of large magnitude. In this case, however, the unsaturated hydraulic conductivity of the dry interspace soil is sufficiently low (Figures 12 and 13) that soil-water flux becomes vapor dominated and is therefore negligible. With depth, gradients between canopy and interspace sample locations are initially large due to the lack of infiltration beneath interspaces. Soils beneath the stem/canopy however show high initial water contents with depth (Figure 17). As soil hydraulic conductivities approach their respective saturated values beneath the canopy, the soil-water flux directed out from the canopy is probably significant. For example, following a monsoon storm event, an expected volumetric soil-water content beneath a shrub canopy and interspace at 15 cm depth would be 25% and 10%, respectively. At 25%, the canopy soil would have  $K(\theta) \approx 1.5 \times 10^{-3} \text{ cm min}^{-1}$ . Over the average distance  $dx = 115 \text{ cm}$  between canopy and interspace measurement locations, the matric potential gradient is  $dh/dx \approx 10^3$  (assuming the absence of hysteretic effects), corresponding to a soil-water flux approximately equal to  $1.5 \text{ cm min}^{-1}$  out from beneath the canopy. The flux would not, of course, traverse the entire 115 cm interval, as the transition distance between canopy soil and bare soil is on the order of tens of centimeters. We merely make the point that the soil-water flux directed out from the canopy into interspace is probably important to plant water availability.

Contrary to observations made in the shrubland, lateral soil-water potential gradients observed in the grassland do not consistently illustrate a soil-water flux directed out from beneath the canopy (Figure 22). Following precipitation, soils measured at 5 cm are not consistently wetter beneath either canopies or interspaces. Such variability is likely due to microtopographic effects, a subject that is later discussed. The potential gradient often, but not always, directs the lateral soil-water flux from the interspace in towards the canopy at early times following precipitation. Over a time period of approximately 2 days, however, the interspace soils at 5 cm dry at a faster rate than the canopy soil as a result of bare soil evaporation. Matric potential gradients subsequently direct the soil-water flux from canopies out into interspaces. The magnitude of this gradient continues to increase at 5 cm depth until both canopy and interspace soils dry to the point that the "no liquid flow" vapor dominated state is achieved. At 15 cm depth, the potential gradient is always directed out from the canopy into interspaces directly following precipitation. Within one to ten days, we observe a reversal of the gradient such that the lateral soil-water flux is directed in towards canopies, indicating that canopy soils at 15 cm dry faster than respective interspace soils. This result and its implication of grass transpiration was previously discussed. At 5 and 15 cm depth, we therefore observe opposed flux directions.

At 25 cm depth, the soil-water flux is always directed from the canopy into the interspace. This is reasonable as a sharp wetting front is never observed (Figure 18) at 25 cm in the interspace.

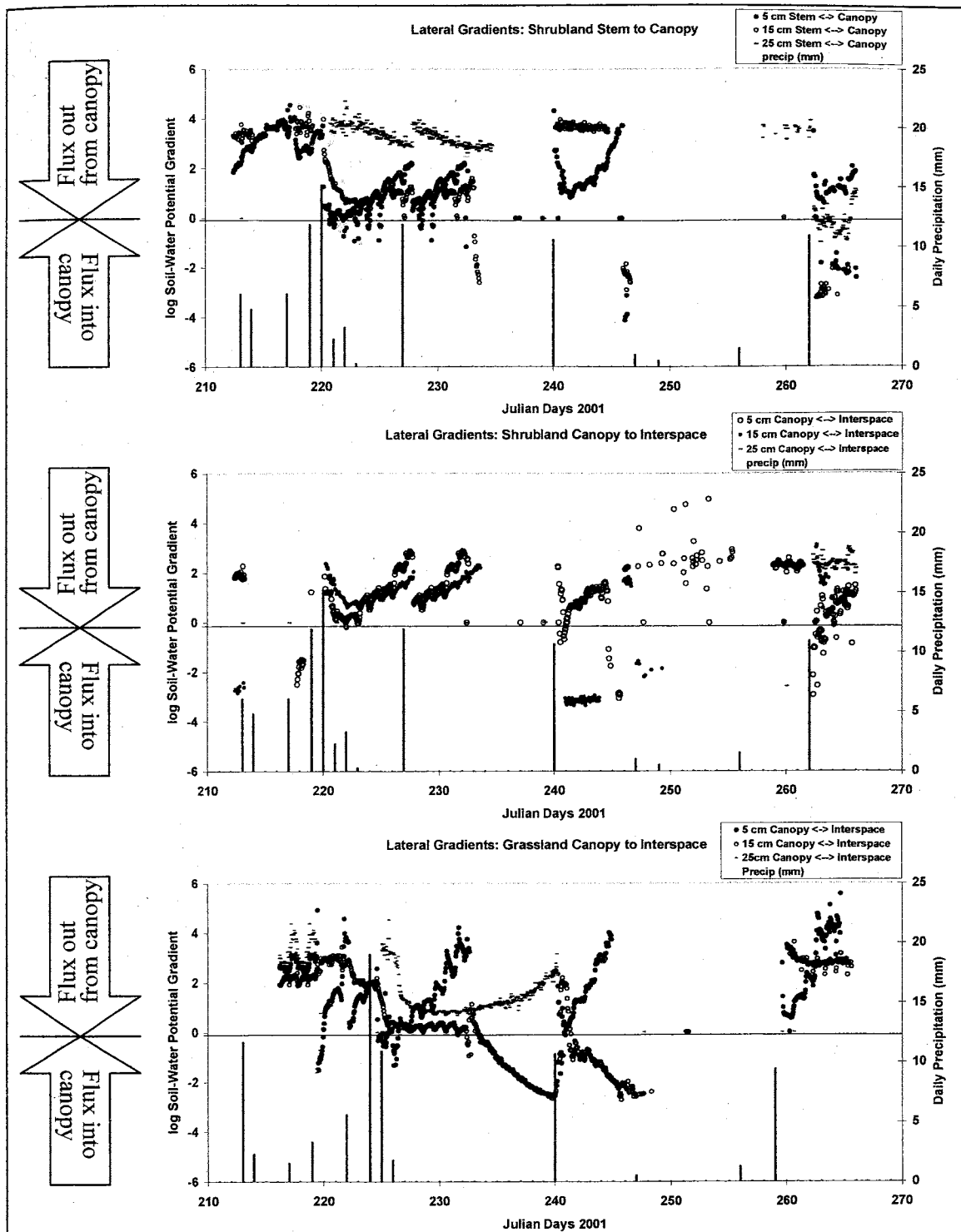


Figure 22: Lateral (horizontal) soil-water potential gradient time series in the shrubland and grassland representing three depths (5, 15, 25 cm) between plant canopy and interspace, and stem and canopy (shrubland only). At 5 and 15 cm depths, gradients are averages of five (5) pairs of heat dissipation sensors (see Section 4.3 and Figures 7 – 9) over shrub canopies S1, S2, S5 and grass canopies G1, G2, G5 (Figure 6). At 25 cm, gradients represent only one (1) location (Figures 8 and 9). A positive gradient value indicates a soil-water flux directed out from canopy into interspace. See section 4.3.2 in the text for equation.

## 5. Discussion

In the introduction we hypothesized that five physical properties constrain the availability of water to plants in the grassland and shrubland ecosystems, both during and after periods of precipitation. These were (1) plant structure and spatial patterns of plant canopy and bare soil patch location, (2) the occurrence of ponding and surface runoff of precipitation, (3) microtopography, (4) surface and near subsurface soil hydraulic parameters at plant canopies and bare soil, and (5) root water uptake. In each environment these parameters naturally are strongly coupled, as discussed in the introduction, and discussed further below. We infer these parameters to exclusively influence the availability of water to plants in both ecosystems. Differences in water availability to shrubs and grasses are therefore a result of different property configurations across the ecotone.

### 5.1. Shrubland

In the shrubland, plant canopies are separated on average by 3 m, the bare soil between which is exposed to wind and water (rainsplash, runoff) erosion, having a finer textured, and therefore less permeable, surface soil layer (Kieft et al., 1998; Abrahams et al., 1995). The surface soil layer beneath shrub canopies is more protected from the effects of erosion. Elevated soil mounds surround shrubs, the heights of which increase toward the stem. We found that shrub interspace surface soils have consistently lower unsaturated hydraulic conductivities than canopy soils at a given soil-water content (Figures 13 and 14), and that the saturated conductivity is less than one-half that of the canopy soil (Table 5). During precipitation, when the rainfall rate exceeds the infiltration capacity of interspace soil, precipitation ponds at the interspace surface and becomes

runoff if a slope is present. Runoff is captured and infiltrates at canopy soil mounds that surround shrub stems, having higher hydraulic conductivity than bare soil. This effect is magnified as the ratio of interspace-to-canopy coverage per unit surface area (3:1 on average) increases. Because of the large bare soil surface area in the shrubland, we suspect that bare soil connectivity is not a limiting factor to surface runoff, however, we did not quantify bare soil connectivity at either ecosystem.

Results further indicate that surface-water ponding and subsequent conversion to runoff is an essential process effecting plant water availability in shrublands. Soil texture, in conjunction with interspace size and connectivity, would therefore appear to be a key surface hydrologic property in shrub ecosystems. Ponding begins when the precipitation rate exceeds the infiltration rate of a surface soil. For example, we measured infiltration rates of 0.91 and 1.50 mm min<sup>-1</sup> for shrubland interspace surface soils, using laboratory and field methods, respectively. Field measurements are larger in magnitude due to soil-water potential gradient driven (three-dimensional) infiltration of the wetting front into dry soil surrounding the infiltrometer ring, discussed in Section 3.1, as opposed to gravity driven (one-dimensional) flow using the constant head method on soil columns in the laboratory. When we relate the saturated hydraulic conductivity measurements to typical precipitation intensity at these ecosystems, we find that ponding is expected to occur during a significant portion of precipitation. In 2001, 10% of total precipitation (231 mm) measured at 5 Points Station (< 1 km from both field sites) fell with intensity greater than 0.91 mm min<sup>-1</sup> (Figure 23), the saturated infiltration capacity of shrubland interspace soil measured in the lab.

We further found that shrub canopy interception can be significant to plant water availability. In our study, such effects are most visible in small storm events ( $\leq 5$  mm), e.g. day 217, where rainfall is captured over the large canopy area and channeled via the stem network to the root (Figure 17). Martinez-Meza and Whitford (1996) showed that creosotebush has on average a canopy rainfall storage capacity of 1.3 mm, beyond which stemflow and channelization to the root was observed. All but two storm events measured in this study are events greater than 1.3 mm.

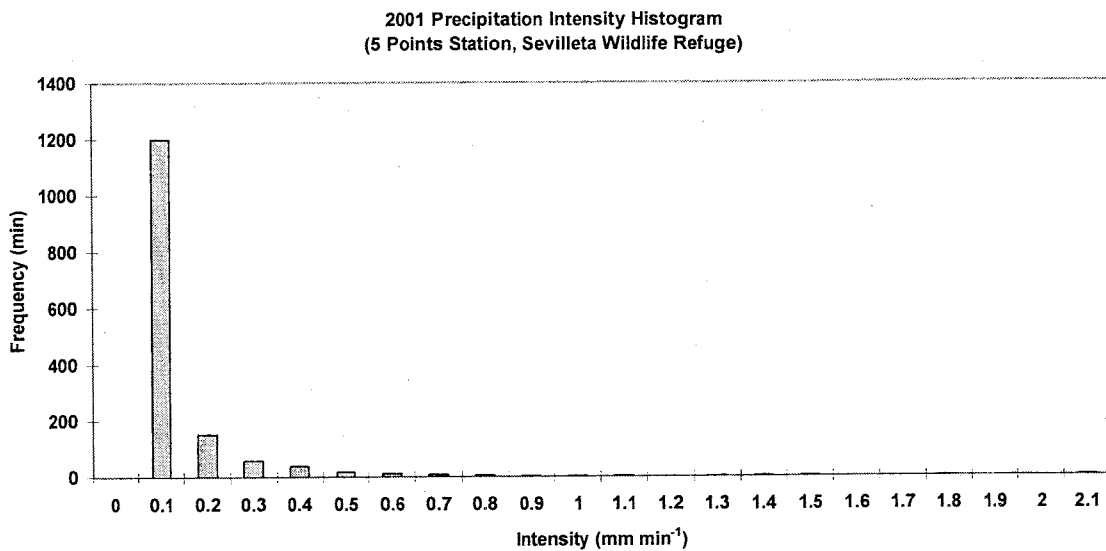


Figure 23: Field site precipitation intensity ( $\text{mm min}^{-1}$ ) histogram for the year 2001 recorded at 5 Points Station, located less than 1 km from both field sites. Precipitation was measured using a tipping bucket rain gage with  $0.1 \text{ mm min}^{-1}$  resolution.

## 5.2. Grassland

In black grama dominated grasslands, grass patches are separated by bare soil patches that are of approximately equal size. Grass patches are elevated above interspaces by a dense biomass/root network, protecting the bare soil from wind and water erosion. Despite the large difference measured between grassland canopy and

interspace hydraulic conductivity (Table 5), we measured significant bare soil infiltration following storm events. Bare soil infiltration was not however significant in the shrubland, where a large difference between shrubland canopy and interspace hydraulic conductivity was also observed. We suggest that the microtopographically elevated grass canopies that surround interspaces do not permit ponded interspace soil-water to enter the grass canopies of higher hydraulic conductivity. Although the proximity of grass patches surrounding an interspace may permit root-water uptake within interspaces (Figure 1), a phenomenon suggested by Gibbenz and Lenz (2001) that would increase soil-water availability to grasses, lateral soil-water potential gradients show that canopy soils at 15 cm dry more rapidly than adjacent unshaded interspace soils, indicating that grass soil-water consumption in interspaces is probably not a primary source of soil-water.

Lastly, our measurements do not indicate any form of grass canopy rainfall interception and/or channelization along grass stalks.

## **6. Conclusions**

In this study we discussed the influence of surface and near-subsurface hydrologic processes on the distribution of soil-water and its availability to plants in shrub and grass dominated semiarid ecosystems. We focused on time periods of precipitation, precipitation being the limiting factor to plant water availability in these semiarid ecosystems. For simplification, our analyses of how hydrologic processes influenced the soil-water distribution were divided into two parts. First, we considered the period during precipitation, which included how precipitation was distributed and redistributed on the ground surface, and subsequently infiltrated into the soil. We hypothesized that

three physical properties controlled the surface hydrologic system: (1) plant structure, e.g., woody, herbaceous, (2) the occurrence of surface ponding of precipitation and runoff, controlled by both surface soil hydraulic properties and spatial patterns of plant canopy and bare soil patch location, and (3) microtopography. Second, we considered the period of soil drying, within days following precipitation, which involved the redistribution of near subsurface soil-water. We attributed this component of water availability to two properties: (1) difference in soil texture and corresponding soil hydraulic properties beneath plant canopies and bare soil patches, and (2) root-water uptake.

We first established that plant canopies in both ecosystems are infiltration sinks during precipitation. This was a result that has been observed in previous studies, e.g. Bhark and Small (Appendix 1), and which we reconfirmed in this study. We were however able to improve upon this result by showing that shrub canopies are infiltration sinks to a greater degree than grasses. We found that (1) the difference between shrub canopy and interspace wetting depths are up to three times greater than that difference observed in the grassland, (2) the wetting depth beneath shrub canopies is greater than beneath grass canopies for a given precipitation event magnitude, and that (3) the soil moisture response to precipitation occurs for a broader range of precipitation events beneath shrubs than grasses.

We next attempted to answer the question 'why does water availability appear to favor plants in the shrub dominated ecosystem?'. We addressed this question with a focus on periods of precipitation, again dividing our investigation into two parts, (1) time periods during precipitation, which included how precipitation was distributed and



redistributed on the ground surface, and subsequently infiltrated into the soil, and (2) time periods during soil drying, within days following precipitation.

In this context, analyses of soil texture and hydraulic properties in both ecosystems provided two key results. First, we found in both shrubland and grassland that soil texture and hydraulic properties are more uniform at 15 cm than at 5 cm. Differences apparent at the surface become less so at 15 cm depth, implying that observed differences in water availability to plants are probably controlled by differences in the surface soils. Second, the differences in soil properties with depth in both ecosystems are not sufficiently different to influence water availability during periods of soil drying.

We therefore concluded that it is the period during precipitation, which includes how precipitation is distributed and redistributed on the ground surface, and subsequently infiltrates into the soil, that has the strongest influence on plant water availability. Remember now that we suggested three physical properties that control the surface hydrologic system.

In the shrubland, it is both the large interspace size, relative to canopies, and plant structure, that control the surface hydrologic system. First, the frequency of ponding during precipitation is similar over grassland and shrubland interspaces. The large shrub interspaces therefore provide a greater volume of surface flow to plant canopies as runoff. Second, the large canopy and stem network of shrub canopies efficiently channels interception to the root system during all but the slightest of precipitation events. We are not able to discern, however, given our spatial system of measurements, whether runoff

infiltration at shrub canopies or canopy interception and stemflow provides more water to shrubs.

In the grassland, we found that it is the elevated plant structure, or microtopography, that is the limiting parameter with respect to plant water availability. Although grass canopies have the highest hydraulic conductivity of any surface soil observed in this study, the conductivity beneath canopies being greater than that at bare soil by almost a factor of three, the depressed interspaces (relative to canopies) isolate ponds and do not permit infiltration into canopies from above. Regardless of grassland interspace connectivity, which was not quantified in this study, a significant portion of surface ponds and runoff will consistently infiltrate at interspaces due to microtopographic effects. While it has been suggested in the literature that grasses may consume infiltration beneath interspaces as root water uptake (e.g., Gibbens and Lenz, 2001), our results indicate primary root-water uptake beneath grass canopies.

In sum, although the grassland and shrubland ecosystems themselves are unquestionably able to thrive in an un-stressed state, both ecosystems are currently pressured by outside factors. High levels of herbivory and the reduced frequency of grassland fires, accompanied by other less significant factors, are the apparent causes of the northern-moving shrub encroachment (Van Auken, O.W., 2000). Although these causes are not the focus of this study, we have shown how under stress shrubs are able to thrive through their ability to better access soil-water than grasses, where soil-water availability is the most critical factor controlling plant productivity and reproduction in arid-to-semiarid environments.

## References

- 1) Abrahams A.D., Parsons, A.J., and Wainwright, J., 1995. Effects of vegetation change on interrill runoff and erosion, Walnut Gulch, southern Arizona. *Geomorphology*, 13: 37-48.
- 2) Archer, S., 1994. Woody plant encroachment into southwestern grasslands and savannas: Rates, patterns, and proximate causes. Pages 13-68 *in* Ecological implications of livestock herbivory in the West, Vavra, M., Laycock, W., and Pieper, R. eds. Society for Range Management, Denver, Colorado.
- 3) Bahre, C.J. and Shelton, M. L., 1993. Historic vegetation change, mesquite increases, and climate in southeastern Arizona. *Journal of Biogeography*, 20: 489-505.
- 4) Breshears, D.D., Rich, P.M., Barnes, F.J. and Campbell, K., 1997. Overstory-imposed heterogeneity in solar radiation and soil moisture in a semiarid woodland. *Ecological Applications*, 7: 1201-1215.
- 5) Buffington, L.C. and Herbel, C.H., 1965. Vegetational changes on a semidesert grassland range from 1858 to 1963. *Ecological Monographs*, 35: 139-164.
- 6) Campbell, G.S., Department of Crop and Soil Science, Washington State Univ., Pullman, WA
- 7) Campbell Scientific, 1998. Application Note: 229 Soil Water Potential Probe
- 8) Cunningham, G.L., Syvertsen, J.P., Reynolds, J.F. and Willson, J.M., 1979. Some effects of soil-moisture availability on above-ground production and reproduction allocation in *Larrea tridentata*. *Oecologia*, 40: 113-123.
- 9) Devitt, D.A. and Smith, S.D., 2002. Root channel macropores enhance downward movement of water in a Mojave Desert ecosystem. *Journal of Arid Environments*, 50: 99-108.
- 10) Drewa, P.B. and Havstad, K.M., 2001. Effects of fire, grazing, and the presence of shrubs on Chihuahuan desert grasslands. *Journal of Arid Environments*, 48: 429-443.
- 11) Dunkerley, D.L., 2000. Assessing the influence of shrubs and their interspaces on enhancing infiltration in an arid Australian shrubland. *Rangeland Journal*, 22: 58-71.

- 12) Dunkerley, D.L., 2000. Hydrologic effects of dryland shrubs: defining the spatial extent of modified soil water uptake rates at an Australian desert site. *Journal of Arid Environments*, 45: 159-172.
- 13) Dunkerley, D.L. and Booth, T.L., 1999. Plant canopy interception of rainfall and its significance in a banded landscape, arid western New South Wales, Australia. *Water Resources Research*, 35: 1581-1586.
- 14) Elrick, D.E. and Parkin, G.W., 1995. Analysis of early-time and steady state single-ring infiltration under falling head conditions. *Water Resources Research*, 31: 1883-1893.
- 15) Ferre, P.A., Department of Hydrology and Water Resources, Univ. of Arizona, Tucson, Arizona
- 16) Gibbenz, R.P. and Lenz, J.M., 2001. Root systems of some Chihuahuan Desert plants. *Journal of Arid Environments*, 49: 221-263.
- 17) Gile, L.H., Gibbens, R.P. and Lenz, J.M., 1998. Soil-induced variability in root systems of creosotebush (*Larrea tridentata*) and tarbush (*Flourensia cernua*). *Journal of Arid Environments*, 39: 57-78.
- 18) Graetz, D., 1994. Grasslands. In *Changes in Land Use and Land Cover: a Global Perspective*, Meyer, W.B. and Turner, B.L. eds. Cambridge Univ. Press.
- 19) Grover, H. D. and Musick, H. B., 1990. Shrubland encroachment in southern New Mexico, U.S.A.: An analysis of desertification processes in the American Southwest. *Climatic Change*, 17: 305-330.
- 20) Hendrickx, J.M.H., Department of Earth and Environmental Science, Hydrology Program, New Mexico Institute of Mining and Technology, Socorro, New Mexico
- 21) Hillel, D., 1998. *Environmental Soil Physics*, Academic Press.
- 22) Kieft T.L., White, C.S., Loftin, S.R., Aguilar, R., Craig, J., and Skaar, D., 1998. Temporal dynamics in soil carbon and nitrogen resources at a grassland-shrubland ecotone. *Ecology*, 79: 671-683.

- 23) Lyford, F.P. and Qashu, H.K., 1969. Infiltration rates as affected by desert vegetation, *Water Resources Research*, 5: 1373-1376.
- 24) Martinez-Meza, E., and Whitford, W.G., 1996. Stemflow, throughfall and channelization of stemflow by roots in three Chihuahuan desert shrubs. *Journal of Arid Environments*, 32: 271-287.
- 25) Mualem, Y., 1976. A new model for predicting the hydraulic conductivity of unsaturated porous media, *Water Resources Research*, 12: 513-522.
- 26) Noy-Meir I., 1973. Desert ecosystems: Environment and producers. *Annual Review of Ecology and Systematics*, 4: 25-51.
- 27) Phene, C.J., Hoffman, G.J. and Rawlins, S.L., 1971. Measuring soil matric potential in situ by Sensing Heat Dissipation within a Porous Body: I. Theory and Sensor Construction. *Soil Sci. Soc. Amer. Proc.*, 35: 27-34.
- 28) Philip, J.R., 1955. The concept of diffusion applied to soil water. *Proc. Natl. Acad. Sci. India*, 24A: 93-104.
- 29) Reece, C.F., 1996. Evaluation of a line heat dissipation sensor for measuring soil matric potential. *Soil Sci. Soc. Am. J.*, 60: 1022-1028.
- 30) Rodriguez-Iturbe, I., 2000. Ecohydrology: A hydrologic perspective of climate-soil-vegetation dynamics. *Water Resources Research*, 36: 3-9.
- 31) Russo, D., 1988. Determining soil hydraulic properties by parameter estimation: On the selection of a model for the hydraulic properties. *Water Resources Research*, 24: 453-459.
- 32) Schlesinger, W.H., Reynolds, J.F., Cunningham, G.L., Huenneke, L.F., Jarrell, W., Virginia, R.A. and Whitford, W.G., 1990. Biological feedbacks in global desertification. *Science*, 247: 1043-1048.
- 33) Schlesinger, W.H., Ward, T.J., and Anderson, J., 2000. Nutrient losses in runoff from grassland and shrubland habitats in southern New Mexico: II. Field plots, *Biogeochemistry*, 49: 69-86.

- 34) Schmutge, T.J., Jackson, T.J. and McKim, H.L., 1980. Survey of methods for soil moisture determination. *Water Resources Research*, 16: 961-979.
- 35) Sharifi, M.R., Meinzer, F.C., Nilsen, E.T., Rundel, P.W., Virginia, R.A., Jarrell, W.M., Herman, D.J. and Clark, P.C., 1988. Effect of manipulation of water and nitrogen supplies on the quantitative phenology of *Larrea tridentata* (creosote bush) in the Sonoran Desert of California. *American Journal of Botany*, 75: 1163-1174.
- 36) Thurow, T. L., W. H. Blackburn, S. D. Warren, and Taylor, C.A., 1987. Rainfall interception by midgrass, shortgrass, and live oak mottes. *Journal of Range Management*, 40: 455-460.
- 37) Topp, G. C., J.L. Davis, and Annan, A.P., 1980. Electromagnetic determination of soil water content: Measurements in coaxial transmission lines. *Water Resources Research*, 16: 574-582.
- 38) Tromble, J. M., 1988. Water interception by two arid land shrubs. *Journal of Arid Environments*, 15: 65-70.
- 39) Van Auken, O. W., 2000. Shrub invasions of North American Semiarid Grassland. *Annual Reviews of Ecology and Systematics*, 31: 197-215.
- 40) van Genuchten, M.Th., 1980. A closed form equation for predicting the hydraulic conductivity of unsaturated soils. *Soil Sci. Soc. Am. J.*, 44: 892-898.
- 41) Wainwright, J., Parsons, A.J. and Abrahams, A.D., 1999. Rainfall energy under creosotebush. *Journal of Arid Environments*, 43: 111-120.
- 42) Whitford, W. G., Anderson, J. and Rice, P. M., 1997. Stemflow contribution to the 'fertile island' effect in creosotebush, *Larrea tridentata*. *Journal of Arid Environments*, 35: 451-457.

**The relationship between plant canopies and the spatial variability of infiltration in  
grassland and shrubland of the northern Chihuahuan desert, NM**

Eric W. Bhark and Eric E. Small

Earth and Environmental Science Department, New Mexico Tech

Socorro, NM, 87801

**Abstract**

Shrubs have invaded extensive areas of grassland in the southwestern U.S. The zones of nutrient-rich soil found beneath plant canopies, referred to as “islands of fertility”, are more intense and spaced further apart in shrubland than in grassland. This difference in the spatial pattern of soil nutrients may reinforce shrub invasion. Changes in water availability in the soil could also influence shrub invasion. Here we compare the spatial patterns of infiltration, defined as the total equivalent water depth entering the soil following individual rainfall events or summed over many events, at adjacent grass and shrub-dominated sites in the Sevilleta National Wildlife Refuge. We use two infiltration datasets. First, following four rainfall events, we measured soil moisture and wetting front depth at 10 cm intervals along 24 meter transects. We estimate infiltration from these data. Second, we use vertical arrays of soil moisture probes to compare infiltration between adjacent canopies and interspaces following 31 storms.

In both the grassland and shrubland, infiltration is typically greater beneath plant canopies than beneath interspaces: canopies are oases where soil moisture is higher than

in the surrounding areas. However, infiltration is not greater beneath canopies when surface runoff is limited. In the shrubland, the canopy-interspace infiltration ratio increases as storm size, and therefore runoff, increases. This relationship also exists in the grassland, but it is not as strong or clear. The magnitude of spatial variability of infiltration is similar in shrubland and grassland. In addition, the distance over which infiltration is correlated is ~50 cm in both environments. Most of the spatial variability exists between the stem and canopy margin in the shrubland and straddling the canopy margin in the grassland. The most notable difference is that sub-canopy oases are spread further apart in the shrubland because canopies are separated by larger interspaces in this environment.

## **1. Introduction**

In the early 19<sup>th</sup> century, large areas of grassland were present in the southwestern U.S. Over the past 200 years, the density of shrubs such as mesquite (*Prosopis glandulosa*) and creosotebush (*Larrea tridentata*) has increased dramatically, converting these ecosystems from herbaceous to woody-dominated (Buffington and Herbel, 1965; Grover and Musick, 1990; Bahre and Shelton, 1993; Archer et al., 1994; Van Auken, 2000). Similar invasions of grasslands by shrubs have been observed worldwide (Graetz, 1994). The following factors have been proposed to explain shrub invasion in the southwest: livestock grazing, altered fire regime, drought, climatic change, and increased atmospheric CO<sub>2</sub> concentration (Archer, 1994). However, it is not possible to establish a clear cause-effect relationship between these factors and observed vegetation changes. There is only limited data to constrain the history of shrub invasion (e.g., Buffington and



Herbel, 1965) and interactions between these different factors could lead to complex ecosystem changes (Archer, 1994).

Previous research has been focused on understanding the changes in processes that accompany the transition from grassland to shrubland ecosystems, with the goal of understanding how different factors such as grazing or droughts may influence shrub invasion. One key difference is that the spatial patterns of soil fertility are different in grassland and shrubland. First, the zones of nutrient-rich soil found beneath plant canopies, referred to as "islands of fertility" (e.g., Schlesinger et al., 1990), are more intense in shrubland than grassland. The intensity of islands was gauged by measuring the canopy-to-interspace ratio of various plant nutrients and carbon, which is typically higher in shrubland than grassland (Schlesinger et al., 1996; Kieft et al., 1998). Second, geostatistical analyses were used to measure the scale of spatial variability in grass and shrub ecosystems. In grasslands, most of the variability in soil fertility exists at distances < 20 cm, interpreted to represent accumulations of nutrients beneath grass clumps (Schlesinger et al., 1996). In contrast, spatial variability of soil fertility increases up to distances of 1-3 m in shrublands, believed to represent cycling beneath individual shrub canopies. These changes in the spatial patterns of soil fertility associated with the transition from grassland to shrubland may act as a positive feedback that reinforces shrub invasion.

The most critical factor controlling plant productivity and reproduction in arid-to-semiarid environments is water availability in the soil (Noy-Meir, 1973; Rodriguez-Iturbe, 2000). The influence of soil fertility, for example available nitrogen, is considered to be of secondary importance, as the effects of enhanced soil fertility are

typically only observed once the limitations from water availability are eliminated (e.g., Sharifi et al., 1988). Schlesinger et al. (1990) proposed that soil moisture is more heterogeneous in shrublands than grasslands, as observed for soil fertility. This soil moisture change could be a feedback that reinforces shrub invasion if the soil water available to grasses is reduced, either due to changes in spatial distribution or temporal variability. Several differences in water cycling between these two ecosystems have been observed. First, intensified rainsplash in large shrubland interspaces reduces infiltration capacity in these areas (Lyford and Qashu, 1969; Abrahams et al., 1995). Second, more overland flow is observed in shrublands (Abrahams et al., 1995; Schlesinger et al., 2000). This increases soil erosion exposing finer textured, and therefore less permeable, soils at the surface (e.g., Kieft et al., 1998). Third, differences in soil moisture have been observed (Schlesinger et al., 1990; Kieft et al., 1998). The soil moisture field exhibits substantial temporal variability in arid and semiarid environments – the soil is typically dry except for brief periods following rainfall events. Therefore, single surveys or repeat sampling at intervals unrelated to wetting and drying cycles provide limited information about soil moisture dynamics (e.g., Schlesinger et al., 1990; Kieft et al., 1998).

In this study, we compare infiltration and soil moisture between grassland and shrubland ecosystems. We define infiltration as the total equivalent depth of water that enters the soil (units of length), resulting either from a single rainfall event or a series of events. This is equivalent to a volume of water passing through a unit area of the soil surface. Our goal is to understand how the transition from grassland to shrubland affects the amount of soil water that is available to plants. Here, we focus on the spatial and temporal variability of infiltration that occurs during individual rainfall events. This

enables us to characterize the soil moisture state immediately following rainfall events in grassland and shrubland, and therefore we can assess how shrub invasion influences the spatial distribution of soil water availability. We do not examine processes that influence soil moisture distribution on longer timescales, such as lateral redistribution within the soil, evaporation, and transpiration. We divide the landscape into sub-canopy and interspace patches for much of our analyses. Previous work has demonstrated that the influence of desert shrubs on soil hydraulic properties extends beyond their canopy margins (e.g., Dunkerley, 2000), so this canopy-interspace binary division is a simplification. Therefore, we also employ geostatistical techniques to gauge the variability throughout the landscape.

We test four hypotheses regarding infiltration in semiarid grassland and shrubland ecosystems. First, there is more infiltration beneath plant canopies than interspaces in both grassland and shrubland, either following a single rainfall event or summed over many events. If this hypothesis is correct, then the fertile islands found beneath plant canopies are also locations where infiltration is highest and soil moisture is concentrated. Second, the difference in infiltration between canopy and interspace is greater in shrublands than grasslands, that is the "oases" beneath canopies are more intense in shrubland, as observed for soil fertility. Third, infiltration is more spatially variable in shrubland than in grassland. And fourth, the correlation length of infiltration variability is greater in shrubland because canopies are spread further apart and infiltration is controlled by the presence or absence of vegetation. If the latter two hypotheses are correct, then the transition from grassland to shrubland is accompanied by increased heterogeneity of soil water, as is the case for soil nutrients.

## 2. Study area and methods

### 2.1 Study area

We measured infiltration in grassland and shrubland ecosystems at the McKenzie Flats research area in the Sevilleta National Wildlife Refuge, central New Mexico (Figure A-1). Our measurements are from the same sites sampled in previous studies (e.g., Schlesinger et al., 1996; Kieft et al., 1998). Annual precipitation is ~250 mm and more than half of the precipitation falls between July and September. The grass-shrub ecotone is narrow at McKenzie Flats – the shrub and grass sites sampled were within 2 km of each other. The grassland is dominated by black grama (*Bouteloua eriopoda*) and has ~50% canopy cover. The shrubland is dominated by creosotebush (*Larrea Tridentata*) with ~25% plant cover. According to historical information and repeat photography, the shrubland was dominated by herbaceous species in the early 20<sup>th</sup> century. Therefore, we are comparing grassland infiltration with infiltration in an area that was recently transformed from grassland to shrubland. The slope at all sites is < 2 degrees and the surface soil is a sandy loam that has developed on fan deposits from the Los Pinos Mountains to the west. Kieft et al. (1998) documented soil texture differences between the grassland and shrubland, and they attributed these differences to the shrub invasion process. The entire area has not been grazed by livestock since the 1970s.

### 2.2 Spatial variability of infiltration and soil moisture

**Data Collection:** We measured infiltration along transects following four rainfall events, two each in the grassland and shrubland ecosystems (Table A-1). Each event had

a rainfall total > 5 mm and infiltration was measured within a few hours of rainfall. Given personnel, equipment, and time constraints, it was not possible to complete infiltration surveys following the same event in both environments. This would have required two days of sampling, so the effects of evapotranspiration and subsurface redistribution would be much more important at the site sampled on the second day following rainfall. Each transect was selected haphazardly, was between 12 – 24 m long, and had sampling intervals of 10 cm. Measurement locations were designated either canopy or interspace, depending upon the presence or absence of standing vegetation above the sample location.

We estimate infiltration by combining water content and wetting front measurements. Volumetric water content was measured using the Time Domain Reflectometry (TDR) method (Topp, 1980; Schlugge et al., 1980). TDR probes were inserted at an angle so that the top end of the rods were located ~1 cm below the soil surface and extended to a depth of 5 cm (Figure A-2), providing an estimate of the average water content over the top 5 cm of the soil. We used 3-pronged probes with 15 cm rods that were spaced 2.0 cm apart. A probe with this geometry samples an elliptical region around the rods: 90% of the signal is derived from the medium between 0.75 cm above and below the rods (Ferre et al., 1998). Given this geometry, the volume sampled by the probe did not extend above the soil surface. All data were collected following rain events sufficient to provide a wetting front of at least 5 cm. Therefore, the probes did not extend into dry soil. TDR provides an indirect measure of volumetric soil moisture. We have checked the accuracy of this method for Sevilleta soils in the laboratory. Soil moisture values from TDR were within several percent of values determined

gravimetrically. We trenched the soil to expose the wetting front, within 1 hour of the TDR measurements along any portion of each transect. The wetting depth was measured at the same locations as water content. The wetting front was identified by the strong color contrast between wet and dry soil (Figure A-3).

At a point, the infiltration,  $I$ , or the total equivalent water depth that enters the soil following a rainfall event (units = cm), can be written as

$$I = \int_{z=0}^{S_f} (\theta_i(z) - \theta_i(z)) dz$$

(1)

where  $\theta_i$  is volumetric water content at some time after the rainfall event,  $\theta_i$  is volumetric water content preceding the rainfall event,  $S_f$  is the wetting front depth [cm], and  $z$  is distance below the surface. In this study, we calculate infiltration based upon the Green and Ampt (1911) model: infiltration proceeds as a plug with uniform water content above the wetting front. Using the water content and wetting front measurements at each location, we approximate infiltration as

$$I = \int_{z=0}^{S_f} (\theta_i(z) - \theta_i(z)) dz \approx (\theta_i - \theta_i) * S_f$$

(2)

This approximation of infiltration is based on two assumptions. First, water content is uniform above the wetting front. We used the average volumetric water content measured in the top 5 cm of soil via TDR for this value. Second, the water content prior to the passage of the wetting front (i.e., the initial water content,  $\theta_i$ ) is also uniform. We used soil moisture values typical of air-dry conditions for the initial value: all four of the rainstorms we studied occurred after rain-free intervals > 15 days in duration.

Previously, we measured volumetric water content of field-dry soil, by re-weighing a known volume of soil following 24 hours of oven drying at 100 °C. In the grasslands, field-dry soil had an average water content of  $2.1 \pm 0.6$  % and  $2.3 \pm 0.5$ % across canopy and interspace patches, respectively. In the shrubland, the canopy and interspace water contents were  $2.7 \pm 0.6$  % and  $2.6 \pm 0.5$ %, respectively. We use values of 2.2% for grass and 2.6% for shrub in our infiltration calculations.

We have not directly tested these two assumptions. However, several lines of evidence indicate that our approximation of infiltration is reasonable. First, we have observed that wetting fronts are sharp: the water content distribution with depth is a step function (Figure A-3) (Philip, 1975). In addition, we did not observe unstable wetting fronts (Raats, 1973), which would indicate that the Green-Ampt model is inappropriate. Second, infiltration calculated using equation 2 is similar to independent estimates based on cored samples and subsequent volumetric water content measurements: the values from the two different methods are within ~10%. And third, the mean infiltration value from each transect is 2-4 mm less than the measured precipitation (Table A-1). This difference is expected given that interception loss in these semiarid environments is on the order of several mm (Navar and Bryan, 1990; Dunkerley and Booth, 1999; Tromble, 1988).

**Statistical Analyses:** Mean and variance were calculated across entire transects and separately for canopy and interspace infiltration. We used t-tests and F-tests to compare mean and variance values, respectively.

We used geostatistics to examine the spatial structure of infiltration variability, as done in previous studies of soil fertility at the Sevilleta and other locations (e.g.,

Schlesinger et al., 1996). We constructed raw variograms for each transect, which show the variance of infiltration,  $\gamma^*$ , as a function of measurement separation or lag distance,  $h$  (Kitanidis, 1997). The variogram data,  $\gamma^*(h)$ , was then used to construct a model variogram for each transect, using an exponential model of the form

$$\gamma(h) = c * \left[ 1 - \exp\left(\frac{-3h}{a}\right) \right] + c_0$$

(3)

where  $c$  is the variance component of the model [ $\text{cm}^2$ ],  $a$  is the variogram range [ $\text{cm}$ ], and  $c_0$  is the nugget [ $\text{cm}^2$ ] (Isaaks *et al.*, 1989). The nugget represents both TDR probe error and spatial variability that exists at scales smaller than the sampling interval, 10 cm.

We used two features of the modeled variogram,  $\gamma(h)$ , to compare the spatial variability of infiltration between grassland and shrubland. First, the range provides an estimate of the correlation length, or the distance at which measurements become independent (Kitanidis, 1997). We used the range to test the hypothesis that spatial correlation of infiltration exists at greater distances in the shrubland because canopies are spread further apart. Second, at distances beyond the range, the modeled variogram approaches the sill. This sill is equivalent to the sample variance,  $\sigma^2$ , across each transect, equal to  $c + c_0$ . We used the sill to identify patterns beyond the range that appear as hole effects, or periodic deviations from the sill. We did not force the modeled variogram to fit the hole effect present in the raw variogram data,  $\gamma^*(h)$ . Instead, we assessed the observed hole effect in terms of the wavelength at which the (raw) variogram data deviates from the modeled sill. Both the range and the sill, and therefore hole effects, are useful statistical measures if infiltration is spatially stationary across



each transect, that is, if soil moisture values vary spatially at a relatively small-scale about a constant mean value that is maintained through the entire sampling domain. A sill only exists if the distribution is stationary.

### **2.3 Temporal variability of infiltration**

We used continuous monitoring of soil moisture to complement the spatially intensive surveys. In both grassland and shrubland, we measured soil moisture beneath a single plant canopy and the adjacent, upslope interspace. The canopy and interspace patches we monitored were selected based on two criteria. First, their dimensions were typical of that observed in each environment. Second, they were close enough to existing data acquisition systems to minimize cable length requirements.

At each of the four locations, we inserted Campbell Scientific water content reflectometers (WCR) at 3 depths: 2.5, 12.5, and 22.5 cm. WCRs provide an estimate of soil moisture based on the TDR method. The WCRs have two 30 cm rods spaced 3.2 cm apart. A probe with this geometry samples a semi-cylindrical region around the rods: 90% of the signal is derived from soil between 2.5 cm above and below the rods (Ferre et al., 1998). Probes were inserted horizontally in the upslope direction from a shallow pit that was subsequently filled. We used the three probes at each location to estimate the average soil moisture throughout the top 27.5 cm of the soil. The value from each probe was weighted assuming it represents soil moisture over the following depth intervals, 0-7.5, 7.5-17.5, 17.5-27.5 cm, a reasonable assumption if soil-wetting is uniform. These depth intervals were chosen according to the mid-points between each probe and to place equal weighting at each depth.

Soil moisture was measured every 15 minutes between June 1, 2000 and January 1, 2002. There were 31 precipitation events that exceeded 2 mm during this interval. We calculated infiltration,  $I$ , for each of these events as

$$I = (\theta_{\max} - \theta) * D$$

(4)

where  $\theta_{\max}$  is the maximum volumetric water content after the event,  $\theta_i$  is the volumetric water content before the event, and  $D$  is the depth over which the measurements were made (27.5 cm). Soil moisture rises to a maximum typically within ~1 hour of each rainfall event, followed by a slow decline due to evapotranspiration and vertical redistribution below 27.5 cm for larger storms. The maximum value following each event was used for our infiltration calculations. We compared infiltration beneath canopy and interspace in both the shrub and grass environments.

### 3. Results

First we describe the relationship between volumetric water content, wetting depth, and infiltration, demonstrating how the method applied here yields estimates of infiltration. Then, we test the hypotheses presented above by analyzing the spatial and temporal variability of infiltration. In each transect, the spatial patterns of water content and wetting depth ( $\theta$ ,  $S_f$ ) were similar: the magnitudes of  $\theta$  and  $S_f$  were typically higher beneath canopies and lower within interspaces (Table A-2). A positive correlation exists between variations in  $\theta$  and  $S_f$ , with values of 0.21 to 0.66 for all four transects. Because infiltration is the product of  $\theta$  and  $S_f$ , it is also higher beneath canopies and lower in interspaces.

In the shrubland, most of the observed variability in  $\theta$  and  $S_f$  exists beneath plant canopies (Table A-2). Because  $\theta$  and  $S_f$  positively covary, most of the variability in infiltration also exists beneath canopies (Figure A-4). The variance of  $\theta$ ,  $S_f$  and  $I$  are all significantly higher beneath shrub canopies than interspaces. In contrast, the variance of grassland  $\theta$ ,  $S_f$ , and  $I$  beneath canopies and interspaces are equal. The greatest variations are found near the junction of adjacent canopies and interspaces. In both environments, the spatial patterns of  $\theta$ ,  $S_f$  and  $I$  are similar. Therefore, we focus the remainder of our analysis on infiltration, which reflects the combined variation in  $\theta$  and  $S_f$ .

### **3.1 Canopy versus interspace infiltration**

We compare the magnitude of infiltration beneath canopy and interspace patches to test the first two hypotheses: (1) there is more infiltration beneath canopies and (2) the canopy-interspace infiltration contrast is greater in shrubland.

Infiltration was higher beneath plant canopies than beneath interspaces, in both grassland transects and one of the shrubland transects (Figure A-4; Table A-2). In these cases, infiltration beneath canopies was greater than the rainfall that accumulates during an event whereas interspace infiltration was less than the accumulated rainfall. The first shrub transect is an exception, as the canopy and interspace values were not significantly different. These results demonstrate that the first hypothesis is sometimes correct: there is more infiltration beneath plant canopies than interspaces. However, the results from the first shrub profile demonstrate that this hypothesis is not always valid.

The results from our spatial analysis do not support the second hypothesis: that the canopy-interspace infiltration contrast is more intense in the shrubland than in the

grassland. The ratios of canopy-to-interspace infiltration in both shrubland transects (0.91 and 1.54) were lower than the ratios measured in the two grass transects (1.64 and 2.18) (Table A-2). These tests of the first two hypotheses were based on measurements of infiltration following different storms in the grassland and shrubland. The partitioning of infiltration between canopies and interspaces may depend on the magnitude and intensity of rainfall events. Therefore, we examined the time series of soil moisture in both grassland and shrubland to test these hypotheses over a broader range of conditions.

In contrast to the spatial surveys, our continuous measurements of soil moisture show that there was more intense canopy infiltration in the shrubland than grassland. In the shrubland, there were 31 events totaling 290 mm of precipitation. Measurements of infiltration beneath a canopy and adjacent interspace show that 405 mm of water infiltrated beneath the shrub canopy and only 198 mm infiltrated in the adjacent interspace, or ~140% and 68% of measured precipitation, respectively (Table A-3). Therefore, the canopy-to-interspace infiltration ratio is nearly 2 in the shrubland, when infiltration is summed over many events. In contrast, the total infiltration measured beneath grassland canopy and interspace was more similar. There was 248 mm and 202 mm of infiltration beneath canopy and interspace, equal to 77% and 64% of the measured precipitation, respectively. Over 31 events, the canopy-interspace ratio was 1.2 in the grassland. Therefore, both the first and second hypotheses are supported when infiltration is considered over many events.

The contrast in results between our spatial and temporal analyses suggests that differences between canopy and interspace infiltration vary dramatically from event-to-event, in both the shrubland and grassland. In the shrubland, the maximum canopy-to-

interspace infiltration ratio observed during a single event is 4.6 and the minimum is 0.1 (Table A-3). The ratio of canopy-to-interspace infiltration is higher during events with greater total precipitation (Figure A-5). When rainfall is  $< \sim 5$  mm, there is more infiltration beneath the shrubland interspace than the canopy. The opposite is true during larger events. In general, the canopy-interspace difference increases logarithmically with precipitation amount ( $r^2 = 0.71$ ). In the grassland, there is also substantial variability from event-to-event: the maximum canopy-to-interspace ratio is 3.1 and the minimum is 0.2. However, the relationship between the ratio of canopy-to-interspace infiltration and precipitation falling during each event is not as strong or clear ( $r^2 = 0.45$ ) (Figure A-5). These results need to be tested with data from multiple plant canopies and interspaces.

### **3.2 Spatial Variability**

The third hypothesis, that the spatial variability of infiltration is greater in shrubland than grassland, was not supported by our infiltration transect data. The profile variance was highest in the first grassland transect and lowest in the second grassland transect whereas the two shrubland transects exhibited intermediate values (Table A-1). This comparison does not account for differences in mean infiltration between the four transects. When variability was normalized by the mean infiltration in each transect, variations in the two shrubland transects were the highest and lowest and the grassland values were intermediate (Table A-1). Therefore, spatial variability of infiltration was not consistently higher in the shrubland than the grassland, regardless of how variability is calculated.

We analyze variograms to test the fourth hypothesis: that the correlation length of infiltration variability is greater in the shrubland because of the larger separation distance between adjacent canopies in this environment. Our results suggest that the radius of plant canopies strongly influences the spatial patterns of infiltration in the shrubland. There was more variability beneath shrub canopies than beneath interspaces (Table A-4). Infiltration maxima existed near the center of canopies and infiltration decreased rapidly towards the canopy margins (Figures A-4 and A-6). In contrast, infiltration was relatively constant within each interspace, except for minor variations that had the appearance of noise rather than of a spatially correlated series. The distance between the canopy infiltration maxima and the lower values found near the canopy-interspace margins controlled the shrubland variogram ranges, 70 cm and 37 cm (Figure A-6 and Table A-5). Therefore, the correlation length of infiltration appeared to be controlled by the length of shrub canopies in the measured transects. The average lengths were 59 cm and 30 cm in the two profiles (Table A-5). The average spacing between shrub canopies was much greater, equal to 270 cm and 380 cm, and does not appear to influence the range. The average length of shrub canopies along the transects is less than the average radii of shrub canopies throughout the landscape, because the transects do not necessarily cross all shrubs through their midpoint. However, the canopy length measured along the transect is the relevant measure for comparison to the spatial patterns of infiltration.

In the grassland, the relationship between infiltration variability and the geometry of canopies and interspaces was not as straightforward. The decrease in infiltration away from grass canopies extends into the adjacent interspace, unlike in the shrubland (Figures A-4 and A-6). Although mean infiltration was greater beneath grass canopies than within

interspaces, canopy and interspace patches exhibit similar variability (Table A-4). Therefore, infiltration variability in both canopies and interspaces contribute to the total variance and affect the range. The range was 41 cm and 44 cm in the first and second transects, respectively (Table A-5, Figure A-6). The range reflects the distance over which the canopy-to-interspace decrease in infiltration occurs, which was not directly controlled by either canopy size or spacing. The range was greater than the average grass canopy radii, which are 22 cm and 26 cm in the two transects (Table A-5). This was consistent with the observed infiltration profiles: the decrease in infiltration from sub-canopy maxima extended into adjacent interspaces.

Based on the four surveys described here, we reject the fourth hypothesis. The correlation length of infiltration was not greater in *Sevilleta* shrubland than grassland, even though shrub canopies were spaced further apart. However, canopy spacing did influence the spatial variability of infiltration. In both the grassland and shrubland, periodic variations about the sill show how canopy spacing influenced infiltration variability at distances greater than the range (Figure A-6). In the shrubland variograms, local minima in variance occurred at ~3 m intervals. Enhanced infiltration beneath the center of shrub canopies, which were spaced at roughly 3 m intervals (Table A-5), is the source of the periodic minima. In the grassland variograms, the periodic variance minima occur every ~1 m. Again, this length is similar to the distance between adjacent canopy centers, where infiltration is typically highest (Figure A-6). Therefore, canopy spacing was the primary control of infiltration variability at scales beyond the range in both the grassland and shrubland.

#### 4.0 Discussion

We now discuss why (1) canopy infiltration is greater than interspace infiltration; (2) the canopy-interspace infiltration contrast varies between storms and locations; and (3) why the canopy-interspace infiltration ratio is typically higher in shrubland than grassland. We assumed that precipitation above the canopy was uniform over an area of  $\sim 100 \text{ m}^2$ , equivalent to the scale at which measurements were collected. Three processes could produce variability of infiltration and soil moisture on the timescales studied here: (1) interception of rainfall and subsequent evaporation, (2) stemflow of intercepted rainfall, and (3) lateral redistribution of water via surface runoff.

Vegetation intercepts rainfall and a substantial fraction of this intercepted rainfall may evaporate directly from the surface of plant leaves and stems (e.g., Tromble, 1988). In the absence of wind, evaporation of intercepted rainfall would result in less water reaching the soil surface beneath plant canopies than in interspaces. The net effect would be greater infiltration within interspaces than beneath canopies, if all water infiltrates where it hits the ground. In the presence of wind, the effects of interception loss on infiltration and soil moisture occur downwind of individual plants, with the downwind distance depending on wind speed and plant dimensions and spacing.

The magnitude of soil moisture variability resulting from evaporation of intercepted rainfall depends on the amount of interception loss, which is controlled by canopy interception storage capacity and rainfall amount and intensity. Compared to forest ecosystems, there are few measurements of interception loss in semiarid shrub and grass systems (e.g., Dunkerley and Booth, 1999). Desert shrubs typically have a canopy storage capacity of several mm (Navar and Bryan, 1990; Dunkerley and Booth, 1999).



For example, creosotebush in southern New Mexico has a canopy capacity of ~3 mm (Tromble, 1988). Fewer measurements of interception loss in semiarid grasslands have been made, but estimates are higher per unit dry weight of plant matter than for shrubland (Thurow et al., 1987).

In the shrubland, the effects of interception loss were apparent in our time series data. The infiltration measured beneath the shrub canopy was lower than that in the interspace (a canopy:interspace ratio <1) during events when the rainfall total was less than ~5 mm (Figure A-5). This suggests that several mm of water were stored and subsequently evaporated from the shrub canopy, consistent with previous observations of creosotebush interception (Tromble, 1988). Effects of interception loss were not as obvious in the grassland, but higher infiltration beneath interspaces was observed during the smallest events. Our spatial sampling shows canopies are typically wetter than interspaces (Table A-2), the reverse of what is expected due to interception loss. The temporal data provides the same result, except in small storms. Based on this information, we believe that evaporation of intercepted rainfall has a small impact on the spatial variability of infiltration.

Stemflow of intercepted rainfall preferentially transports water towards shrub stems. Whitford et al. (1997) measured that 16% of rainfall was converted to stemflow in creosotebush. Martinez-Meza *et al.* (1996) found that creosotebush typically has a canopy storage capacity of 3 mm, beyond which significant stemflow occurs. They reported that the stem-root system of creosotebush channels water to depths significantly greater than the wetting front in the surrounding soil (Martinez-Meza *et al.*, 1996), similar to the results of Devitt and Smith (2002). For example, Martinez-Meza *et al.*

found that following natural rainfall, a maximum root channel flow of 35 cm was observed when the ambient wetting front was only 10 cm. Lyford et al. (1969) found that infiltration capacity at the stem of creosotebush is nearly three times greater than that in the areas between plants. In grassland, stemflow is probably less important due to the lack of a single woody stem to focus flow.

Stemflow should influence both the spatial and temporal measurements discussed above, as canopy storage was exceeded in all four spatial surveys and most of the 17 events sampled by our automated system. We expect that stemflow is the source of the infiltration maxima located near the center of shrub canopies (Figure A-4 and A-6). The higher variance beneath shrub canopies than interspaces is the result of these peaks. Stemflow may redirect water intercepted by canopies. However, it cannot yield canopy-to-interspace infiltration ratios much greater than 1.0, unless canopy shading robs interspaces of precipitation in the presence of wind.

Our infiltration data and observations during rainfall events suggest that lateral redistribution of water via surface runoff is the key process that resulted in higher canopy infiltration, in both the grassland and shrubland. Surface ponding and overland flow originate when the precipitation rate exceeds the infiltration capacity. Infiltration capacity is typically higher in canopy soils than interspaces in a variety of environments (Lyford et al., 1969; Reid et al., 1999; Dunkerley, 2000). Therefore, ponding and overland flow will occur sooner and during more rainfall events in interspaces than in canopy patches. The runoff from interspace areas then runs on to canopy patches and may infiltrate there (Reid et al., 1999). We have observed this transfer of surface water from interspace to canopies in the Sevilleta shrubland. In the grassland, we observed that

rainfall that does not immediately infiltrate in the interspaces ponds on the uphill side of grass canopies. This was the result of the raised topography associated with grass clumps.

If surface redistribution leads to differences between canopy and interspace infiltration, then the canopy-to-interspace infiltration ratio should be higher in situations with greater runoff. Surface runoff is enhanced when storm intensity or magnitude is high and when areas with low infiltration capacity are pervasive (Cordova and Rodrigues-Iturbe, 1985). The canopy-to-interspace infiltration ratio we measured was typically higher under these conditions. First, canopy infiltration did not exceed interspace infiltration along the second shrub profile only. This was the only profile measured on nearly flat ground, where runoff should be negligible. The other three transects were measured on slopes of  $\sim 1.5^\circ$ . Second, the canopy-to-interspace infiltration ratio clearly increases with storm size, and therefore runoff (Figure A-5). This relationship was not as strong in the grassland, perhaps due to the lack of connectivity between adjacent interspaces. And third, the canopy-interspace ratio was higher in the shrubland when summed over the range of storms sizes and intensities included in the 31 sampled events. The area covered by interspace is roughly twice as high in the shrubland than in the grassland. Therefore, more low-infiltration areas exist that provide runoff to canopies in the shrubland.

The four transects described here do not show that the magnitude of the spatial infiltration variability was different in shrubland and grassland. Data documenting the spatial variability of infiltration over a range of storms was necessary to fully test our third hypothesis. However, our data did show that there were similarities and differences

between the spatial structure of infiltration in grassland and shrubland. There were three key similarities between infiltration variability in the two environments. First, most of the spatial variability exists in the vicinity of plant canopies: between the stem and canopy margin in the shrubland and straddling the canopy margin in the grassland. Second, the distance over which most of this variability exists was ~50 cm. And third, there was often more infiltration beneath canopies than in interspaces: following rainfall events, canopies were oases where water availability was greater than in the surrounding areas. The notable difference between the two environments was that oases are more intense and spread further apart in the shrubland because canopies are separated by larger interspaces in this environment.

We examined the spatial patterns of infiltration in grassland and shrubland. Investigating how the observed differences between canopy and interspace infiltration impact plants should be addressed in future research. We expect that the observed canopy-interspace infiltration contrast will influence plant productivity in two ways. First, water that infiltrates beneath the canopy will more likely be absorbed by plant roots. Root density is greater beneath canopies than beneath bare soil in the Sevilleta grassland and shrubland. In addition, direct evaporation from sub-canopy soil is much less than from interspace soil because the canopy reduces midday surface temperatures by ~10 °C or more. Second, a synergistic interaction between soil moisture and nutrient cycling should exist beneath plant canopies. Enhanced infiltration beneath canopies will promote more intense and longer-duration pulses of nitrogen mineralization following rainfall (e.g., Cui and Caldwell, 1997).

## References

- 1) Abrahams A.D., Parsons, A.J., and Wainwright, J., 1995, Effects of vegetation change on interrill runoff and erosion, Walnut Gulch, southern Arizona. *Geomorphology*, 13, 37-48.
- 2) Abrahams, A. D., Parsons, A.J., and Wainwright, J., 1994, Resistance to overland flow on semiarid grassland and shrubland hillslopes, Walnut Gulch, southern Arizona. *Journal of Hydrology*, 156, 431-446.
- 3) Abrahams, A.D. and Parsons, A.J., 1991, Relation between infiltration and stone cover on a semiarid hillslope, southern Arizona. *Journal of Hydrology*, 122, 49-59.
- 4) Archer, S., 1994, Woody plant encroachment into southwestern grasslands and savannas: Rates, patterns, and proximate causes. Pages 13-68 in *Ecological implications of livestock herbivory in the West*, Vavra, M., Laycock, W., and Pieper, R. eds. Society for Range Management, Denver, Colorado.
- 5) Bahre, C.J. and Shelton, M. L., 1993, Historic vegetation change, mesquite increases, and climate in southeastern Arizona. *Journal of Biogeography*, 20, 489-505.
- 6) Buffington, L. C. and Herbel, C. H., 1965, Vegetational changes on a semidesert grassland range from 1858 to 1963. *Ecological Monographs*, 35: 139-164.
- 7) Cordova, J. R., and I. Rodriguez-Iturbe. 1985. On the probabilistic structure of storm surface runoff. *Water Resources Research* 21:755-763.
- 8) Cui, M. and Caldwell, M. M., 1997, A large ephemeral release of nitrogen upon wetting of dry soil and corresponding root responses in the field. *Plant and Soil*, 191: 291-299.
- 9) Devitt, D.A. and Smith, S.D., 2002, Root channel macropores enhance downward movement of water in a Mojave Desert ecosystem. *Journal of Arid Environments*, 50: 99-108.
- 10) Dunkerley, D.L. and Booth, T.L., 1999, Plant canopy interception of rainfall and its significance in a banded landscape, arid western New South Wales, Australia. *Water Resources Research*, 35, 1581-1586.
- 11) Dunkerley, D.L., 2000, Hydrologic effects of dryland shrubs: defining the spatial extent of modified soil water uptake rates at an Australian desert site. *Journal of Arid Environments*, 45: 159-172.
- 12) Ferre, P.A., Knight, J.H., Rudolph, D.L., and Kachanoski, R.G., 1998, The sample areas of conventional and alternative time domain reflectometry probes. *Water Resources Research*, 34, 2971-2979.

- 13) Graetz, D., 1994, Grasslands. In Changes in Land Use and Land Cover: a Global Perspective, Meyer, W.B. and Turner, B.L. eds. Cambridge Univ. Press.
- 14) Green, W. H. and Ampt, G. A., 1911, Studies in soil physics. I. The flow of air and water through soils. *J. Agric. Sci.* 4:1-24.
- 15) Grover, H. D. and Musick, H. B., 1990, Shrubland encroachment in southern New Mexico, U.S.A.: An analysis of desertification processes in the American Southwest. *Climatic Change*, 17, 305-330.
- 16) Kieft T.L., White, C.S., Loftin, S.R., Aguilar, R., Craig, J., and Skaar, D., 1998, Temporal dynamics in soil carbon and nitrogen resources at a grassland-shrubland ecotone. *Ecology*, 671-683.
- 17) Kitanidis, P. K., 1997, Introduction to Geostatistics, Cambridge University Press.
- 18) Lyford, F.P. and Qashu, H.K., 1969, Infiltration rates as affected by desert vegetation, *Water Resources Research*. 5, 1373-1376.
- 19) Martinez-Meza, E., and W. G. Whitford. 1996. Stemflow, throughfall and channelization of stemflow by roots in three Chihuahuan desert shrubs. *Journal of Arid Environments* 32:271-287.
- 20) Mutchler, C. K., and K.C. McGregor. 1983. Erosion from low slopes. *Water Resources Research* 19:1323-1326.
- 21) Navar, J., and R. Bryan. 1990. Interception loss and rainfall redistribution by three semi-arid growing shrubs in northeastern Mexico. *Journal of Hydrology* 115:51-63.
- 22) Noy-Meir I., 1973, Desert ecosystems: Environment and producers. *Annual Review of Ecology and Systematics* 4:25-51.
- 23) Parsons, A.J., Abrahams, A.D., and Wainwright, J., 1996, Responses of interrill runoff and erosion rates to vegetation change in southern Arizona. *Geomorphology*, 14, 311-317.
- 24) Philip, J. R. 1975. Stability analysis of infiltration. *Soil Sci. Soc. Amer. Proc.* 39:1042-1049.
- 25) Raats, P. A. C. 1973. Unstable wetting fronts in uniform and nonuniform soils. *Soil Sci. Soc. Amer. Proc.* 37:681-685.
- 26) Reid, K.D., Wilcox, B.P., Breshears, D.D., MacDonald, L., 1999, Runoff and erosion in a pinon juniper woodland: influence of vegetation patches. *Soil Science Society of America Journal*, 63: 313-325.

- 27) Rodriguez-Iturbe, I., 2000, Ecohydrology: A hydrologic perspective of climate-soil-vegetation dynamics. *Water Resources Research*, 36, 3-9.
- 28) Schlesinger, W.H., Raikes, J.A., Hartley, A.E., and Cross, A.F., 1996, On the spatial pattern of soil nutrients in desert ecosystems. *Ecology*, 77, 364-374.
- 29) Schlesinger, W.H., Reynolds, J.F., Cunningham, G.L., Huenneke, L.F., Jarrell, W., Virginia, R.A., Whitford, W.G., 1990, Biological feedbacks in global desertification. *Science*, 247, 1043-1048.
- 30) Schlesinger, W.H., Ward, T.J., and Anderson, J., 2000, Nutrient losses in runoff from grassland and shrubland habitats in southern New Mexico: II. Field plots, *Biogeochemistry*, 49, 69-86.
- 31) Thurow, T. L., W. H. Blackburn, S. D. Warren, and C. A. Taylor. 1987. Rainfall interception by midgrass, shortgrass, and live oak mottes. *Journal of Range Management* 40:455-460.
- 32) Topp, G. C., J.L. Davis, and A. P. Annan. 1980. Electromagnetic determination of soil water content: Measurements in coaxial transmission lines. *Water Resources Research* 16:574-582.
- 33) Tromble, J. M., 1988, Water interception by two arid land shrubs. *Journal of Arid Environments*, 15, 65-70.
- 34) Van Auken, O. W., 2000, Shrub invasions of North American Semiarid Grassland. *Annual Reviews of Ecology and Systematics*, 31: 197-215.
- 35) Whitford, W. G., Anderson, J., Rice, P. M., 1997, Stemflow contribution to the 'fertile island' effect in creosotebush, *Larrea tridentate*. *Journal of Arid Environments*, 35: 451-457.
- 36) Wood, M. K., Jones, T. L., and VeraCruz, M. T., 1998, Rainfall interception by selected plants in the Chihuahuan desert. *Journal of Range Management*, 51, 91-96.

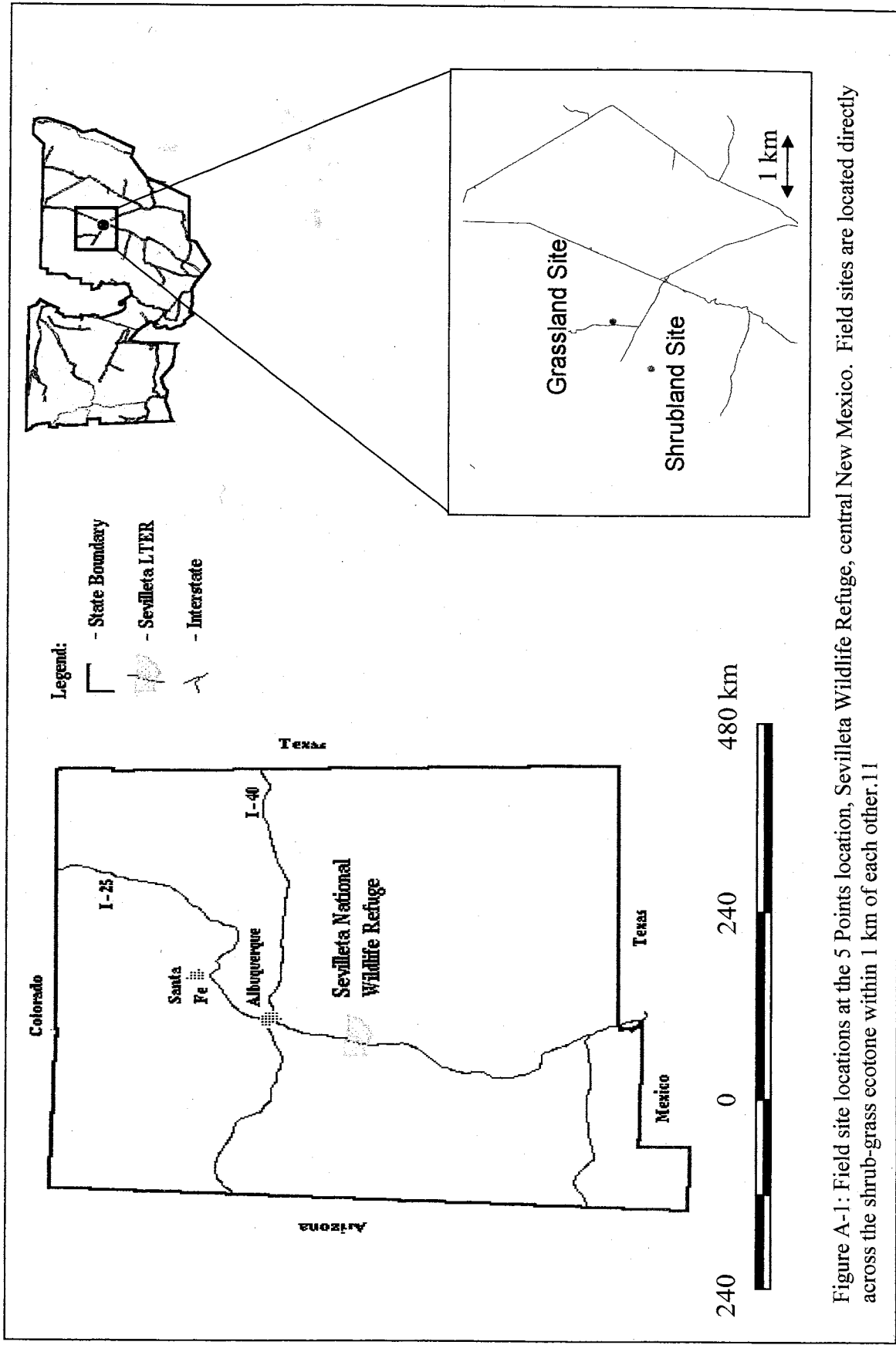


Figure A-1: Field site locations at the 5 Points location, Sevilleta Wildlife Refuge, central New Mexico. Field sites are located directly across the shrub-grass ecotone within 1 km of each other.11



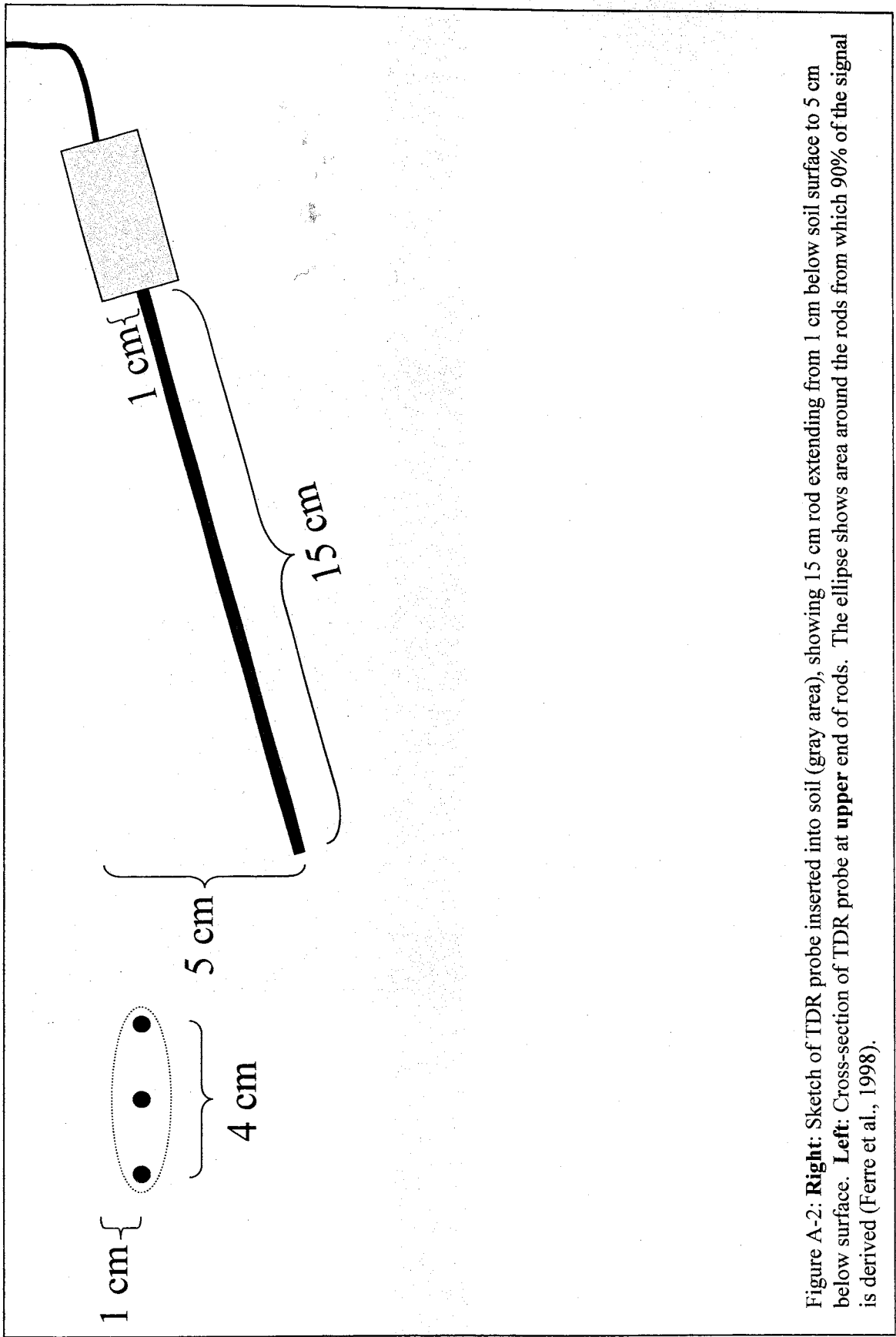


Figure A-2: **Right:** Sketch of TDR probe inserted into soil (gray area), showing 15 cm rod extending from 1 cm below soil surface to 5 cm below surface. **Left:** Cross-section of TDR probe at **upper** end of rods. The ellipse shows area around the rods from which 90% of the signal is derived (Ferre et al., 1998).

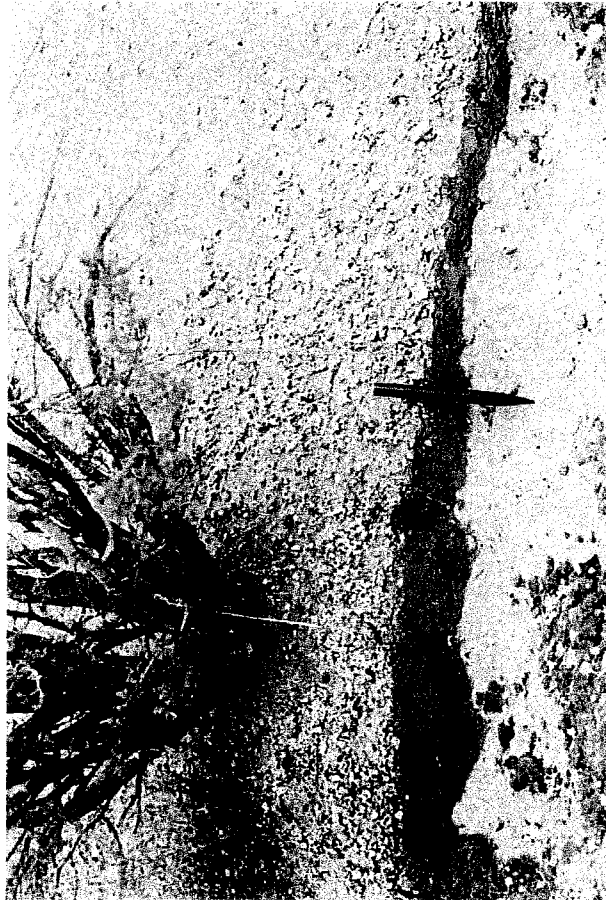


Figure A-3: A wetting front in the *Sevilleta* shrubland is exposed in a trench face. The wet soil above the front is dark and the dry soil below the front is light. The trench was completed and the photograph was taken ~1 hour after a several mm rainfall event. The wetting front is deeper beneath the canopy than in the interspace. The absence of fingering indicates wetting front stability. Wetting fronts in the adjacent grassland are also sharp and distinct.

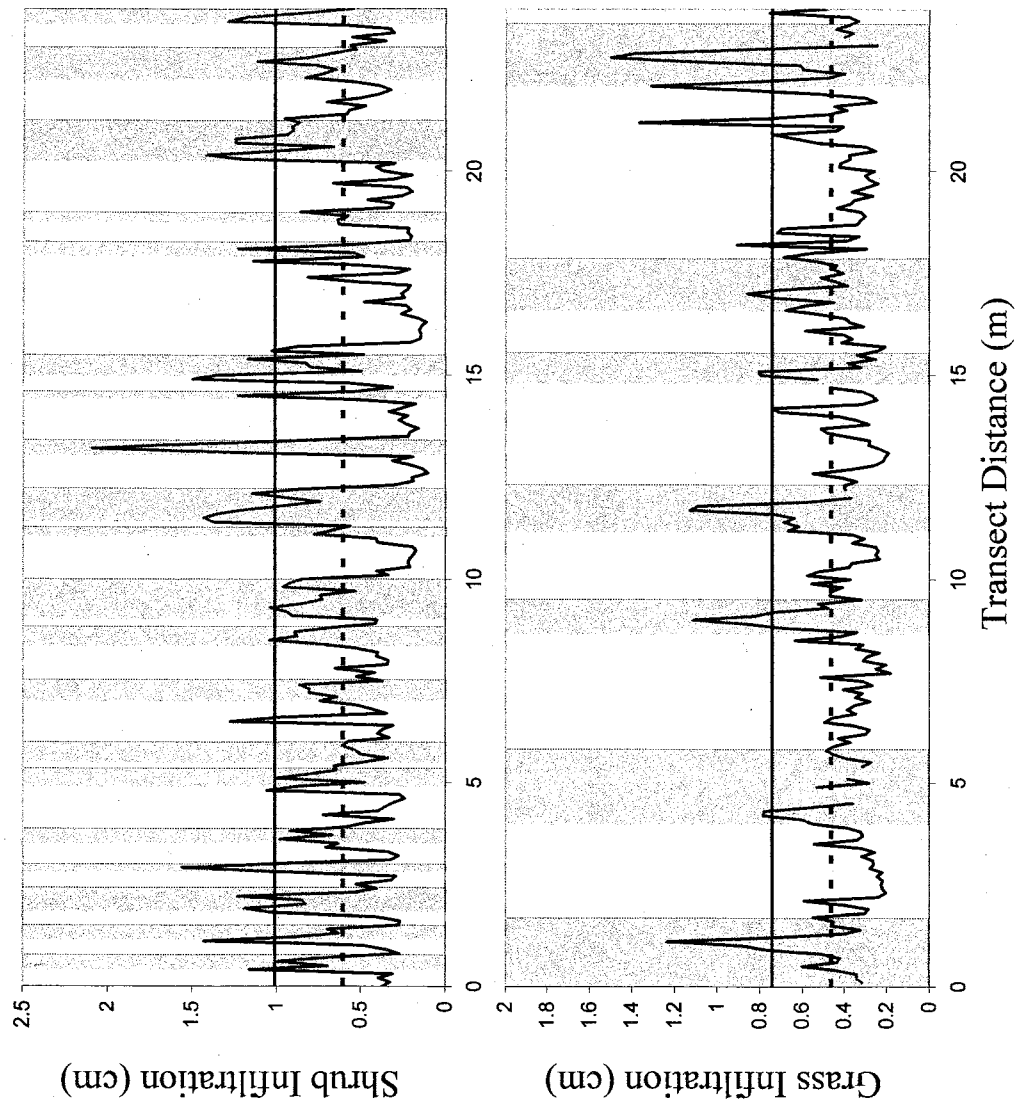


Figure A-4: Profiles of infiltration from grassland (top) and shrubland (bottom) transects. Shaded areas indicate the presence of plant canopies. The upper horizontal line indicates the measured rainfall and the lower dashed line the average infiltration.

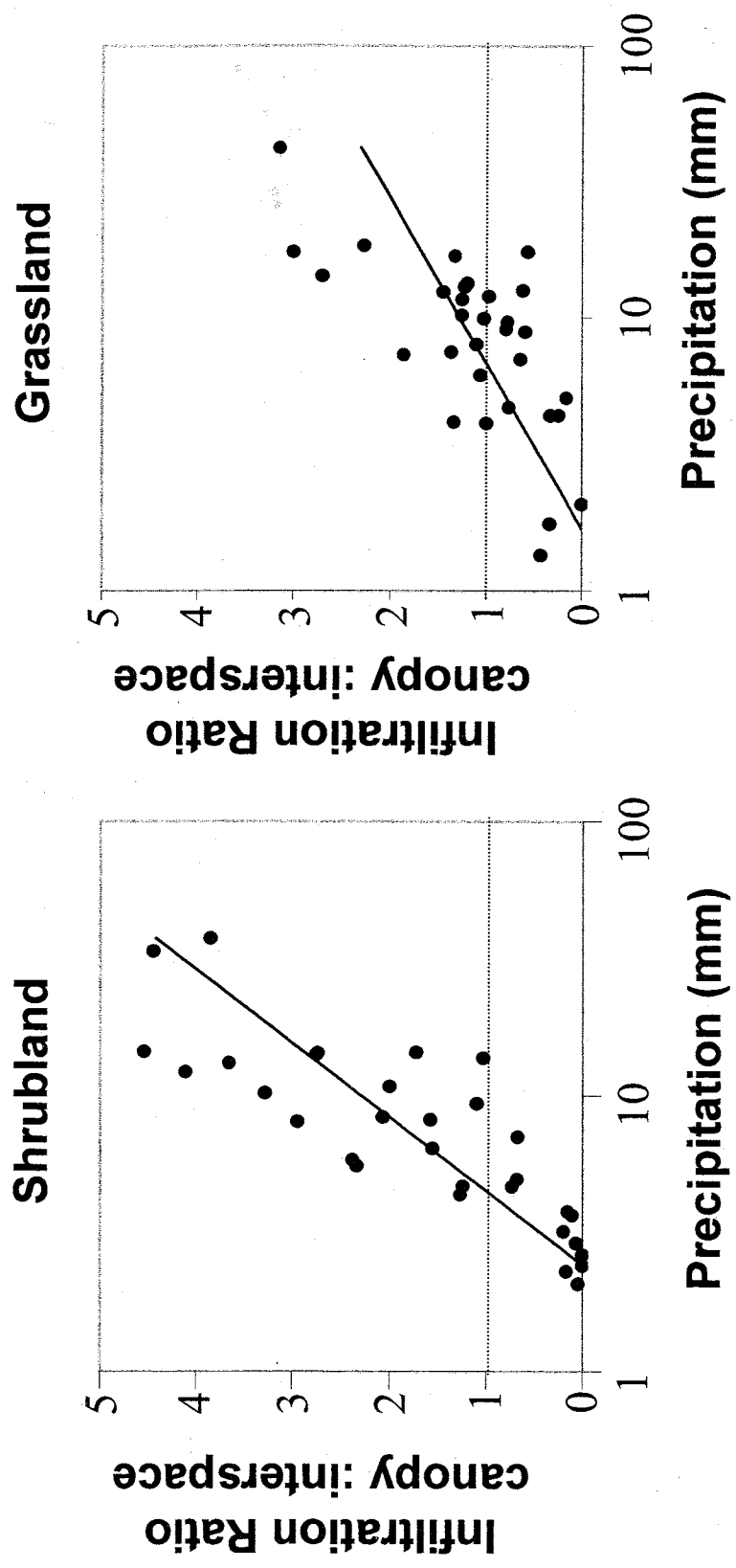


Figure A-5: The ratio of canopy to interspace infiltration plotted against the rainfall total during each of 31 precipitation events in the grassland and shrubland. If the difference is greater than one (dashed line), then canopy infiltration is greater than interspace infiltration. Lines are least squares linear fit to the data with the form  $r^2$  is 0.71 in shrubland and 0.45 in grassland.

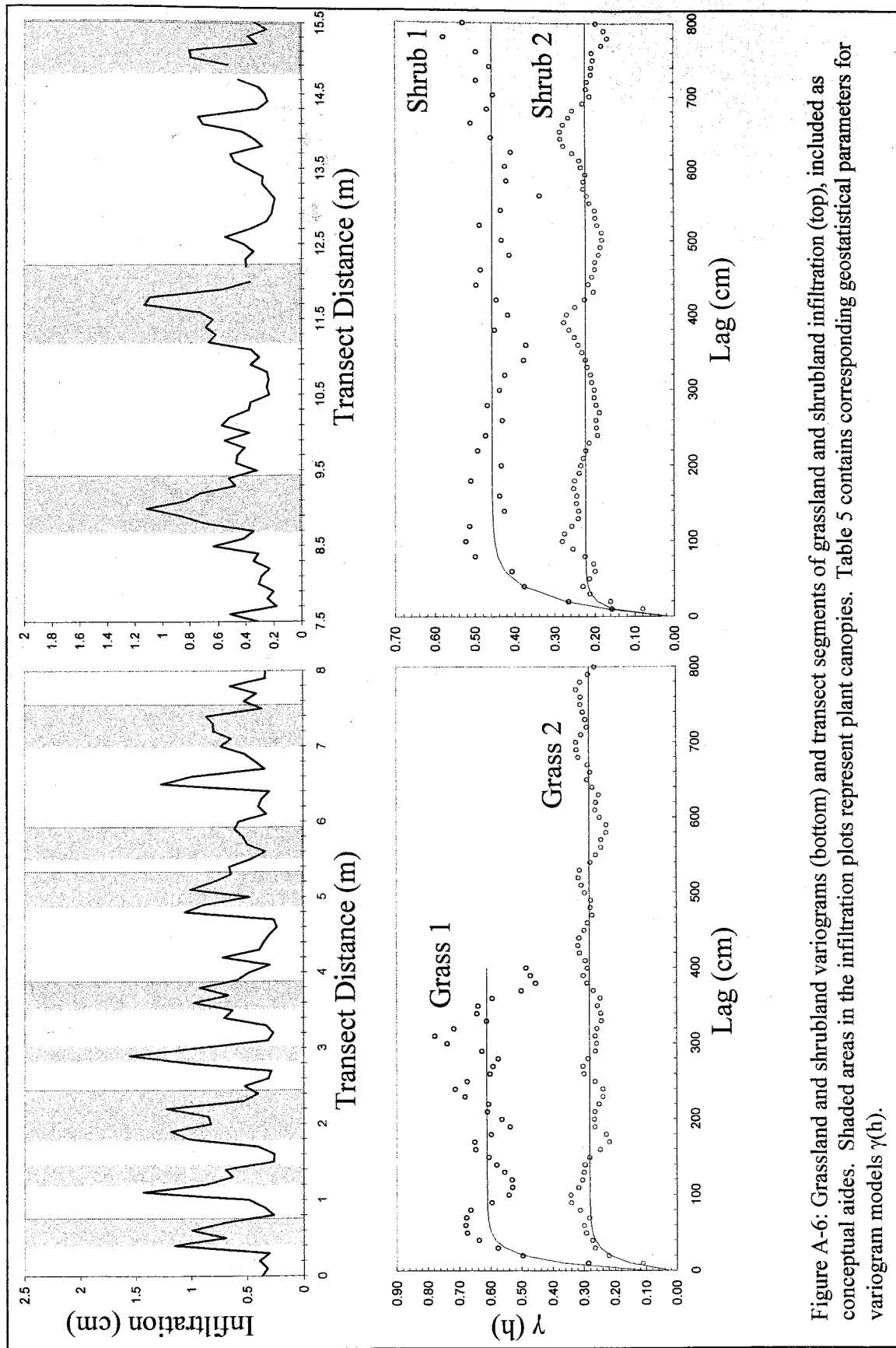


Figure A-6: Grassland and shrubland variograms (bottom) and transect segments of grassland and shrubland infiltration (top), included as conceptual aides. Shaded areas in the infiltration plots represent plant canopies. Table 5 contains corresponding geostatistical parameters for variogram models  $\gamma(h)$ .